ISSN 1590-8844
Vol. 08 No 02
2007

International Journal of Mechanics and Control

Honorary Editor: Guido Belforte

Editor: Andrea Manuello Bertetto

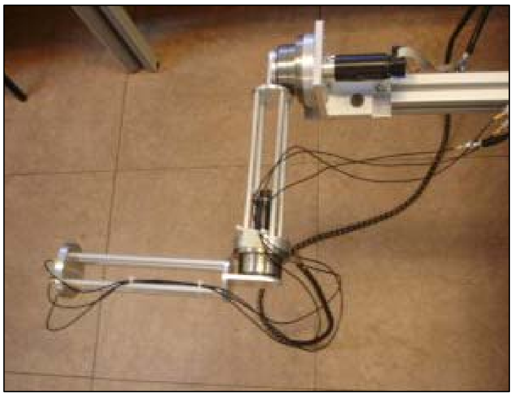

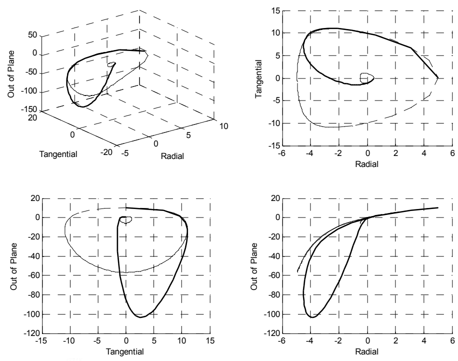

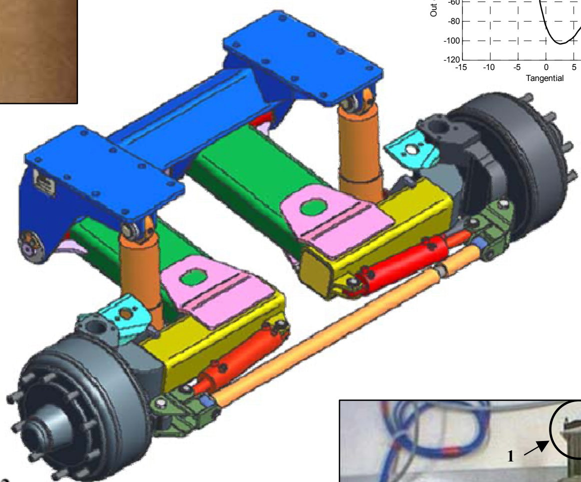

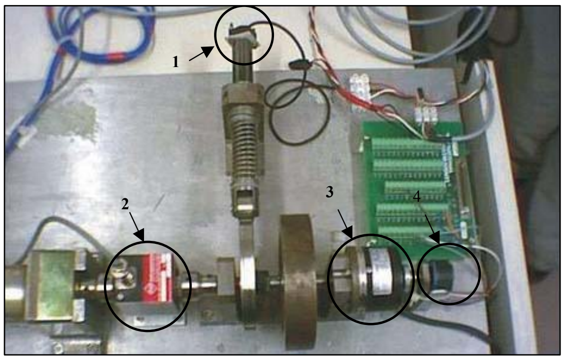

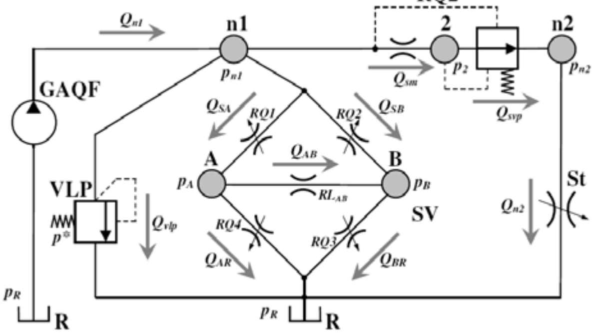

LIBRERIA EDITRICE UNIVERSITARIA
LEVROTTO & BELLA
TORINO

Editorial Board of the

International Journal of Mechanics and Control

Published by Levrotto&Bella – Torino – Italy E.C.

Honorary editors

Guido Belforte **Kazy Yamafuji**

Editor: **Andrea Manuello Bertetto**
General Secretariat: **Elvio Bonisoli**

Anindya Ghoshal
Arizona State University
Tempe – Arizona – USA

Domenico Appendino
Prima Industrie
Torino – Italy

Kenji Araki
Saitama University
Shimo Okubo, Urawa
Saitama – Japan

Guido Belforte
Technical University – Politecnico di Torino
Torino – Italy

Bruno A. Boley
Columbia University,
New York – USA

Marco Ceccarelli
LARM at DIMSAT
University of Cassino
Cassino – Italy

Amalia Ercoli Finzi
Technical University – Politecnico di Milano
Milano – Italy

Carlo Ferraresi
Technical University – Politecnico di Torino
Torino – Italy

Nunziatino Gualtieri
Space System Group
Alenia Spazio
Torino – Italy

Giovanni Jacazio
Technical University – Politecnico di Torino
Torino – Italy

Takashi Kawamura
Shinshu University
Nagano – Japan

Kin Huat Low
School of Mechanical and Aerospace Engineering
Nanyang Technological University
Singapore

Andrea Manuello Bertetto
University of Cagliari
Cagliari – Italy

Stamos Papastergiou
Jet Joint Undertaking
Abingdon – United Kingdom

Mihailo Ristic
Imperial College
London – United Kingdom

Jànos Somlò
Technical University of Budapast
Budapest – Ungary

Jozef Suchy
Faculty of Natural Science
Banska Bystrica – Slovakia

Federico Thomas
Instituto de Robótica e Informática Industrial
(CSIC-UPC)
Barcelona – Espana

Lubomir Uher
Institute of Control Theory and Robotics
Bratislava – Slovakia

Furio Vatta
Technical University – Politecnico di Torino
Torino – Italy

Kazy Yamafuji
University of Electro-Communications
Tokyo – Japan

Official Torino Italy Court Registration
n.5390, 5th May 2000

Deposito presso il Tribunale di Torino
numero 5390 del 5 maggio 2000
Direttore responsabile:
Andrea Manuello Bertetto

International Journal of Mechanics and Control

Editor: **Andrea Manuello Bertetto**

Honorary editor: **Guido Belforte** ***General Secretariat:*** **Elvio Bonisoli**

The Journal is addressed to scientists and engineers who work in the fields of mechanics (mechanics, machines, systems, control, structures). It is edited in Turin (Northern Italy) by Levrotto&Bella Co., with an international board of editors. It will have not advertising.
Turin has a great and long tradition in mechanics and automation of mechanical systems. The journal would will to satisfy the needs of young research workers of having their work published on a qualified paper in a short time, and of the public need to read the results of researches as fast as possible.
Interested parties will be University Departments, Private or Public Research Centres, Innovative Industries.

Aims and scope
The *International Journal of Mechanics and Control* publishes as rapidly as possible manuscripts of high standards. It aims at providing a fast means of exchange of ideas among workers in Mechanics, at offering an effective method of bringing new results quickly to the public and at establishing an informal vehicle for the discussion of ideas that may still in the formative stages.

Language: English
International Journal of Mechanics and Control will publish both scientific and applied contributions. The scope of the journal includes theoretical and computational methods, their applications and experimental procedures used to validate the theoretical foundations. The research reported in the journal will address the issues of new formulations, solution, algorithms, computational efficiency, analytical and computational kinematics synthesis, system dynamics, structures, flexibility effects, control, optimisation, real-time simulation, reliability and durability. Fields such as vehicle dynamics, aerospace technology, robotics and mechatronics, machine dynamics, crashworthiness, biomechanics, computer graphics, or system identification are also covered by the journal.

Please address contributions to

Prof. Guido Belforte
Prof. Andrea Manuello Bertetto
PhD Eng. Elvio Bonisoli

Dept. of Mechanics
Technical University - Politecnico di Torino
C.so Duca degli Abruzzi, 24.
10129 - Torino - Italy - E.C.

e_mail: jomac@polito.it

Subscription information

Subscription order must be sent to
the publisher:

Libreria Editrice Universitaria
Levrotto&Bella
2/E via Pigafetta – 10129 Torino – Italy

www.levrotto-bella.net
e_mail: info@levrotto-bella.net
tel. +39.011.5097367
+39.011.5083690
fax +39.011.504025

ISSN 1590-8844
International Journal of Mechanics and Control, Vol. 08, No. 02, 2007

A MULTI-OBJECTIVE OPTIMIZATION DESIGN FOR A 4R SERVICE ROBOT

Cristina Castejón * Giuseppe Carbone ** Juan-Carlos García-Prada * Marco Ceccarelli **

* MAQLAB group. Department of Mechanical Engineering, Carlos III University of Madrid, Spain
** LARM: Laboratory of Robotics and Mechatronics, DiMSAT, University of Cassino, Italy

ABSTRACT

The aim of this contribution is to propose a suitable design procedure for service robots. In particular, main characteristics and peculiarities of service robots are investigated in order to propose design criteria in the form of computationally efficient objective functions. Then, these objective functions are implemented in a multi-objective optimisation algorithm in order to obtain optimal design solutions for service robots. The proposed procedure has been applied to a service robot composed of two-2R robotic arm modules called SIDEMAR (Spanish acronym of Mechatronics Design of an Integrated System for Service Robots) that has been designed and built at Carlos III University of Madrid as a module for service robots [1]. The 4R robotic arm will be applied to perform tasks of attendance people with certain degree of handicap referred to its mobility, so that they were able to approach objects in home or offices. The results of this case of study are used for demonstrating both the soundness and engineering feasibility of the proposed multi-objective optimal design procedure.

Keywords: Robotics, Robot Design, multi-objective optimization.

1 INTRODUCTION

In the last two decades service robots has attracted significant interest of researchers in the mechatronics field. The wide range of possible applications of service robots covers elderly or handicapped care, education, assistance in hospitals, but also several other repetitive, boring, or dangerous tasks that could be carried out by robots within the humans environment, [1-4].

The specific field of service robots application makes not advisable to use a conventional approach for their design. In fact, one of the main skills of a service robot is to interact with human beings and to operate with them. Therefore, human-robot interaction and safety become most significant aspects in the design process while there is usually no need of high payload or high speed performances.

In literature we can find approximations to optimal environment [5], or to prevent serious injuries to human in the human beings and also to the robot integrity, [6], for example with an inertia minimization in order to suddenly stop a robot [8]. An optimisation of the stiffness can be also very useful in order to have a good accuracy with a lightweight design as proposed, for example, in [7,8]. Power consumption and path planning strategies should be taken into account for improving the autonomy and flexibility as proposed for example in [9].

All the above-mentioned design aspects should be taken into account in the design process. Nevertheless, optimizing a robot with respect to a design criterion usually produces a design that is not optimal with respect to other design criteria. A possible solution for overcoming this limit, proposed in this paper, is the implementation of a multi-objective design approach that can take into account several design criteria at the same time as proposed, for example, in [10]. Then, the proposed procedure has been applied to a specific case of study in order to show feasibility and effectiveness of the proposed design approach.

Contact authors: Cristina Castejon[1], Giuseppe Carbone[2]

[1] Av. de la Universidad 30, 28911 Leganés, Spain
E-mail: castejon@ing.uc3m.es
[2] Via Di Biasio 43, 03043 Cassino (Fr), Italy
E-mail: carbone@unicas.it

2 THE PROBLEM AND ITS FORMULATION

The problem for achieving optimal results from the formulated multi-objective optimization problem consists mainly in two aspects, namely to choose a proper numerical solving technique and to formulate the optimality criteria with computational efficiency.
There is a wide range of possible solving techniques. At LARM in Cassino, since the beginning of 90's a research line has been dedicated to the development of analysis formulation of manipulator performances that could be used in proper optimization problems by taking advantage of the peculiarity of the solving techniques in commercial softwares [7].
Once the numerical technique is chosen or is advised for solving the proposed multi-objective optimization problem, the main efforts can be addressed to the formulation of common algorithms for numerical evaluation of optimality criteria and design constraints.

3 OPTIMALITY CRITERIA FOR SERVICE ROBOTS

The choice and mathematical formulation of optimality criteria usually require a deep understanding of the specific application tasks of a robot. In this work, we are interested in service robots requiring manipulative skills, since they require a more careful mechanical design to be effective. It is also worth noting that this type of robots is supposed to help/substitute human beings in manipulative operations. Therefore, it is advisable to use human behavior as benchmark for the following optimality criteria. Detailed information about the objective function selection criteria and their normalized dimensionless can be found in [11].

3.1 REACHES AND WORKSPACE

The maximum reach of a robot R_{robot} could be computed is

$$R_{robot} = \sqrt{x_{max}^2 + y_{max}^2 + z_{max}^2} \tag{1}$$

where x_{max}, y_{max}, z_{max}, indicate coordinates of the maximum reach point. A reasonable and computationally efficient expression of reach and workspace performance of a service robot is defined as

$$f_1(X) = \left|1 - \left(R_{robot} / R_{human}\right)\right| \tag{2}$$

in which R_{human} stands for the maximum reach of the human arm and | | stands for absolute value.
In this optimality criterion, the upper and lower bound of link lengths must be given as manufacturing constraints that can be expressed as

$$L_i - L_{i\,max} < 0 \tag{3}$$

$$L_{i\,min} - L_i < 0 \tag{4}$$

where L_i is the link length and $L_{i\,min}, L_{i\,max}$ are the maximum and minimum design lengths.

3.2 LIGHTWEIGHT DESIGN

The robot must have a lightweight structure since it is going to interact with human beings. A reasonable and computationally efficient expression of the lightweight design criterion can be given by

$$f_2(X) = \left|1 - M_T / M_d\right| \tag{5}$$

where M_T is the overall mass of a robot and M_d is the desired overall mass of the same robot, where

$$M_T = \sum_{i=1}^{n_{link}} M_i + \sum_{j=1}^{n_{act}} M_j + \sum_{k=1}^{n_{comp}} M_k \tag{6}$$

The mass of the links can be easily related with their volumes and density. Thus, the minimization process given by Eq.(5) will try to reduce link lengths and cross section sizes. Nevertheless, a constraint should be added in the form

$$A_i - A_{i\,min} < 0 \tag{7}$$

where A_i is the cross section area of i-th link and A_{imin} is the minimum acceptable cross section area for i-th link. This value depends on manufacturing constraints.

3.3 ACCURACY AND STIFFNESS

The previous optimal criteria tries to reduce the weight of motors and links. Nevertheless, if links are very thin and lightweight they cannot be considered rigid as in the case of industrial robots and their accuracy will be strongly affected by compliant displacements. In order to optimize the stiffness behavior Eq.(8) is presented.

$$f_i(X) = 1 - \left(\left|\Delta S_{max}\right| / \left|\Delta S_d\right|\right) \quad (i = 3,4,5 \text{ for } \Delta x_{max}, \Delta y_{max}, \Delta z_{max}) \tag{8}$$

where ΔS_{max} and ΔS_d are the maximum and design compliant displacements along X, Y, and Z-axes, respectively. The stiffness properties can be defined through a matrix called 'Cartesian stiffness matrix K'. This matrix gives the relation between the compliant displacements vector $\Delta S_{max}[\Delta X, \Delta Y, \Delta Z]^T$ occurring at the system when a static wrench $W=[F_x,F_y,F_z]^T$ acts upon it, and W itself in the form

$$\Delta S = K^{-1}\,\Delta W \tag{9}$$

It is worth noting that Eq.(9) can be obtained if and only if

$$\det K \neq 0 \tag{10}$$

Therefore, Eq.(10) should be assumed as additional constraint equation in order to avoid singularities on the stiffness matrix K.

3.4 PATH PLANNING

Path planning regarded as the way to obtain the constrained trajectory given only the initial and final points [12]. Path planning optimization will be carried out by considering the optimal traveling time, which takes the robot, to perform a trajectory defined by two points in Cartesian coordinates. Therefore, one can write

$$f_6(\mathbf{X}) = 1 - \left(t_{path} / t_{straight} \right) \tag{11}$$

where t_{path} is the time that takes the robot to accomplish the trajectory and $t_{straight}$ is the time that would take if the robot could plan the trajectory as a straight line. To obtain this objective function, the position of the motors will be considered that evolve in time as a polynomial as

$$q_i(t) = \sum_{j=0}^{n-2} a_j t^j \tag{12}$$

where n is the number of conditions; a_j are constants, which are calculated based on initial and goal conditions.
An additional constraint equations can be added to Eq.(11) in order to guarantee that trajectory belongs to the workspace:

$$0 \le q_i \le 2\pi \tag{13}$$

On the other hand, limiting restriction in the movement actuators must be fulfilled as related to velocity, acceleration and jerk that can be expressed as

$$\dot{q}_i \le \omega_{i\,max} \quad \ddot{q}_i \le \alpha_{i\,max} \quad \dddot{q}_i \le \gamma_{i\,max} \tag{14}$$

with prescribed maximum values of joint velocities ω_{max}, accelerations α_{max}, and jerks γ_{max},, respectively.

3.5 INERTIA AND SAFETY

Risks derived from a possible collision between robots and humans should be reduced at the design stage yet. The reduction of collision effects has been widely exploited, in particular, in crash test which results are used for assessing car safety by means of several criteria, [14]. In order to obtain an equation useful for the optimization process, the basic case of a single rigid joint moving at uniform velocity v before impact is used, in this paper, to calculate the Head Injury Criterion (HIC) [13],

$$HIC = 2\left(2/\pi\right)^{3/2} \left(K_{cov}/M_{oper}\right)^{3/4} \left(M_T/M_T + M_{oper}\right)^{7/4} v^{5/2} \tag{15}$$

where M_T is the total effective mass, M_{oper} is the impacted operator mass and K_{cov} is the lumped stiffness of a compliant cover on the arm. So, an objective function related to the safety issue ca be defined as,

$$f_7(X) = 1 - \left(HIC / HIC_{sd} \right) \tag{16}$$

where HIC is computed with Eq.(15) by replacing the velocity v with the end-effector standard velocity value that is computed based on the rotational motor velocities; the HIC_{sd} can be chosen as a design value of the head injury criterion. Experimental tests demonstrate that, for a maximum velocity in the end-effector of 2m/s the HIC value must be less than 100. So, the following constraint function has been implemented

$$HIC < 100 \tag{17}$$

4 A CASE OF STUDY

The system used to test the optimization formulation is a two-2R robotic arm modules called SIDEMAR (see Fig. 1). The robot presents four rotational and orthogonal joints as shown in Fig.2.

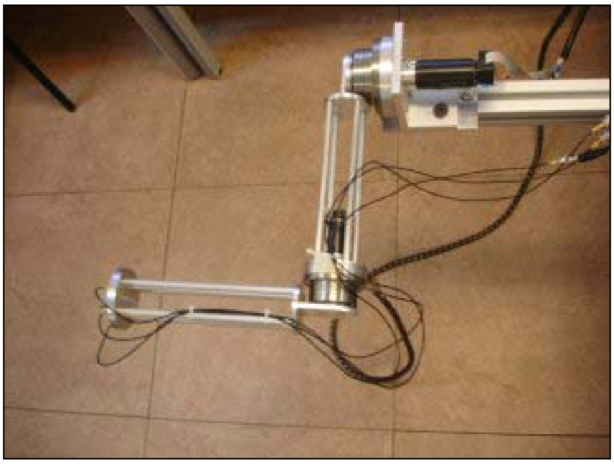

Figure 1 2D SIDEMAR module

As a first approximation, bar lengths L_i and equivalent areas A_i (i=1, ..., 4) are chosen as parameters to optimize.
Based on the above-mentioned assumption the objective functions f_i can be expressed for SIDEMAR by substituting in previous equations.

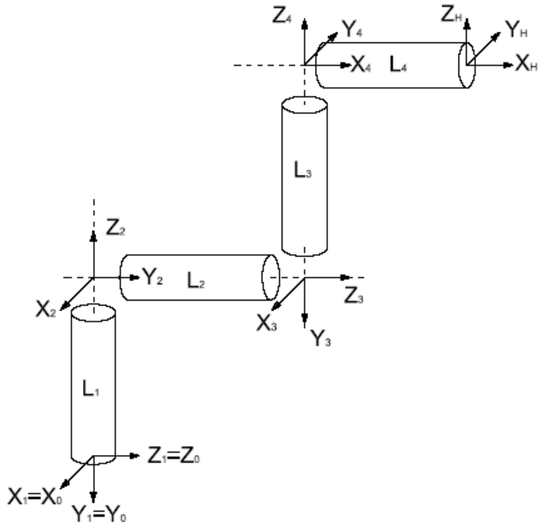

Figure 2 4R service robot

The stiffness matrix for this system is calculated through the lumped parameter model in Fig.3 to give the complete stiffness matrix through equation (18)

$$K = J_M K_\theta J_M^T \tag{18}$$

where

$$J_M = \begin{bmatrix} \frac{\partial X_H}{\partial \theta_1} & \frac{\partial X_H}{\partial L_1} & \frac{\partial X_H}{\partial \theta_2} & \frac{\partial X_H}{\partial L_2} & \frac{\partial X_H}{\partial \theta_3} & \frac{\partial X_H}{\partial L_3} & \frac{\partial X_H}{\partial \theta_4} & \frac{\partial X_H}{\partial L_4} \\ \frac{\partial Y_H}{\partial \theta_1} & \frac{\partial Y_H}{\partial L_1} & \frac{\partial Y_H}{\partial \theta_2} & \frac{\partial Y_H}{\partial L_2} & \frac{\partial Y_H}{\partial \theta_3} & \frac{\partial Y_H}{\partial L_3} & \frac{\partial Y_H}{\partial \theta_4} & \frac{\partial Y_H}{\partial L_4} \\ \frac{\partial Z_H}{\partial \theta_1} & \frac{\partial Z_H}{\partial L_1} & \frac{\partial Z_H}{\partial \theta_2} & \frac{\partial Z_H}{\partial L_2} & \frac{\partial Z_H}{\partial \theta_3} & \frac{\partial Z_H}{\partial L_3} & \frac{\partial Z_H}{\partial \theta_4} & \frac{\partial Z_H}{\partial L_4} \end{bmatrix} \tag{19}$$

and

$$K_\theta = \begin{bmatrix} k_{T1} & 0 & 0 & 0 & 0 & 0 & 0 & 0 \\ 0 & k_1 & 0 & 0 & 0 & 0 & 0 & 0 \\ 0 & 0 & k_{T2} & 0 & 0 & 0 & 0 & 0 \\ 0 & 0 & 0 & k_{T2} & 0 & 0 & 0 & 0 \\ 0 & 0 & 0 & 0 & k_{T3} & 0 & 0 & 0 \\ 0 & 0 & 0 & 0 & 0 & k_3 & 0 & 0 \\ 0 & 0 & 0 & 0 & 0 & 0 & k_{T4} & 0 \\ 0 & 0 & 0 & 0 & 0 & 0 & 0 & k_4 \end{bmatrix} \tag{20}$$

The k_i lumped stiffness parameters can be computed as $E_i A_i / L_i$; k_{Ti} lumped stiffness parameters can be computed as the superposition of compliance of i-th motor that is given by $k_{\text{motor i}}^{-1}$ and bending compliance of beams about Z_i-axes that is given by $k_{\text{beam i}}^{-1}$ as proposed by [12]. Thus, one can write

$$k_{Ti}^{-1} = k_{\text{beam i}}^{-1} + k_{\text{motor i}}^{-1} \tag{21}$$

Therefore, the objective functions f_3, f_4, and f_5, in Eq.(8) can be computed through calculus of the maximum compliant displacement within a workspace when a wrench is applied on point H whose x, y, z components are equal to 10N.

Concerning with path planning optimisation, the conditions in Eqs. (12) to (14) are calculated for each joint.

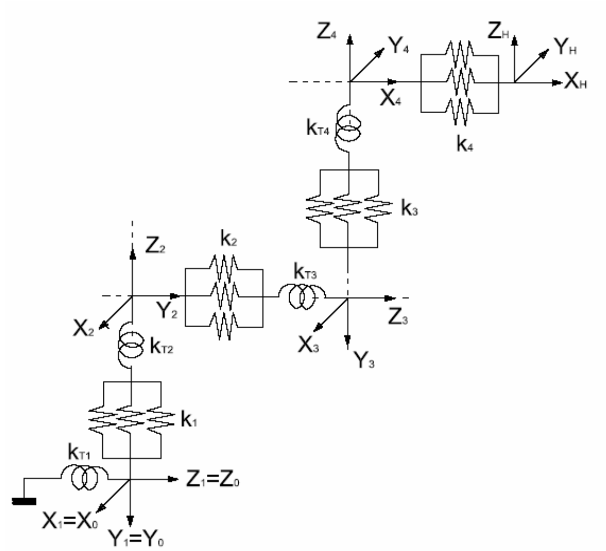

Figure 3 A stiffness model for 4R system in Fig.1

Moreover, the objective function f_6 in Eq.(11) has been computed by assuming $t_{straight}$ as equal to $1{,}3.10^{-2}$ sec.

HIC parameter for safety characteristics of SIDEMAR system can be computed as referring to the Eq.(15). Parameters have been considered as standard values [11] and K_{cov} is calculated for the last link considering Fig.(2). Eq.(19) presents the calculus.

$$f_1(X) = \left|1 - \left(R_{robot} / R_{human}\right)\right| \tag{22}$$

$$K_{cov} = \max(K_x, K_y, K_z) \tag{22}$$

where Kx, Ky and Kz are the diagonal elements of the last link lumped beam stiffness matrix without considering the actuator lumped parameter.

Results of the proposed design procedure as applied to 4R SIDEMAR system are reported in Figs. 4, 5, 6 and Table I and II. In particular, the evolution of the objective functions, when the design parameters are modified in order to achieve the optimal values, is reported in Fig. 4, the numerical procedure takes less than 100 iterations to converge to the optimum values, which are reported in Table I. Besides, evolution of design parameters and constraints are shown in Figs. 5 and 6. Design characteristics for the optimum solution are reported in Table II.

Numerical results show the optimal minimization of the objective functions (Fig. 4), by reducing the geometry of the third link, reducing the areas and incrementing the length of the first link, which increases the workspace.

Table I - Design parameters for 4R-SIDEMAR robot

	L_1 (mm)	L_2 (mm)	L_3 (mm)	L_4 (mm)	A_1 (cm^2)	A_2 (cm^2)	A_3 (cm^2)	A_4 (cm^2)
Initial Guess	221	202	221	202	50.27	12.57	50.27	12.57
Optim Value	500	100	220	227	0.71	0.24	0.14	8.42

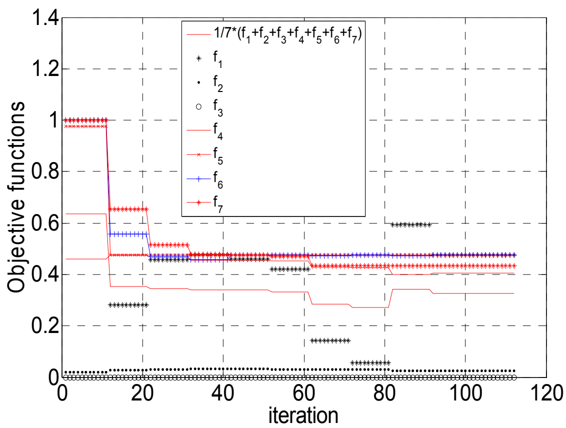

Figure 4 Evolution of the optimization functions versus number of iterations for the 4R-SIDEMAR system optimal design

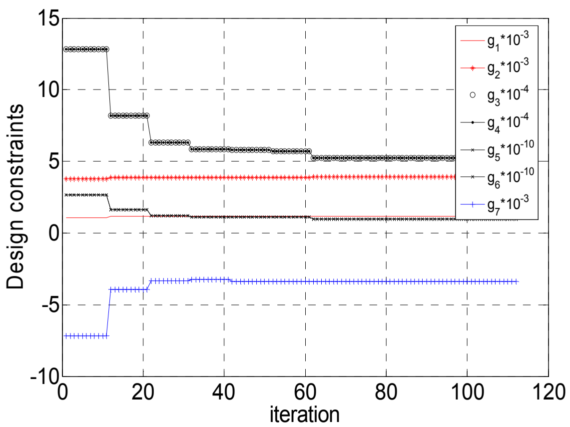

Figure 5 Evolution of design constraints versus number of iterations for the example of 4R-SIDEMAR optimal design

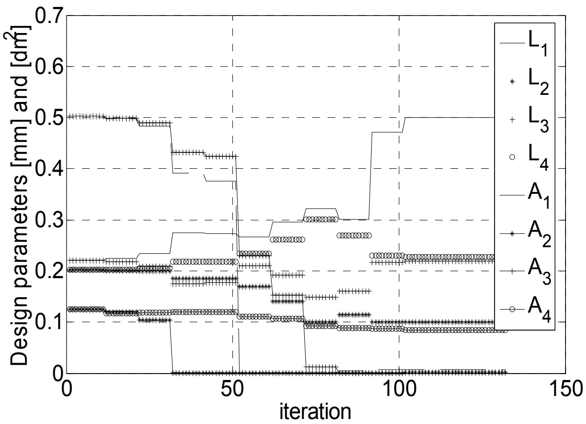

Figure 6 Evolution of design parameters versus number of iterations for the example of 4R-SIDEMAR optimal design

Table II - Design characteristics of optimum solution

	R_{Robot} (mm)	M_T (Kg)	ΔX_{Max} (mm)	ΔY_{Max} (mm)	ΔZ_{Max} (mm)	t_{path} (sec)	HIC
Initial Guess	599.1	11.97	0.189	0.398	0.190	0.91	7246
Optim. Value	739.2	5.48	0.093	0.368	0.094	0.40	12.67

5 CONCLUSIONS

In this manuscript, main optimal design criteria for service robots have been addressed. Then, these design criteria have been expressed in a mathematical form as objective functions to be minimized in a multi-objective optimisation algorithm. The proposed procedure has been applied to a 4R SIDEMAR two-module. Numerical results of the optimisation process show the soundness of the proposed design procedure.

6 AKNOWLEDGEMENTS

The financial support of Spanish government is gratefully acknowledged for the construction of a SIDEMAR prototype through the Project MCYT DPI2003-084790-C02-01.

REFERENCES

[1] Castejon C., Giménez A., Garcia-Prada, J.C., and Balaguer C., Integrated system of assisted mechatronic design for oriented computer to automatic optimising of structure of service robots. *8th International Conference on Climbing and Walking Robots Clawar'05*, London, 2005.

[2] Balaguer C., Giménez A., and Jardón A., The MATS robot: Service Climbing Robot for Personal Assistance. *IEEE Robotics & Automation Magazine*, Vol. 13, No. 1, pp. 51-58, 2006.

[3] Meng Q., and Lee M.H., Design Issues for Assistive Robotics for the Elderly. *Advanced Engineering Informatics*, Vol. 20, No. 2, pp. 171-186, 2006.

[4] Gosselin C.M., The optimum design of robotic manipulators using dexterity indices. *Robotics and autonomous systems*, Vol. 9, pp. 213–226, 1992.

[5] Blanco D., Castejon C., Kadhim S., and Moreno L., Predesign of an Anthropomorphic Lightweight Manipulator. *8th International Conference on Climbing and Walking Robots Clawar'05*, London, 2005.

[6] Gao F., Liu X.J., and Jin S.L., Optimum design of 3-dof spherical parallel manipulators with respect to the conditioning and stiffness indices. *Mechanism and Machine Theory*, Vol. 35, No. 9, 2000.

[7] Carbone G., Lim H.O., Takanishi A., and Ceccarelli M., Optimum Design of a New Humanoid Leg by Using Stiffness Analysis. *12th International Workshop on Robotics in Alpe-Andria-Danube Region RAAD 2003*, Cassino, 2003.

[8] Zinn M., Khatib O., Roth B., and Salisbury J.K., Playing it safe. *IEEE Robotics and Automation Magazine*, June 2004.

[9] Saramago S.F.P., and Ceccarelli M., Effect of Numerical Parameters on a Path Planning of Robots Taking into account Actuating Energy. *Mechanism and Machine Theory*, 2004, Vol. 39, No. 3, pp. 247-270.

[10] Ceccarelli M., Carbone G., and Ottaviano E., Multi Criteria Optimum Design of Manipulators. *Bullettin of the Polish Academy of Sciences, Technical Sciences*, Vol. 53, No. 1, pp. 9-18, 2005.

[11] Castejón C., Carbone G., García-Prada J.C., and Ceccarelli M., A multi-objective optimization for designing service robots. *12th IFToMM World congress*, Besançon, 2007.

[12] Ceccarelli M., *Fundamentals of Mechanics of Robotic Manipulation*, Kluwer, Dordrecht, 2004.

[13] Snyder, R.G., State-of-the-Art – Human Impact Tolerances. SAE 700398, *International Automobile Safety Conference Compendium*, 1970.

[14] Bicchi A., and Tonietti G., Fast and soft-arm tactics. *IEEE Robotics & Automation Magazine*, June 2004.

ISSN 1590-8844
International Journal of Mechanics and Control, Vol. 08, No. 02, 2007

OPTIMIZATION OF RELATIVE ORBIT TRANSFER WITH LOW THRUST PROPULSION

Mauro Massari

Department of Aerospace Engineering, Politecnico di Milano

ABSTRACT

In this paper the problem of optimizing a low thrust trajectory for transfer between relative orbits is addressed. The problem can be stated as the solution of an optimal control problem in which an objective function related to controls is minimized satisfying a series of constraints on the trajectory which are both differential and algebraic. The problem has been faced transcribing the differential constraints with a parallel multiple shooting method into a NLP problem which has been solved with an interior point method. The method has been applied to the design of relative orbit transfer which can be considered as the first step in designing reconfiguration manoeuvres for spacecrafts flying in formation.

Keywords: Optimization, Transfer, Relative Orbit, Low Thrust

1 INTRODUCTION

In the field of space trajectory design the optimization of the resources is vital. In an environment where the refuelling is not possible and it is necessary to reduce the overall weight of the satellites, the amount of propellant needed can highly influence the operative life of the satellites. For this reason low thrust propulsion is becoming quite popular as it is characterized by high value of specific impulse, which allows to reduce the amount of propellant needed for a mission.
The relative dynamics used for the description of formation flying and rendezvous or docking is governed by differential gravitational attractions which are low with respect to full gravitational acceleration in case of limited relative states. In this case low thrust propulsion is an effective way of controlling the spacecraft motion in a relative reference frame.
Expressing the dynamics of satellites on orbits in a relative reference frame, it is possible to identify the peculiar conditions which allow a bounded periodic motion in the relative reference frame.

Contact author: Mauro Massari

Politecnico di Milano
Department of Aerospace Engineering
Via La Masa 34, 20156, Milano, Italy
E-mail: massari@aero.polimi.it

This kind of motion will be referred as relative orbit, as the relative motion of a spacecraft with respect to a reference point which is orbiting on a circular orbit is represented by an ellipse. The concept of relative orbits can be used to design formation flying missions which require that the slave members remain in a limited region around the master.
In this work the solution of the optimal control problem for the design of optimal low thrust relative orbit transfer will be shown. The use of continuous thrust propulsion will lead to the necessity to find the optimal continuous control law which should be applied to obtain the optimal trajectory. This problem can be stated as the solution of an optimal control problem in which an objective function which is usually related to controls is minimized, satisfying a series of constraints on the trajectory which are both differential and algebraic.
The numerical solution of the optimal control problem which is at the base of the trajectory optimization is usually based on the idea of discretizing the continuous problem using a transcription technique into a discrete problem which can be faced with the algorithms developed for parameter optimization which are usually based on the Newton method [1]. Using this approach, the differential constraints representing the dynamics are translated in non linear constraints on discrete variables, while continuous terms of the objective function are usually computed exploiting numerical quadrature methods. Following this paradigm, the problem is conceptually divided in two parts: a transcription of the differential optimal control problem in

a parameters optimization problem and the solution of the associated discrete problem.
For what concerns the transcription of the optimal control problem in a Non Linear Programming (NLP) problem, a direct transcription method based on parallel multiple shooting technique has been developed. It allows to exploit the advantages of parallel computing reducing at the same time the dimension of the resulting parameters optimization problem.
The parameters optimization deriving from the transcription of the optimal control problem with the multiple shooting technique is characterized both by nonlinear constraints and nonlinear objective function, leading to a NLP problem. The solution of this NLP problem is usually based on Sequential Quadratic Programming (SQP) methods associated with active set approach for active inequalities identification [2]. In space application this approach has been successfully applied by Betts and Huffman [2] and by Fahroo and Ross [3].
In the case of problems with a high number of inequality constraints, this approach can be highly inefficient, so the method developed for the solution of this problem is based on an interior point approach, which allows to consider inequality constraints directly in the objective function, reducing the overhead due to active constraints identification [4]. The method developed considers the optimization of a series of equality constrained subproblems in which the objective function is adjoined with a weighted barrier term that allow to implicitly satisfy the inequality constraints. Progressively reducing the weight in the barrier term, the method leads the solution toward the minimum of the original problem.
The algorithm developed has been applied to the problem of relative orbit transfer with low thrust propulsion in the case of a general Earth orbit. In particular, transfers which allow to initialize relative orbit and to change relative orbit dimension maintaining the geometry have been considered, in case of both circular and eccentric reference orbit. In the following section an overview of the relative dynamics models used in the optimization are reported, together with the derivation of the conditions that allow relative orbit motion. Afterwards the transcription method developed will be presented, followed by the description of the approach used for the solution of the NLP problem. Finally the results of a series of test cases considered will be shown.

2 RELATIVE ORBITS

One of the feature desired for spacecrafts flying in formation is that they orbit remaining in the neighbourhood of the other satellites or, in other words, it is desirable that all the members of the formation remain in the vicinity of the origin of the relative reference frame. From orbit theory it is clear that in case of circular orbit this cannot be achieved if the satellites orbit at different altitude, as they will have different orbital periods which make them drift apart [5]. The desired feature can be clearly achieved using propulsion to counteract the drifting effect of the difference in velocity but this will not be a clever choice. Looking deeply at the reason which cause that drift it is clear that the satellites which drift apart are characterized by different energy level with respect to the reference orbit, so imposing that the energy associated with their motion is equal to that associated with the reference orbit it is possible to obtain a limited bounded relative motion. In particular in the case of ideal two body problem the condition that must be imposed is that the semi-major axis are equal:

$$a_s = a_0 \tag{1}$$

This is the basic condition which must be satisfied in order to obtain a bounded limited motion which does not require any control. This condition is expressed in an absolute reference system and does not allow to clearly identify the relative motion. In order to do that it is necessary to face the problem from a different point of view, describing the dynamics in a relative reference frame.

2.1 RELATIVE DYNAMICS

In order to study and describe the dynamics which governs the relative motion of a chaser satellite with respect to a target one it is possible to write the well known differential equations, which govern the motion of satellites on orbit, for each satellite and compute the relative distance between them considering the solution of those equations [6].
This could be a good choice for the computation of relative distance between satellites which are part of a constellation, because the relative distance is of the same magnitude of orbit semi major axis. On the other hand, in the case of docking manoeuvres or formation flying, where relative distance could not be compared with orbit semi major axis, it is better to use dynamical equations written in a relative reference frame. The origin of the relative reference frame can be chosen to be coincident with the target or with a member of the formation, but usually it is considered as a special orbiting point mass.
The development of such relative dynamics models have been carried out for the analysis and design of control systems, which could control relative distance in rendezvous and docking manoeuvres or which could maintain a fixed distance between satellites composing in-track formations. For this reason almost all the models developed are based on linearized equations which can be used for the controller design. Those linear models lead to a reduced accuracy in conditions far away from the cases considered for the linearization. However those equations represent a suitable instrument for the conceptual study of the relative orbital motion, as they have analytical solutions which allow to exploit general features of the relative dynamics.

2.1.1 Clohessy-Wiltshire Equations

The first model of relative dynamics was developed for the simulation of rendezvous and docking operation of the Apollo spacecraft and has retained the name of the

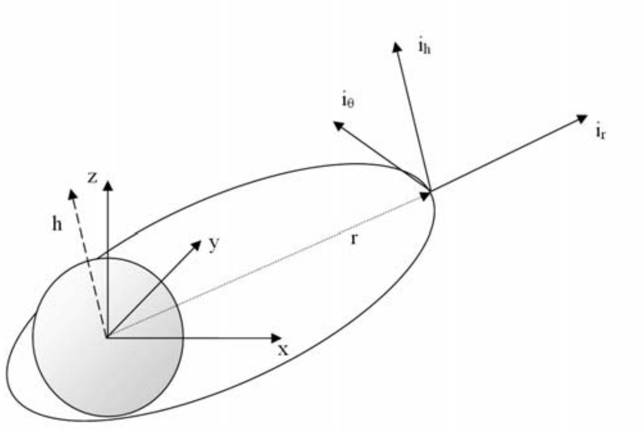

Figure 1 Relative reference frame

researchers which have developed it, the famous Clohessy-Wiltshire relative model [7].

This model is valid for circular unperturbed reference orbit and for relative motion which have small relative states in comparison with the orbit radius, as the equations are derived by a linearization.
The equations are written with respect to a rotating orbital reference frame which has the origin coincident with the position of a point mass orbiting on a circular orbit and subject only to the ideal gravity field of a point mass. The three axes of the reference frame are aligned with the radial, tangential and binormal directions as seen in figure 1.
The unit vectors that represent the reference frame $\hat{i}_x, \hat{i}_y, \hat{i}_z$ can be expressed as:

$$\begin{aligned} \hat{i}_x &= \hat{i}_r = \frac{\mathbf{r_0}}{|r_0|} \\ \hat{i}_y &= \hat{i}_\theta = \hat{i}_r \wedge \hat{i}_h \\ \hat{i}_z &= \hat{i}_h = \frac{\mathbf{h}}{|h|} \end{aligned} \tag{2}$$

where $\mathbf{r_0}$ is the vector representing the position of the origin of the reference frame and **h** is the orbital angular momentum vector.
Considering a spacecraft orbiting near the reference point, its position can be expressed in the absolute reference frame as the sum of relative position vector plus reference frame origin position vector:

$$\mathbf{r_s} = \mathbf{r_0} + \mathbf{r} = (r_0 + x)\hat{i}_r + y\hat{i}_\theta + z\hat{i}_h \tag{3}$$

Equating the satellite acceleration expressed in the relative reference frame with the gravity acceleration it is possible to find the general relative equations of motion which are valid for each unperturbed reference orbit in the case of ideal two body problem:

$$\begin{aligned} &\ddot{x} - 2\dot{\theta}\left(\dot{y} - y\frac{\dot{r}_0}{r_0}\right) - x\dot{\theta}^2 - \frac{\mu}{r_0^2} = -\frac{\mu}{r_s^3}(r_0 + x) \\ &\ddot{y} + 2\dot{\theta}\left(\dot{x} - x\frac{\dot{r}_0}{r_0}\right) - y\dot{\theta}^2 = -\frac{\mu}{r_s^3} y \\ &\ddot{z} = -\frac{\mu}{r_s^3} z \end{aligned} \tag{4}$$

In those equations the only assumption is that both the origin of the relative reference frame and the satellite move under the effect of the gravity field of a point mass, in an ideal Kepler motion.
However, imposing that the relative coordinates are small with respect to the relative reference frame origin position, and that the reference orbit is circular, it is possible to obtain the well known Clohessy-Wiltshire equations:

$$\begin{aligned} &\ddot{x} - 2n\dot{y} - 3n^2 x = 0 \\ &\ddot{y} + 2n\dot{x} = 0 \\ &\ddot{z} + n^2 z = 0 \end{aligned} \tag{5}$$

where $n\hat{i}_h$ is the constant angular velocity of the relative reference orbit.
Those equations represent a valuable instrument for the conceptual study of the relative orbital dynamics, as they have analytical solutions:

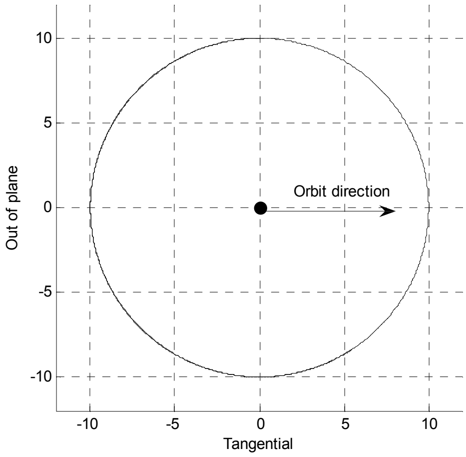

Figure 2 Ground projection of relative orbit in Clohessy-Wiltshire model

$$
\begin{aligned}
x(t) &= \frac{\dot{x}_0}{n}\sin nt - \left(\frac{2\dot{y}_0}{n} + 3x_0\right)\cos nt + \left(\frac{2\dot{y}_0}{n} + 4x_0\right) \\
y(t) &= \frac{2\dot{x}_0}{n}\cos nt + \left(\frac{4\dot{y}_0}{n} + 6x_0\right)\sin nt + \left(y_0 - \frac{2\dot{x}_0}{n}\right) \\
&\quad - \left(3\dot{y}_0 + 6nx_0\right)t \\
z(t) &= z_0 \cos nt + \left(\frac{\dot{z}_0}{n}\right)\sin nt
\end{aligned} \tag{6}
$$

It can be seen that the motion on the out of plane axis **z** is independent from the other two coordinates and represents a typical harmonic oscillation while the other two represent a coupled harmonic motion. The motion along the tangent direction presents a secular term which will grow indefinitely with time, causing the satellite to drift from the origin of the reference frame. However, considering that the coefficient of the secular term depends only on initial conditions, it is possible to derive constraints on initial conditions which grant a bounded relative motion, simply imposing:

$$\dot{y}_0 + 2nx_0 = 0 \tag{7}$$

which constitutes a constraint in the definition of the initial relative velocity along the tangential direction.
With the secular term forced to zero, the solutions describe a bounded relative motion which is an ellipse not centred in the origin of the reference frame. This relative orbit presents a displacement along the **y** axis due to the remaining term in the tangential equation of (6).
Imposing also this remaining term to be null:

$$2\dot{x}_0 - ny_0 = 0 \tag{8}$$

we have a constraint on the velocity along the radial direction. The combination of the two constraints allows to obtain bounded relative orbits centred around the origin of the relative reference frame.
Considering that the ellipse corresponding to the closed relative orbit has an amplitude along **y** axis which is double than that along the **x** axis, but is not dependent on the amplitude on the **z** axis, it is possible to obtain relative orbits which produce ground elliptic projections of different eccentricity simply imposing appropriate values of those amplitudes.
In figure 2 a circular projection on ground (plane $\hat{i}_\theta - \hat{i}_h$) is reported.

2.1.2 Elliptic reference orbits

The Clohessy-Wiltshire equations are based on three assumptions: the use of ideal two body problem dynamics for reference orbit description, circular reference orbit and small relative distance from the origin of the relative reference system compared with the reference orbit radius.
In this section a development which will allow to remove the assumption of circularity of the reference orbit will be presented [8]. As the assumption of two body dynamics remains, it is possible to maintain the equations (4), impose the conditions on small relative motion with respect to orbit semi major axis and transform the time derivative in derivative with respect to the true anomaly with the following relations:

$$
\begin{aligned}
\dot{(\cdot)} &= (\cdot)'\dot{\theta} \\
\ddot{(\cdot)} &= (\cdot)''\dot{\theta}^2 + \dot{\theta}\dot{\theta}'(\cdot)'
\end{aligned} \tag{9}
$$

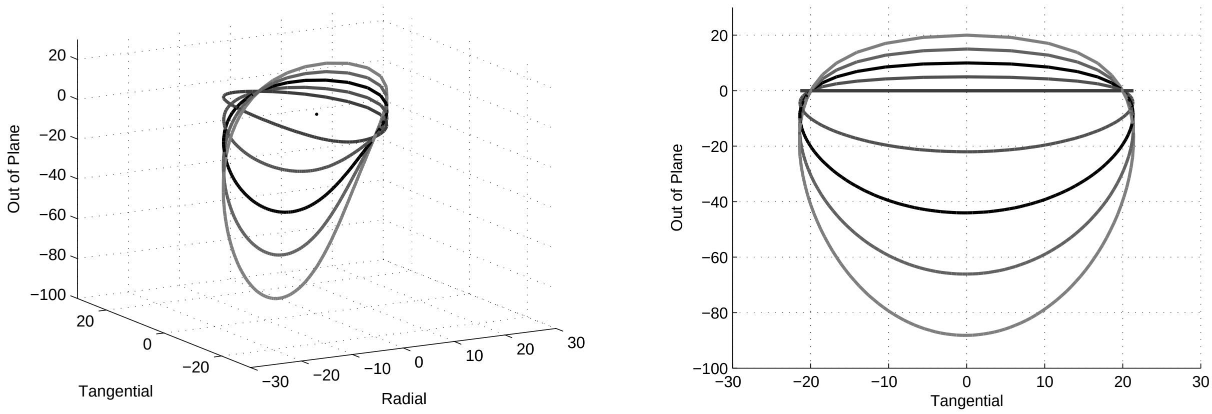

Figure 3 Relative Orbits in linearized model considering eccentricity

It is then possible to write a set of linear time varying (LTV) equations which represent the relative motion for a generic eccentric reference orbit:

$$\begin{bmatrix} x'' \\ y'' \\ z'' \end{bmatrix} = \begin{bmatrix} \frac{2e\sin\theta}{1+e\cos\theta} & 2 & 0 \\ -2 & \frac{2e\sin\theta}{1+e\cos\theta} & 0 \\ 0 & 0 & \frac{2e\sin\theta}{1+e\cos\theta} \end{bmatrix} \begin{bmatrix} x' \\ y' \\ z' \end{bmatrix} + \\ + \begin{bmatrix} \frac{3+e\cos\theta}{1+e\cos\theta} & \frac{-2e\sin\theta}{1+e\cos\theta} & 0 \\ \frac{2e\sin\theta}{1+e\cos\theta} & \frac{e\cos\theta}{1+e\cos\theta} & 0 \\ 0 & 0 & \frac{-1}{1+e\cos\theta} \end{bmatrix} \begin{bmatrix} x \\ y \\ z \end{bmatrix} \tag{10}$$

Also these equations have solutions which are expressed in terms of eccentric anomaly:

$$\begin{aligned} x(\theta) &= \sin\theta\left(d_1 e + 2d_2 e^2 H(\theta)\right) - \cos\theta\left(\frac{d_2 e}{(1+e\cos\theta)^2} + d_3\right) \\ y(\theta) &= \sin\theta\left(\frac{d_3 e}{(1+e\cos\theta)^2} + d_3\right) + \cos\theta\left(d_1 e + 2d_2 e^2 H(\theta)\right) + \\ &\quad + \left(d_1 + \frac{d_4}{(1+e\cos\theta)} + 2d_2 e H(\theta)\right) \\ z(\theta) &= \sin\theta\left(\frac{d_5}{(1+e\cos\theta)}\right) + \cos\theta\left(\frac{d_6}{(1+e\cos\theta)}\right) \end{aligned} \tag{11}$$

where d_1, d_2, d_3, d_4, d_5 and d_6 are integration constants which can be related to initial conditions and:

$$H(\theta) = -(1-e^2)^{\frac{5}{2}}\left(\frac{3eE}{2} - \left(1+e^2\right)\sin E + \frac{e}{2}\sin E\cos E\right) \tag{12}$$

where E is the eccentric anomaly.

Those solutions describe a relative motion in terms of eccentric anomaly instead of time, and looking at the equation it is not clear how to impose conditions that allow bounded periodic motion. In literature this condition has been obtained imposing continuity condition after a period, producing relative orbits which are limited to small relative distances.

Considering that the motion on axis **z** is purely harmonic and is decoupled from the other two coordinates, it is possible to limit the imposition of continuity constraints to the **x** and **y** coordinates:

$$\begin{aligned} x(0) &= x(2\pi) \\ x'(0) &= x'(2\pi) \\ y(0) &= y(2\pi) \\ y'(0) &= y'(2\pi) \end{aligned} \tag{13}$$

These produce a relation which binds **y'(0)** to **x(0)** and grants that the motion is bounded. The relative orbit obtained is not symmetric with respect to the radial direction, and in order to impose the symmetry it is necessary to impose a second condition which will constraint **x'(0)** to be null.
Imposing those conditions it is possible to obtain relative orbits which have a symmetric projection on ground, like those shown in figure 3. Relative orbits shown have been obtained imposing **z' (0)** to be null and different values of **z(0)**.

2.2 PROPULSION MODEL

In the model of the dynamics described above it has been assumed that the mass of the spacecraft is constant. This assumption is not a problem when studying the simple dynamics, as the mass variation does not influence gravitational forces acting on the satellite, so it does not influence the dynamic condition of the spacecraft, assuring

that the periodicity condition, once established, could not be altered by the decrease of mass due to manoeuvring.
On the other hand it is a rough approximation to consider constant mass in the case of propelled manoeuvres design. In that case it is necessary to model the mass flow involved in propulsion, which produces a decrease of the overall mass of the spacecraft when manoeuvring.
In the case of impulsive manoeuvres which can be modelled as instantaneous discontinuity in velocity, the mass flow can be easily introduced as instantaneous decrease in mass considering engine performances, with the well known rocket equation:

$$\Delta m = m_0 \left[1 - e^{-\left(\frac{\Delta V}{I_{sp} g_0} \right)} \right] \tag{14}$$

where $\mathbf{m_0}$ is the mass before the manoeuvres, $\mathbf{I_{sp}}$ is the specific impulse of the engine and $\mathbf{g_0}$ is the Earth gravity constant at sea level.
In the case of low thrust propulsion it is not possible to approximate the manoeuvres as impulsive, but they must be considered as continuous application of control actions. In that case it is not possible to use the rocket equation any more, but it is necessary to model the mass flow and adjoin the differential equation to the model of the dynamics. In this way, mass can be considered as a new state which is coupled to the other equations trough the control actions. The relation describing the mass flow can be expressed as:

$$\dot{m} = -\frac{|\mathbf{u}|}{I_{sp} g_0} \tag{15}$$

where $\mathbf{u}$ is the control vector expressed in terms of thrust.

3 OPTIMIZATION

Relative orbit transfer with low thrust propulsion can be approached as a trajectory optimization in which the satellite has to move from a relative orbit to the desired final position on the target orbit. From the point of view of a single satellite this can be regarded as an optimal control problem that can be stated as:

Find the control law which minimizes a certain objective function being subject both to differential and algebraic constraints.

In space applications, the control law is usually related to thrust level in low thrust propulsion or to engine firings if chemical propulsion is used, while the objective function is usually related to the propellant mass or to a quadratic measure of the control action but also manoeuvring time can be used as optimization target. The algebraic constraints are related to position and velocity to guarantee the insertion on a particular orbit while differential constraints are the equations which govern the phenomenon and which relate control actions to trajectory variations.

This problem has been faced and successfully solved for different space applications such as interplanetary transfer with low thrust or launcher trajectory definition [9] [2].
An optimal control problem is seldom solved analytically because the differential equations in states and costates are usually hard to solve for real life problems. The numerical solution of the problem can be performed with different techniques, which can be divided in two main categories, indirect methods and direct methods [10]. The distinction is on the way the problem is faced, as indirect methods solve numerically the Euler-Lagrange Equations derived by the imposition of optimality condition, while direct methods try to minimize the objective function at each step without using those equations. At the base of both classes of methods there is the application of a Newton method for the solution of a system of non linear equations as both translate the optimal control problem solution into a parameters optimization, which is usually characterized by non linear objective function and nonlinear constraints, and is commonly addressed as a Non Linear Programming (NLP) problem.

Indirect methods have been largely used for the solution of optimal control problems when computing performances were not available at low cost, because the number of parameters of the resulting parameters optimization remain low. Today the trend is to use direct methods that generally require more computational power but can be more easily formulated to solve different kind of problems.

The idea behind direct methods is to transcribe the differential constraints into a set of algebraic constraints on a series of parameters which derive from the discretization of the states and controls in time. This can be done with two classes of methods, shooting methods and collocation methods. In this work a direct transcription based on a shooting method has been implemented, while the solution of the resulting NLP problem is performed with an interior point method described below.

3.1 TRANSCRIPTION

Relative orbits have limited extension so the control actions needed for the transfer between two different orbits are usually very low. As it has been said in the introduction this kind of transfer are the base manoeuvres which can be used to implement formation flying reconfiguration manoeuvres, so, even if the control actions are low, they will be required more often then on a single satellite. This aspect enforces the use of low thrust and high impulse propulsion like solar electrical propulsion, imposing to the transcription algorithm to take into account general control laws which are functions of time.

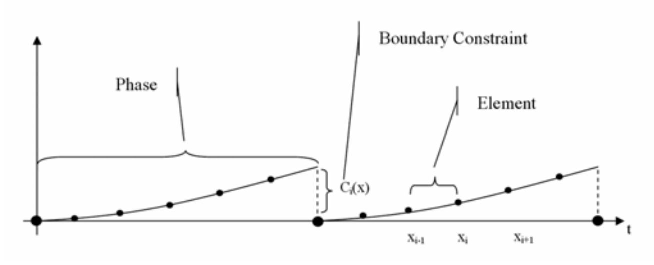

Figure 4 Multiple Shooting Method

Among direct transcription methods, collocation methods produce a NLP parameters optimization problem which is generally composed by a great number of parameters and constraints. Usually this is not a problem as the sparsity of the produced matrixes allows an efficient solution of the problem using sparse solvers. However, in the case of formation flight, the number of parameters will be too high, and the existence of relative distance constraints used to avoid collisions reduce the sparsity of the matrixes, reducing the benefits that a sparse solver will introduce.
Shooting methods, on the other hand, produce a dense problem, but with decisively less parameters, and this will allow to increase the performance of the solution of the resulting NLP parameters optimization problem. If from one side shooting methods seem to be more suitable in terms of computing resources, from the other it has to be said that the process of constraints evaluation will be much more costly in shooting methods than in collocation methods. This is due to the fact that shooting methods require the numerical solution of initial value problems for the computation of the constraints.

The problem of computing resources can be easily solved considering the possibility to use parallel computation techniques which allow to take advantage of multi-processor workstations or cluster of computers which are rapidly becoming attractive in terms of costs and resources. In order to exploit those computing systems it is necessary to detect a possible parallel structure of the algorithm which will allow the execution of different parts of it concurrently. In the case of collocation and pseudo spectral methods, the most resource consuming part is the solution of the NLP problem. It is not easy to find a parallel structure in the solution of that problem, as the Newton method is inherently sequential. In the case of shooting methods, and in particular multiple shooting methods, the parallelism of the transcription is quite clear, as each numerical integration can be carried out in parallel. In this way the part which will be more resource consuming can take advantage of parallel architecture and an increase in performance can be easily achieved [11].

For these reasons a parallel multiple shooting method has been designed to transcribe the optimal control problem resulting from the trajectory optimization of relative orbit transfer.

3.1.1 Multiple Shooting

Multiple shooting methods are based on the idea of splitting the time domain in small intervals, and considers the states at the initial time of those intervals as the parameters of the transcription adjoined by a set of control parameters which are defined along each time interval. In order to grant the satisfaction of differential constraints over the entire time domain, it is necessary to impose continuity constraints between time intervals.

The time domain is subdivided in **N** phases, which are on their turn subdivided in **M** elements, producing the following list of time nodes:

$$\Delta t = \left[t_1^1, t_2^1, \ldots, t_m^1, t_1^2, t_2^2, \ldots, t_1^n, \ldots, t_m^n\right] \tag{16}$$

where $\mathbf{t_m^n}$ represent the $\mathbf{m^{th}}$ time node of the $\mathbf{n^{th}}$ phase. Figure 4 shows this subdivision.

The continuity constraints are expressed only between elements and can be represented as:

$$d_i^n = x_{i,f}^n - x_{i,0}^{n+1} = 0 \quad n \in \left[1, Num\, phases - 1\right] \tag{17}$$

where the index **i** represent the different states, the indexes **f** and **0** indicate the final and initial nodes of an element, while the index **m** represent the element number.

The constraints $\mathbf{C_i}$ between phases can be imposed as continuity constraints adjoined to eventual algebraic constraints derived by the original control problem, or, if no particular constraint is defined, can be left unconstrained in order to allow the introduction of discontinuities in some states, useful for the introduction of impulsive manoeuvres or for the simulation of eventual mass separations.

The original optimal control problem, which can be stated as:

$$\min_{u \in C^0} J[x(t), u(t), t] = \varphi[x(t_f), t_f] + \int_{t_0}^{t_f} L[x(t), u(t), t] dt \tag{18}$$

subject to the differential constraints:

$$\dot{x} = f[x(t), u(t), t] \tag{19}$$

and to the algebraic constraints:

$$b[x(t), u(t), t] \geq 0 \tag{20}$$

is transcribed using the multiple shooting method in the following NLP parameters optimization problem:

$$\min_{s \in R^n} J = \varphi(x_f, t_f) + \sum_{j=0}^{n} \sum_{k=0}^{m} \sum_{i=0}^{p} w_i L[x_i, u_i, t_i]_k^j \tag{21}$$

subject to the continuity constraints:

$$d_i[x_m, u_m, t_m] = 0 \quad i = [0 \cdots n] \tag{22}$$

and to the boundary constraints:

$$c_i[x_n, t_n] \geq 0 \quad i = [0 \cdots m] \tag{23}$$

where the objective function is computed summing the numerical quadrature terms on each element in each phase.

Usually, in multiple shooting application, the control law is imposed as a predefined function of a small number of parameters such as:

$$u(t) = p_1 + p_2 t \tag{24}$$

In this work it has been decided to approximate the control function with Lagrange polynomials. In this way the control law is introduced in the optimization though a series of parameters which control the polynomials and allows the definition of a general function. The order of the polynomials is not fixed and can be used to increase the degree of freedom of the optimization problem increasing the convergence ability. The control is approximated on each element through the following parameters:

$$U_m = \left[u_1^m, u_2^m, \ldots, u_p^m\right] \tag{25}$$

which control the Lagrange polynomial:

$$U_m(t) = \sum_{j=1}^{m} P_j(t) \tag{26}$$

where:

$$P_j(t) = u_j \prod_{\substack{k=1 \\ k \neq j}}^{m} \frac{x - x_k}{x_j - x_k} \tag{27}$$

The solution of the initial value problem along each element is carried out with a numerical integration rule. In literature different rules have been proposed, both simple and fast rules like Euler methods and complicate variable step integration rules. In this work it has been decided to avoid the use of variable step integration rules as they could bring to numerical problems in the parameters optimization solution. Variable step methods are usually more accurate than fixed step methods and are able to automatically adapt the grid to achieve the desired accuracy, but introduce inconsistency in the way in which the constraints are computed. This is due to the fact that computing the Jacobian of the constraints with finite differences, the initial conditions are slightly modified to obtain gradient information, and the variable step integration rule modifies the grid to obtain the same accuracy in the integration, producing increments which are no more representative of the gradient. This effect is usually addressed as inconsistency in constraints definition and can be easily solved using fixed step integration rules.
The integration rules adopted in this work is the classical Runge-Kutta method of the fourth order, which assures a good compromise between accuracy and performance, allowing to reduce the number of integration steps inside the elements.

3.2 NLP OPTIMIZATION

Once that the optimal control problem is transcribed, it is necessary to choose a suitable method for the solution of the NLP optimization resulting from the particular transcription adopted. The choice of a shooting method for the transcription reduces the overall number of parameters with respect to collocation methods, allowing the transcription in a smaller NLP problem. However, the introduction of path constraints typical of formation flying will produce many algebraic inequality constraints which will be imposed on the elements of the transcription. To handle inequality constraints two different approaches have been developed, active set methods and interior point methods. Active set methods try to identify at each iteration the set of inequality constraints active at the solution, while interior point methods try to adjoin the inequality

constraints to the objective function avoiding the need of active constraints identifications.
The use of an active set method for the identification of the active constraints will suffer performance decrease due to the high number of constraints, so it seems that the best choice for the solution of this kind of problem is the use of interior point methods, which allows to solve the problem related to the identification of active constraints.

3.2.1 Interior Point Method

Interior point methods are based on the idea that the general inequality constrained optimization problem which is stated by:

$$\min_{x \in R} F(x) \tag{28}$$

subject to:

$$c(x,u) \geq 0 \tag{29}$$

and that leads to the following optimality conditions, that must be satisfied at the solution:

$$\begin{aligned} &c(\bar{x}) \geq 0 && (\mathit{feasibility}) \\ &g(\bar{x}) = J(\bar{x})^T \lambda && (\mathit{stationarity}) \\ &\lambda \geq 0 && (\mathit{nonnegativity\ of\ the\ multipliers}) \\ &c(\bar{x})\lambda = 0 && (\mathit{complementarity}) \end{aligned} \tag{30}$$

can be solved as a series of unconstrained sub problems in which the objective function is augmented by an appropriate term depending on the constraints. The states **x** are addressed as primal variables, while the costates λ are the dual variables, as this is the usual naming in linear programming community, where interior point methods have been extensively used.
The more common modification of the objective function is the well known logarithmic barrier function:

$$B(x) = F(x) - \mu \sum_{i=1}^{m} \ln c_i(x) \tag{31}$$

which allows to solve a series of unconstrained problems which stay well inside the feasible region, as the logarithmic term grows to infinity approaching the constraints.

The series of unconstrained problems is generated reducing the barrier parameter μ which reduces the influence of logarithmic barrier term, allowing to the unconstrained problems to reach the real solution of the constrained problem following what is called an interior path.

In literature there are essentially two categories of interior point methods which are based on the same idea of solving a sequence of problems which depend on a barrier parameter, but with a different approach: primal-dual methods and barrier methods.
Primal-dual methods are based on the idea of considering primal variables (states) and dual variables (multipliers) as independent and solve the problem composed by the stationarity conditions and by the complementarity conditions [12]. The barrier approach is then introduced solving a series of problems where the barrier parameter is used to perturb the complementarity conditions.

Barrier methods are based on the original idea of modifying the objective function with the barrier term associated with inequalities and to solve a series of equality constrained problem with a decreasing barrier parameter. This kind of methods allows the use of classical SQP methods for the solution of intermediate problems, and are particularly indicated when the number of inequalities is very high compared to equality constraints, or when the computation of inequalities is difficult and time consuming, as there is no need of computing the Jacobian of inequalities.
The problem arising from the transcription of optimal control problem for formation flying has those peculiar features, so it has been decided to implement, even for the relative orbit control, a barrier method for the solution of the NLP parameters optimization problem.

The method implemented for the solution of the NLP parameters optimization problem is a barrier method which exploits the particular structure of the optimal control problem transcribed using the multiple shooting transcription method. It produces an NLP problem which has a limited number of parameters and a comparable number of equality constraints related to differential equations satisfaction, while, in the case of formation flying, it can be characterized by an high number of inequality constraints deriving from the relative distance constraints. So it has been decided to solve the equality constrained problem with a classical SQP solver adjoining the inequalities in the objective function with a barrier term and to apply an interior point method procedure on a series of those SQP problems.
One of the drawbacks of interior point method based on logarithmic barrier functions is that the initial guess must be inside the feasible region, otherwise the method will not be able to converge to the solution, even if the initial guess is in the region which could assure a convergence of the unmodified objective function.

One of the most difficult task in trajectory optimization is the definition of a good initial guess, and often the object of this kind of optimization is to find a trajectory which satisfies all the constraints. From this point of view it is desirable that the method allows the imposition of initial guess which does not satisfy all the constraints. In order to

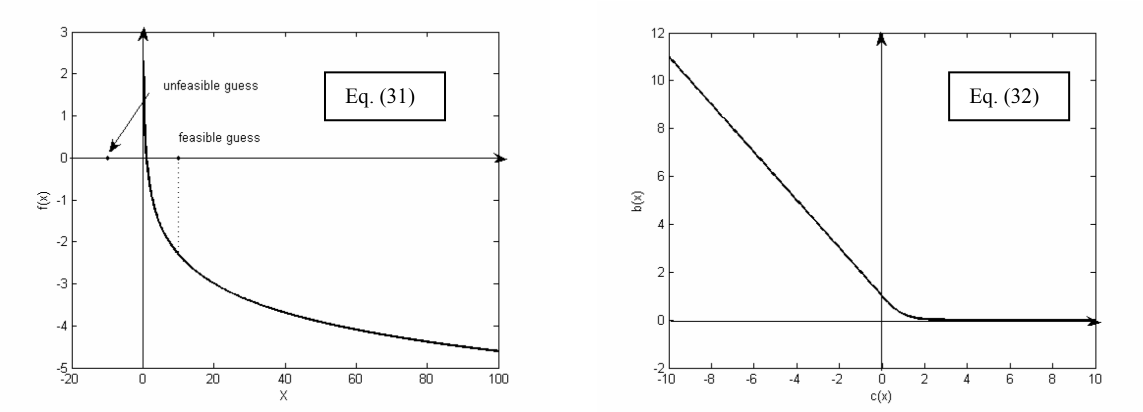

Figure 5 Barrier functions

assure the possibility to the barrier method implemented to accept an unfeasible starting guess it has been decided to modify the barrier function. This modification consists in the definition of two different barrier functions which are applied to constraints on the basis of their level of satisfaction.

In order to allow unfeasible initial guess solutions it has been decided to consider the following barrier function, which is defined on all the domain and which is monotonic towards the constraints satisfaction, and that goes to zero in the feasible area:

$$B(x)=\begin{cases} F(x)-\mu\sum_{i=1}^{m}(1-c_i(x)) & c_i(x)\le 0 \\ F(x)-\mu\sum_{i=1}^{m}1-\tanh(c_i(x)) & c_i(x)>0 \end{cases} \tag{32}$$

In figure 5 both the logarithmic barrier and the modified barrier function are shown. It is possible to see that the modified function is continuous at the linking point, which is a necessary requirement to avoid bad Jacobian computation in correspondence of constraint satisfaction. Once that all the constraints are satisfied and the solution is inside the feasible region the barrier term is switched to the classic logarithmic barrier.

The NLP problem resulting from the transcription will be generally characterized by a small number of parameters and matrixes which are densely populated, reducing the benefits of using sparse solver. For this reason the equality constrained problems which have to be solved are solved with an SQP solver which does not exploit eventual sparsity of the Jacobian of the constraints, but use dense linear algebra to solve the linear system at the base of the SQP iteration.

To solve the SQP sub problem it has been decided to use the solver available from the Harwell Subroutine Library which implements a variable metric method for the Hessian successive approximation, and a line search method for the globalization of the algorithm using a watchdog method developed by Chamberlain et al. [13], which relaxed the request that the iteration produce a decrease of the merit function only one time in a fixed number of iterations. This solver requires to compute the gradient of the objective function and the Jacobian of the constraints, which have been computed using finite differences.

The efficiency of the interior point method is largely dependent on the decrementing policy of the barrier term, as the idea of interior point is based on the fact that the new iteration modifies the objective function reducing the weight of the constraints, but the solution of the previous problem must be sufficiently near to the solution of the new problem to be used as a guess for it. If the reduction of the barrier parameter is too fast, the new problem take an initial guess which is too far from the solution, increasing the amount of iterations that the SQP sub problem needs to reach the solution. On the other end, if the reduction is too slow, and the requested tolerance on the solution of intermediate problems is too stringent, the number of sub problems can increase too much reducing the efficiency of the method.

In the algorithm developed, it has been decided to reduce linearly the barrier term, a good compromise between the necessity of obtaining a good initial guess and the need of reducing the number of intermediate SQP sub problems.

$$\mu_{k+1}=b\mu_k \qquad 0.25<b<1 \tag{33}$$

The constant **b** can be chosen depending on the particular problem faced. The choice influences the balance between the number of SQP sub problems and the number of iterations needed by each of them.

4 RESULTS

The proposed trajectory optimization method has been applied to the problem of relative orbit transfers. These are the first step in the design of reconfiguration manoeuvres for spacecrafts flying in formation. For this reason the transfers reported here have been chosen in order to test possible operative condition that could be faced by formations of satellites which make use of relative orbit for their deployment. In the test cases considered in the following, the linearized relative dynamics presented above has been used considering both circular and eccentric reference orbit. In each case the model neglects the effect of gravitational perturbation due to J_2 coefficient and of atmospheric and solar pressure drags.

Continuous low thrust propulsion has been considered. It is therefore necessary to adjoin the relative dynamics model with the mass flow model described in section 2.2 and to adjoin the mass state to dynamic states. For this reason it has been decided to consider an initial mass of 100 kg for the typical spacecraft and an engine with a specific impulse of 4000 s, which is typical of ion engine propulsion. The thrust level has been considered to be less than 2 mN which again is typical for ion engine propulsion.

The first transfer analyzed is that of a single satellite from one orbit to another one considering both a circular and an eccentric reference orbit. In particular the reference orbits considered for all the cases analyzed in this section are characterized by the orbital elements summarized in Table I.

Table I - Reference Orbits Elements

Elements	Unit	Circular	Eccentric
a	Km	7378	26570
e	-	0	0.7
I	Rad	0	1.01
ω	Rad	0	0
Ω	Rad	0	0

The problem can be easily stated as the minimization of an objective function related to fuel usage for the manoeuvre. The mass flow is linked to the control actions, so it has been decided to minimize a quadratic function of the control actions:

$$J = \int_{t_0}^{t_f} u_x(t)^2 + u_y(t)^2 + u_z(t)^2 \, dt \tag{34}$$

where u_x, u_y and u_z are the components of the control action projected on the axis of the relative reference system.

The problem is then completed with a series of boundary constraints which allow to impose that the states of the spacecraft at the beginning of the manoeuvre are on the starting relative orbit, and at the end are on the final relative orbit:

$$\begin{array}{ll} x_0 = x_{p1} & x_f = x_{p2} \\ y_0 = y_{p1} & y_f = y_{p2} \\ z_0 = z_{p1} & z_f = z_{p2} \\ \dot{x}_0 = \dot{x}_{p1} & \dot{x}_f = \dot{x}_{p2} \\ \dot{y}_0 = \dot{y}_{p1} & \dot{y}_f = \dot{y}_{p2} \\ \dot{z}_0 = \dot{z}_{p1} & \dot{z}_f = \dot{z}_{p2} \end{array} \tag{35}$$

As the mass flow equation is adjoined to the dynamic system it is necessary to constrain also the value of the mass variable at the beginning of the manoeuvre:

$$m_0 = \overline{m} \tag{36}$$

Finally, a set of path constraints derive from the engine performances, as it is necessary to constrain the modulus of the control actions to the value of the admissible thrust:

$$U_i(t) < U_{MAX} \quad \forall t \in \left[t_0, t_f\right] \tag{37}$$

where:

$$U_i(t) = \sqrt{u_x(t)^2 + u_y(t)^2 + u_z(t)^2} \tag{38}$$

The first kind of manoeuvre analysed consists in a transfer between two relative orbits which are characterized by the same relative amplitude, but have different relative inclination in the relative reference frame. The optimization has been carried on considering one orbital period of the reference orbit as time domain, bringing to the trajectory shown in figure 6 for the case of circular reference orbit together with the mass history and the control action.

Following the same procedure, the relative orbit transfer in the case of eccentric reference orbit has been studied. Even in this case the manoeuvre consists in a transfer between two relative orbits characterized by the same relative amplitude and different inclination with respect to the relative reference frame. Moreover the initial point of the manoeuvre has been constrained to be at the time in which the reference point is at the pericenter of the reference orbit, allowing the design of a trajectory which exploits some symmetry.

Figure 7 shows that trajectory together with the mass history and control action.

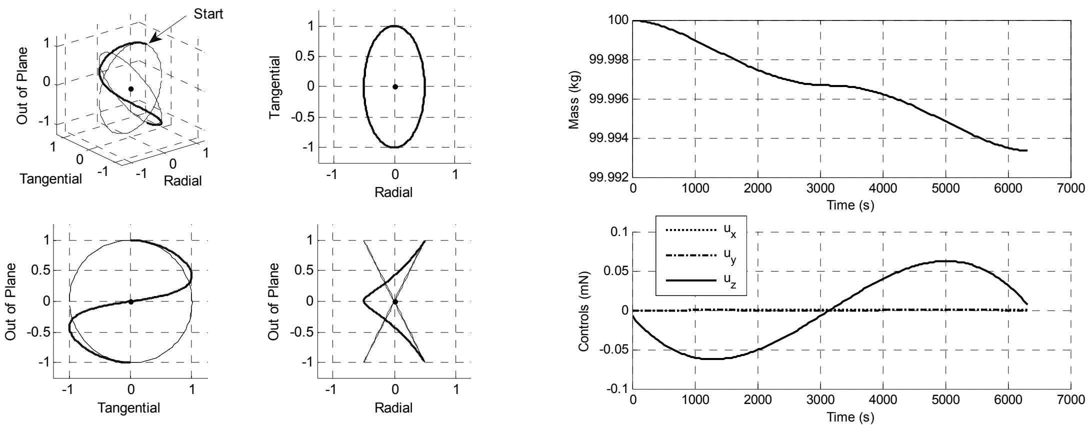

Figure 6 Circular reference Relative Orbit transfer

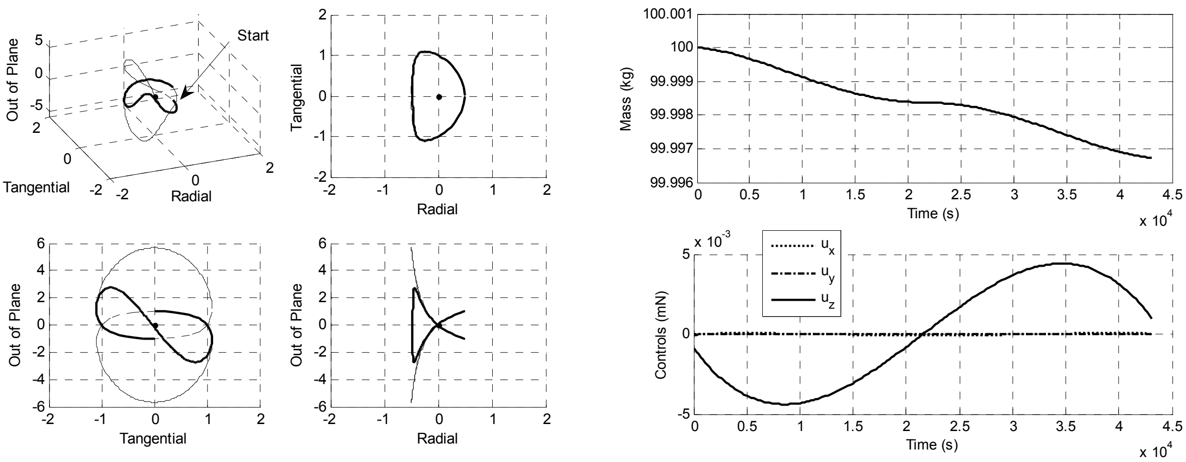

Figure 7 Eccentric reference Relative Orbit transfer

A particular case of relative orbit transfer is the trajectory that a spacecraft follows to initialize a bounded relative periodic orbit, starting from an initial fixed position in the relative frame which can be considered as a degenerated orbit. Following the same procedure used for transfer between two relative periodic orbits, and constraining the initial state to be fixed, it has been possible to design the trajectory that allows to initialize a relative orbit in the case of both circular and eccentric reference orbit. Figure 8 shows the trajectories obtained in those cases.

The second kind of relative orbit transfer taken into consideration have been chosen to represent the reconfiguration manoeuvre that a formation must be able to exploit to change its size. Relative orbit transfer to change orbit dimension in the case of circular and eccentric reference orbit have been considered.

The case of circular reference orbit consists in augmenting the radius of the ground projection of the relative orbit. The initial and final states of the satellite have been imposed to grant an increase of the radius of the ground projection by ten times. The optimization has been performed considering as time domain of the manoeuvre a single period of the reference orbit.

The case of eccentric reference orbit is slightly different, as it is not possible to define a radius of the ground projection. In order to define the final orbit an increase of the extension of the relative orbit in the tangential direction has been considered.

Figure 9 shows the trajectories obtained for the increase of relative orbit dimension, both in the case of circular and eccentric reference orbit

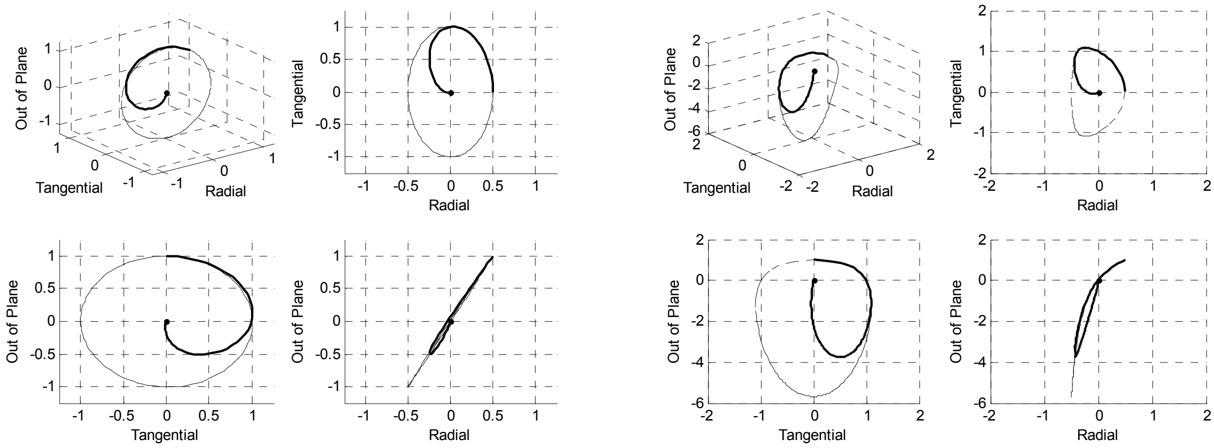

Figure 8 Relative Orbits Initialization

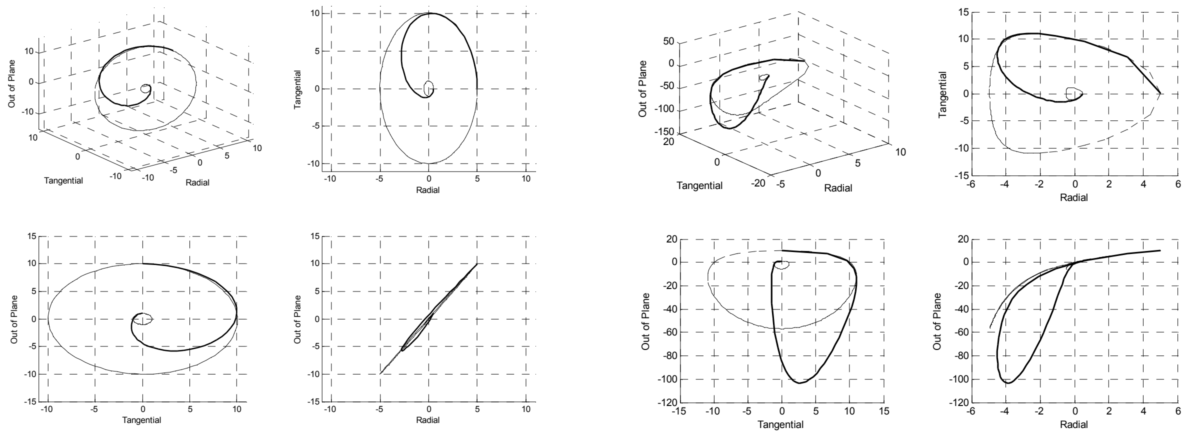

Figure 9 Relative Orbit dimension increase

All transfers considered above are based on the assumption that the time domain is equal to only one period of the reference orbit. This assumption has been done because relative orbits have the same period of the reference orbit, and the generation of guess solution can be smarter considering the same period for the manoeuvres.

However, if the trajectory can be computed over a longer period of time, even if the fuel consumption will remain almost the same, the required level of thrust could be considerably lower. For this reason it has been decided to consider manoeuvres that span more then one orbit period, resulting in what has been called a multi-revolution transfer.

The only case considered for this kind of transfer consists in the change of relative orbit dimension in case of circular reference orbit over four orbital periods, and has been optimized imposing thrust level constraints along the entire manoeuvre.

Figure 10 shows the trajectory obtained in the case of an increase of relative orbit ground projection identical to that shown in figure 9, together with the control action.

CONCLUSIONS

The parallel multiple shooting transcription adopted has lead to small NLP problems, which are characterized by hundreds of variables. It allows to reduce the computational burden and, at the same time, to exploit the inherent parallel structure of the multiple shooting approach, leading to the possibility to use parallel computing to reduce the time needed to solve the problem.

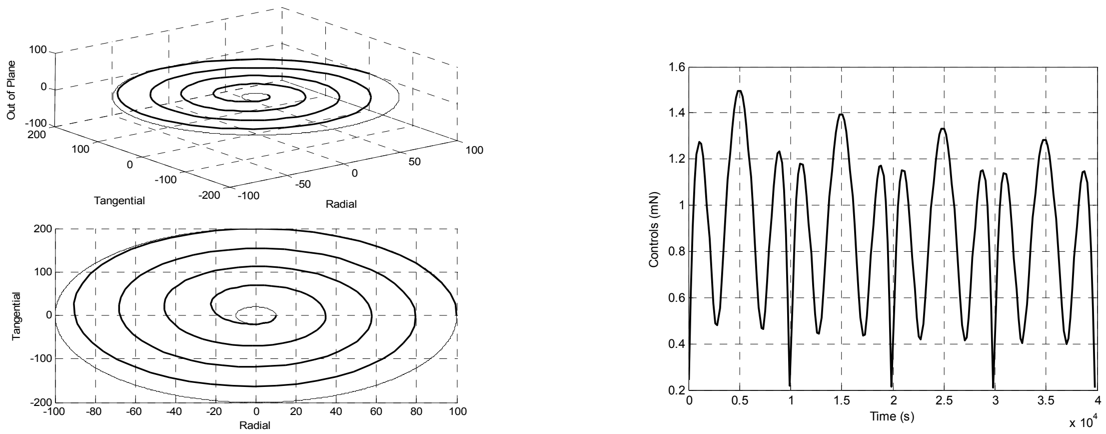

Figure 10 Multi-revolution relative orbit transfer

The interior point method that has been developed for the solution of the NLP problem allows a great improvement over classical active set SQP methods as the constraints are included directly in the objective function, allowing the efficient treatment of problems characterized by high number of inequality constraints. The classical problem of unfeasible initial guess, which affects interior point methods, has been solved with a particular strategy on the barrier term, which allows to impose an unfeasible initial guess.

Concluding, it can be said that the developed method allows to face a general problem of low-thrust relative orbit transfer and is well suited for problems with an high number of inequalities deriving from path constraints. This can be regarded as the first step in designing reconfiguration manoeuvres for formation of satellites. For this reason the particular orbit transfer shown in the results have been chosen to represent possible formation flying manoeuvres.

REFERENCES

[1] Betts J.T, Survey of numerical methods for trajectory optimization. *Journal of Guidance, control and Dynamics,* Vol. 21, No. 2, 1998.

[2] Betts J.T. and Huffman W.P., Path-constrained trajectory optimization using sparse sequential quadratic programming. *Journal of Guidance, control and Dynamics,* Vol. 16, No. 1, 1993.

[3] Fahroo F. and Ross I.M., Direct trajectory optimization by chebyshev pseudospectral method. *Journal of Guidance, control and Dynamics,* Vol. 25, No. 1, 2002.

[4] Forsgreen A., Gill P.E. and Wright M.H., Interior methods for nonlinear optimization. SIAM Review, Vol. 44, No. 4, pp. 525-597, 2002.

[5] Junkins J.L. and Schaub H., *Analytical Mechanics of Space System*. Education Series. AIAA, New York, 2003.

[6] Vallado D., *Fundamental of Astrodynamics and Applications*. Mc-Graw Hill, 1997.

[7] Clohessy W.H. and Wiltshire R.S., Terminal guidance for satellite rendezvous. *Journal of Aerospace Sciences*, Vol. 27, No. 9, pp. 653-658, 1960.

[8] Inalhan G., Tilerson M. and How P.J., Relative dynamics and control of spacecraft formations in eccentric orbit, *Journal of Guidance, control and dynamics*, Vol. 25, No. 1, 2002.

[9] Brusch R.G., Constrained impulsive trajectory optimization for orbit-to-orbit transfer. *Journal of Guidance, control and Dynamics,* Vol. 2, No. 3, 1979.

[10] Betts J.T., *Practical Methods for Optimal Control using Nonlinear Programming*. The Boing Company, 2000.

[11] Betts J.T. and Huffman W.P., Trajectory optimization on a parallel processor. *Journal of Guidance, control and Dynamics,* Vol. 14, No. 2, 1991.

[12] Gertz E.M. and Gill P.E., *A primal-dual trust-region algorithm for nonlinear optimization*. Technical Report NA 02-1, Department of Mathematics, University of California, San Diego, 2002.

[13] Chamberlain R.M., Powell M.J.D., Lemarechal C. and Pedersen H.C., The watchdog technique for forcing convergence in algorithms for constrained optimization. *Mathematical Programming,* Vol. 16, pp.1-16, 1982.

ISSN 1590-8844
International Journal of Mechanics and Control, Vol. 08, No. 02, 2007

MULTI-BODY DYNAMIC MODELLING OF THE EXPECTED PERFORMANCE OF ACCELERATED PAVEMENT TESTING FACILITIES

Ezio Santagata * Davide Lioi * Mauro Velardocchia ** Enrico Galvagno ** Elvio Bonisoli ***

* Dipartimento di Idraulica, Trasporti e Infrastrutture Civili, Politecnico di Torino
** Dipartimento di Meccanica, Politecnico di Torino
*** Dipartimento di Sistemi di Produzione ed Economia dell'Azienda, Politecnico di Torino

ABSTRACT

Accelerated Pavement Testing (APT) facilities are nowadays considered fundamental for the thorough understanding of the performance of pavements. The amount of information that can be derived from APT investigations can serve as the basis for a more performance-related pavement design but also for the development of new pavement types and innovative materials. In the design and use of such facilities, special care should be placed in the modelling of the loading systems which are employed to produce accelerated damage. Such an analysis is important both in the preliminary design phase, in which technological solutions are found in order to simulate the effects of heavy vehicles on the pavement, and in the various phases of investigation, when the recorded damage has to be clearly related with effective loading conditions. In this respect, modelling can be a valuable support to the evaluation of the data which can be acquired by means of a proper instrumentation of the facility. In order to address such issues, the Authors have developed a design procedure which together with typical stationary calculations includes the adoption of Multi-Body (MB) and Finite Elements (FE) models of the testing system. As proven by the first implementation exercises of the design procedure, the use of MB and FE models allows the evaluation of the dynamics of the system in a wide variety of testing conditions. Thus, stresses and strains in the structure of the APT facility can be estimated and the dynamic forces and torques which arise during testing at the tire-pavement interface can be predicted. Given the width of the design problem, this paper gives only a general overview of the structure of the proposed procedure, with its application to a specific case which has been studied in depth. Refinements are still under way and will hopefully yield a set of modelling methods which in the future will be available for the design of new APT facilities and for the assessment of the performance of existing systems.

Keywords: Accelerated Pavement Testing, tire-pavement interaction

1 INTRODUCTION

The design and construction of long-lasting pavements is one of the goals which highway engineers have continuously tried to reach for centuries. Such an effort has required experimental and theoretical research which in time has increased its level of complexity: while initial studies were essentially based on the observation of pavement sections subjected to traffic and on the index characterization of the materials used in construction, current investigations are based on a more detailed description of material behaviour and on the modelling of pavement performance under controlled or monitored loading conditions. In such a context, Accelerated Pavement Testing (APT) facilities have proven to be extremely powerful research tools, since they can simulate long-term effects of traffic loading in a relatively short time period, with the corresponding evaluation of the progressive changes in pavement response and distress.

Contact authors: Ezio Santagata[1], Mauro Velardocchia[2]

[1] E-mail: ezio.santagata@polito.it

[2] E-mail: mauro.velardocchia@polito.it

Quite obviously, the accelerated character of this kind of testing is a key element for the development of projects focused on the design and modelling of perpetual pavements, conceived in such a way to extend service life well beyond the levels associated to standard pavement structures.
APT programs are nowadays active worldwide and address almost all relevant aspects of pavement engineering. Valuable sources of information with respect to past achievements and future perspectives are provided by TRB Committee AFD40 (formerly A2B09) and by the European COST-Transport action COST 347.
When compared with the original prototypes developed at the beginning of the 20th century [1,2], current APT devices are quite complex, with a wide array of operative options and technological refinements which are implemented in order to maximize the simulation of the effects caused by actual heavy vehicles and/or aircraft landing gears. Moreover, whether of the linear of circular type, all APT systems are designed in such a way to make their use economically feasible, with a convenient limitation of energy consumption and testing time. In many cases research institutions have developed their own testing prototypes, conceived to suit specific needs; however, in other cases they have preferred to adopt systems already used in other countries which to some extent could be considered as standard devices with a rich set of test data available for comparative purposes.
In the Politecnico di Torino, the whole issue of vehicle-road interaction has been recently approached by combining the efforts and resources of the Pavement Engineering and Vehicle Dynamics research groups. Topics of interest which have been treated both experimentally and theoretically range from the evaluation of the effects caused by pavement roughness to the dynamic design of geometrical road elements. More recently, the joint research group has also started working on the design of APT facilities which is in fact a theme at the boundary between pavement and vehicle engineering: as illustrated in this paper, this has been done by developing a design procedure which together with typical stationary calculations includes the adoption of Multi-Body (MB) and Finite Elements (FE) models of the testing system.
As proven by the first implementation exercises of the design procedure, the use of MB and FE models allows the evaluation of the dynamics of the system in a wide variety of testing conditions. Thus, stresses and strains in the structure of the APT facility can be estimated and the dynamic forces and torques which arise during testing at the tire-pavement interface can be predicted. This second aspect of analysis is especially important when considering side and longitudinal forces, the importance of which is generally overlooked in the design of APT facilities even though it has been clearly recognized that they may greatly affect both the interaction between the components of the test system and the development of structural and functional distresses in the pavement. As shown in the design example illustrated in this paper, such a limitation can be overcome by means of an adequate modelling of the APT system: in fact, its results provide the basis for the definition of the location and type of on-board sensors used to measure shear forces applied to the pavement and of methods to be employed for their active control.
The development and use of the proposed design procedure requires a deep knowledge of tire and vehicle dynamics and should be supplemented by direct testing in order to make realistic assumptions of the many structure and materials parameters utilized in modelling. Given the width of the design problem, this paper gives only a general overview of the structure of the proposed procedure, with its application to a specific case which has been studied in depth. Refinements are still under way and will hopefully yield a set of modelling methods which in the future will be available for the design of new APT facilities and for the assessment of the performance of existing systems.

2 DESIGN PROCEDURE

Figure 1 gives a schematic illustration of the design procedure which is being developed by the Pavement Engineering and Vehicle Dynamics research groups.
The first step in design consists in performing the basic static calculations which are necessary to establish the main dimensions of the structure. The basic parameters of the APT device (circular or linear layout, engine power, number of wheels of the trolleys, static load acting on the wheels, etc.) have to be chosen at this step. As better explained in the following paragraphs, the adoption of an MB model in this first step of design would be too expensive in terms of time, due to the large number of uncertain parameters which should be evaluated and modified. In fact, an MB model considers the inertia of all the main components, which are connected by elements characterized by their own stiffness and damping coefficients.

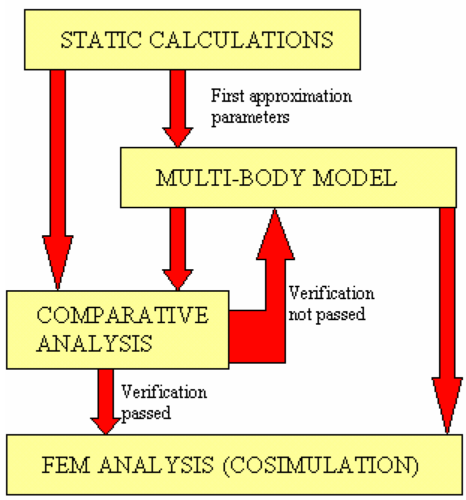

Figure 1 Flux diagram of the design procedure.

After the definition of a first approximation layout, it is possible to implement the MB model of the APT facility. First of all, in semi-stationary conditions, it is necessary to make a comparison between the results of the static calculations and the output of the model, in order to assess its validity. Then it is possible to carry out an analysis of the behaviour of the system in dynamic conditions, for example when the pavement surface is not perfectly flat, to investigate the forces and the torques acting at the tire-pavement interface and between the different components of the testing facility. The MB model can also be useful to optimize the structural design of the APT system and, as mentioned previously, to decide how to locate the sensors on its moving parts in order to measure or estimate the dynamic tire-pavement forces.

Finally, for an in-depth design of the structure of the APT facility, it is necessary to set up an FE model of the machine and to make it run in co simulation with the MB model. This type of modelling is quite complex and should be performed on the final layout of the facility; the corresponding results can be used to better understand the performance of the APT system and to provide a continuous feedback to measurements carried out during testing.

This paper presents the results obtained in the design steps of Figure 1 which correspond to the static calculations and to the implementation and use of the MB model. The calculation examples refer to the specific case of a rotational APT system which has been thoroughly examined to test the applicability of the procedure and which could be actually built by employing the indicated technological components.

3 PRELIMINARY ASSUMPTIONS

The first choice for the designer of an APT facility consists in defining the configuration of the system, which can be either of the rotational or linear type. Both configurations have several advantages and disadvantages, so the choice should be made based on a balanced evaluation of a number of factors which may have different weights depending upon the intended use of the facility.

The linear configuration has the advantage of occupying a small area; furthermore, it is usually transportable and can be located in different sites depending upon specific needs. However, it has the limitation of permitting only small values of longitudinal speed of the loading trolleys. The inertial force necessary to obtain a speed of 40-50 km/h with an acceptable (not too large) spatial length of the test facility is too high both in terms of power required by the system of propulsion and of strains exerted on the structure.

The rotational configuration permits a very slow acceleration of the testing equipment (only during transients, necessary to make the machine start and stop) without significant dynamic forces or torques on the structure and on the system of propulsion. The power system of the testing facility can be designed as a function of the static load acting on the trolleys of the testing equipment.

Taking into account the observations illustrated above, the design procedure was applied to the case of a rotational APT facility, with a loading system composed of four trolleys connected by means of rigid horizontal arms to a rotating central shaft (Figure 2). In order to avoid the superposition of dynamic loading effects on the pavement, it was hypothesized that the trolleys should have a single axle configuration (Figure 3) with the possibility of using super single tires. Such a choice also allows a more simple modelling of pavement damage, which according to traditional approaches is always referred to single axles.

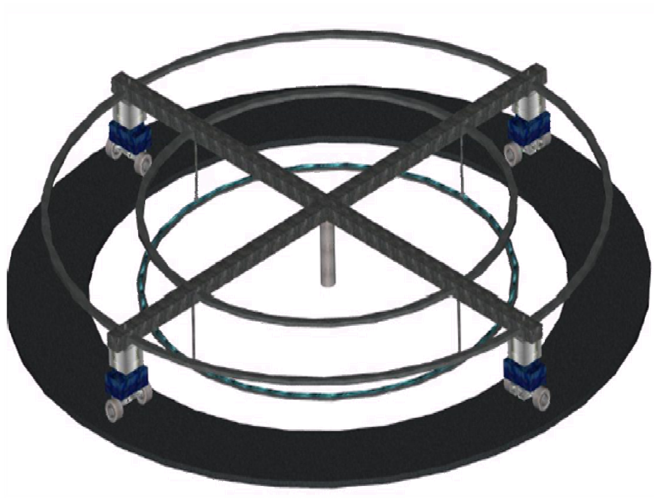

Figure 2 Sketch of the APT facility considered in the study.

For a system of the type indicated in Figure 2, the connection between the arms and the trailers should be made by employing ball recirculation bearings, characterized by a low friction. Their function is to prevent the rotation of each trolley around the axis of the wheels and to transmit the horizontal force necessary to make the system rotate along a circular trajectory.

In the preliminary phase of design some hypotheses had also to be made on the type of loading trolleys. Therefore, it was assumed that commercial suspensions, such as the one shown in Figure 3, should be utilized: this allows the dynamics of the loads to be very similar to the typical behaviour of a heavy truck. The system represented in Figure 3 is a trailing arms suspension, with an integrated steering system based on a hydraulic power circuit. It can be equipped with a system of hydraulic springs, which can be used for the dynamic variation of the load acting on the pavement.

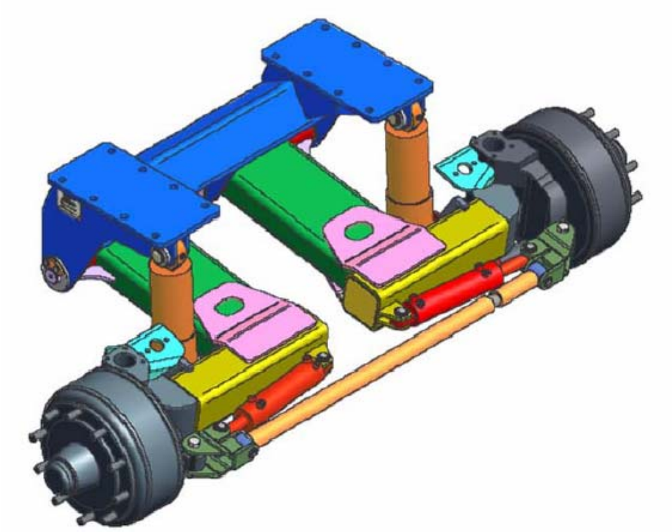

Figure 3 Sketch of the suspension system of the trolley.

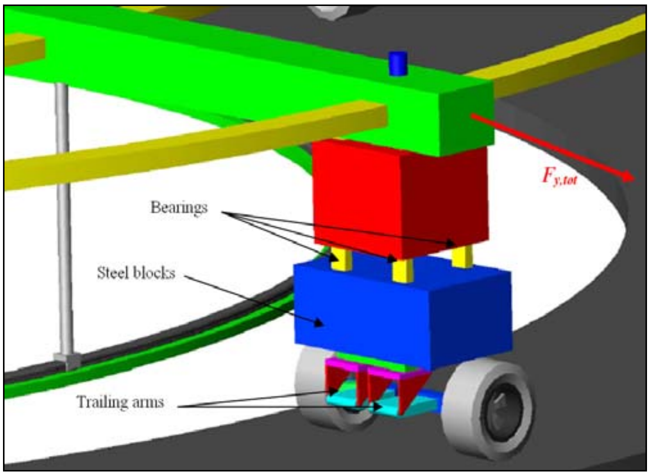

Figure 4 Sketch of a trolley and its connection to a lever arm.

With respect to the maximum static load acting on each trolley, in the calculations reference was made to a value of 120 kN, which can be obtained by means of a system of steel blocks piled on the each individual chassis (Figure 4). It is important to highlight the fact that by adopting the abovementioned solution for the trolley-arm connection, the vertical load, even in dynamic conditions, is entirely sustained by the tires and not by the bearings which connect the structure of the APT facility to the trolleys.
For the configuration schematically shown in Figure 4, centrifugal forces, which are generated by the motion of the trolleys, are absorbed by the lever arms (through the bearings) and not by the tires of the moving trolley. Only the sideslip angles due to the steering angle of the wheels give origin to a force which is transmitted to the structure of the trolley (suspension and chassis).
It has to be underlined that a commercial trailer for a truck can sustain a maximum level of lateral acceleration equal to 0.5 g. A typical configuration (for example, with a diameter of 20 m) of a circular APT facility can easily give origin to a level of lateral acceleration greater than 1.5 g, which corresponds to the force absorbed by the arms of the machine (and not by the suspensions). As a consequence, in designing the facility it is possible to refer to a level of lateral acceleration of the trolleys which exceeds the maximum value which it could have on the road. However, care should be taken in checking that the imposed steering angle does not give origin to a force which exceeds the structural resistance of the trolley.

4 STATIC CALCULATIONS

The first point to be addressed through static calculations is the evaluation of the forces acting along the axis of the arms of the testing machine ($F_{y,tot}$). These can be calculated as the sum of two components, $F_{y,\alpha}$ and $F_{y,c}$, respectively due to the sideslip angle α of the tires of the trolley [3] and to the centrifugal effects due to the radius of curvature of the trajectory of the trolleys during their motion around the pivot axis of the facility.

$$F_{y,tot} = F_{y,\alpha} + F_{y,c} \tag{1}$$

The equations necessary for the evaluation of the two components are the following:

$$F_{y,\alpha} = C_{\alpha}\ \alpha \tag{2}$$

$$F_{y,c} = m\ a_y = m\frac{v^2}{R} \tag{3}$$

where C_{α} is the equivalent cornering stiffness of the axle of the trolley (considered constant for low values of α), m is the mass of the trailer, a_y is its lateral acceleration, v is its speed and R is the radius of trajectory.
It can be observed that since small values of the radius R imply large strains for the arms of the test machine, the choice of the size of the APT facility is also directly connected to structural issues. It should also be underlined that sideslip angle effects can be due both to the motion of the tie rod, which can be used to increase in controlled conditions the shear forces acting on the pavement, and to the elasto-kinematical behaviour of the suspensions. Finally, the value of $F_{y,tot}$ should be considered for a first estimate of the bending torque acting on the arms of the APT facility.
Another very important issue which has to be treated by means of static calculations is the evaluation of the power of the motor adopted to make the system rotate. This can be either an electrical motor or an internal combustion engine,

but in any case it has to be correctly chosen to guarantee the expected performance of the APT facility.
First of all, it is necessary to consider the power contribution (for each trolley) due to rolling resistance. The following equation can be therefore used:

$$P_{roll} = W_{tot}\ v\left(f_0 + Kv^2\right) \tag{4}$$

where W_{tot} is the vertical load acting on the axle of the trolley, f_0 and K are the speed-independent and speed-dependent contributions to the rolling resistance coefficient of the tires.
Secondly, the power due to the aerodynamic resistance is considered according to the expression:

$$P_{air} = \frac{1}{2}\rho\ S\ C_x\ v^3 \tag{5}$$

where ρ is air density, S is the front surface of the trolley, C_x is the aerodynamic drag coefficient.
Finally, additional power contributions should be calculated to take into account the effects due to tire sideslip angle and to the presence of longitudinal forces acting at the tire-pavement interface while running at constant speed. The corresponding equations are the following:

$$P_\alpha = C_\alpha\ \alpha^2\ v \tag{6}$$

$$P_s = C_s\ s\ v \tag{7}$$

where C_s is axle equivalent longitudinal stiffness [3] and s is longitudinal slip.
The total power required to make a single trolley move at a constant speed v is therefore given by the following expression:

$$P_{tot} = P_{roll} + P_{air} + P_\alpha + P_s \tag{8}$$

The different contributions in terms of power necessary for the motion of the system as a function of the speed of the trolleys can be observed in Figure 5, in the case of absence of longitudinal and lateral slips (P_α and P_s equal to zero). The static calculations demonstrate that the effect of the spin of the tires due to the curvature of the trajectory can be neglected. The contribution due to tire rolling resistance is prevalent on the contribution due to aerodynamics. By comparing equations (6) and (7), it is clear that, for reasonable values of α and s, the contribution of (6) is coherent with a value of power of the motor of the APT facility of some hundreds of kW, whereas contributions (7) easily exceed the power limit of existing motors. This suggests that it is economically feasible to design an APT system in which sideslip angles are imposed during testing in order to increase shear forces transferred to the pavement surface: this can be done through the controlled motion of the tie rods which can be hand actuated before the beginning of the test or electrically or hydraulically actuated during the test. However, active control of longitudinal forces is not easily obtainable when operating in constant speed conditions.

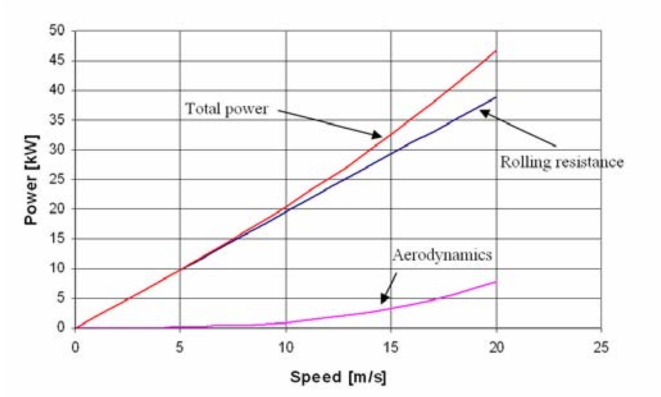

Figure 5 Power necessary for the motion of a trolley of the APT facility.

After choosing the motor and the driveline of the facility, it is necessary, through static calculations, to define the regulation diagrams of the system, fundamental both during the design process and for the final use of the APT facility in order to have the best performance of the system.
For example, it is useful to compute the maximum value of sideslip angle (α_{max}) as a function of motor power. This can be done by referring to the energy balance of the system which translates in the following equation:

$$\alpha_{max} = \sqrt{\frac{\eta_t\ P_{mot} + P_{4,tot}(v)}{4\ C_\alpha\ v}} \tag{9}$$

where: η_t is the efficiency of the driveline of the facility, P_{mot} is the power of the adopted motor unit and $P_{4,tot}$ is the power contribution comprehensive of (4), (5) and (7) for the four trolleys.
Figure 6 is an example of such a kind of regulation diagram in which the longitudinal slip contribution has not been considered. The design target of a sideslip angle of 3° can be reached at a maximum speed of about 13 m/s, but much larger values of sideslip angle can be obtained at lower speeds.
In a similar way, it is possible to compute the maximum speed v_{max} of the trailers (having a total weight equal to W) of the testing facility as a function of sideslip angle, thereby obtaining the regulation diagram shown in Figure 7. In this

case, the following equations, which do not consider tire longitudinal slip, can be employed:

$$\eta_t \; P_{mot} = A\,v + B\,v^3 \tag{10}$$

where:

$$A = W\,f_0 + 4\,C_\alpha\,\alpha^2 \tag{11}$$

$$B = W\,K + 2\,\rho\,S\,C_x \tag{12}$$

To obtain v_{max}, it is possible to adopt Cardano's rule [4]:

$$v_{\max}(\alpha) = A^*\left(\sqrt[3]{B^*+1} - \sqrt[3]{B^*-1}\right) \tag{13}$$

where:

$$A^* = \sqrt[3]{\frac{\eta_t\,P_{mot}}{2\,B}} \tag{14}$$

$$B^* = \sqrt{1 + \frac{4\,A^3}{27\,P_{mot}^2\,\eta_t^2\,B}} \tag{15}$$

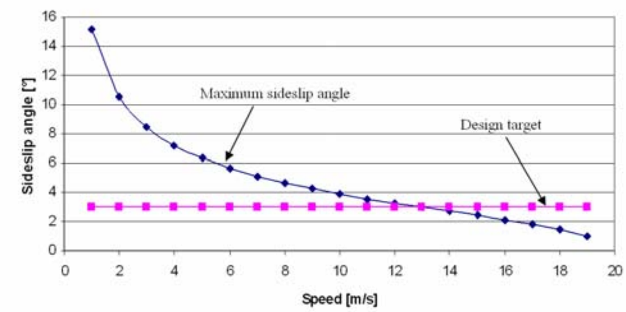

Figure 6 Typical α_{max} - v regulation diagram of the APT facility.

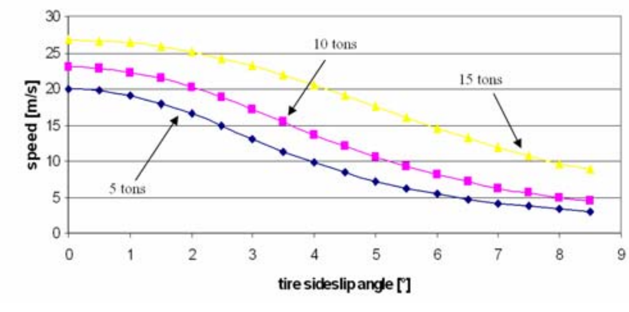

Figure 7 Typical v_{max} - α regulation diagram of the APT facility.

On the basis of regulation diagrams like those of Figure 6 and 7 and of equations (1), (2) and (3), it is possible to find the axial forces acting on the four arms of the test system as a function of the working parameters of the APT facility. Figure 8 shows the values of these forces (for their orientation, see Figure 4) plotted against the longitudinal speed of the trolleys, in the conditions of usage of the maximum power of the motor. It can be observed that the maximum value of sideslip angle (and of side force) decreases as a function of lateral speed according to a regulation diagram similar to the one of Figure 6.

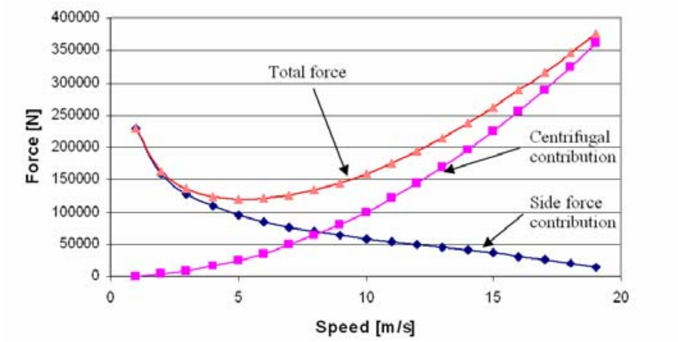

Figure 8 Forces acting along the axis of the arms of the APT device.

5 MULTI-BODY MODELLING

Static calculations have to be followed by the development of a Multi Body (MB) model which by means of the simulation of the dynamics of the system allows the evaluation of the forces and torques acting between the different components of the test machine and on the pavement surface. As anticipated previously, this kind of dynamic modelling can not only provide information on the general behaviour of the test facility, but can also guide in selecting and positioning various sensors for the measurement and/or active control of forces and displacements.

In the specific case of the APT facility described in the previous sections, the MB model was implemented by making use of the software ADAMS View® [5]. Equations (4) and (5) were considered to estimate the resistance to motion of the test facility.

The tire model which was selected for implementation is based on Fiala's formulation [6], which takes into account the interactions between longitudinal and side forces. Side and longitudinal stiffness vary as a function of the working conditions of the tire and are not constant as hypothesized for static calculations.

In the MB model, the contributions to the power necessary for the motion of the trolleys related to longitudinal and lateral forces are not computed through equations (6) and (7), but directly as a function of the outputs of Fiala's model.

The elasto-kinematical characteristics of the suspensions of the trolley are taken into account by the MB model, which considers both unsprung and sprung masses, the geometry of the steering system, the stiffness of the bearings and the bushings of the components of the whole system. The arms of the testing facility, the trailing arms of the suspensions of the trolleys and the wheel hubs are considered infinitely stiff. As mentioned previously, the connection between the chassis of the loading trolleys and the arms of the testing device was hypothesized to be done by using low friction ball recirculation bearings. More specifically, in the MB model each trolley was connected to a horizontal arm by means of four rails, one for each corner of the trolley, with two bearings for each rail. This is shown in Figure 9, which gives a complete representation of the MB model of the loading trolley.

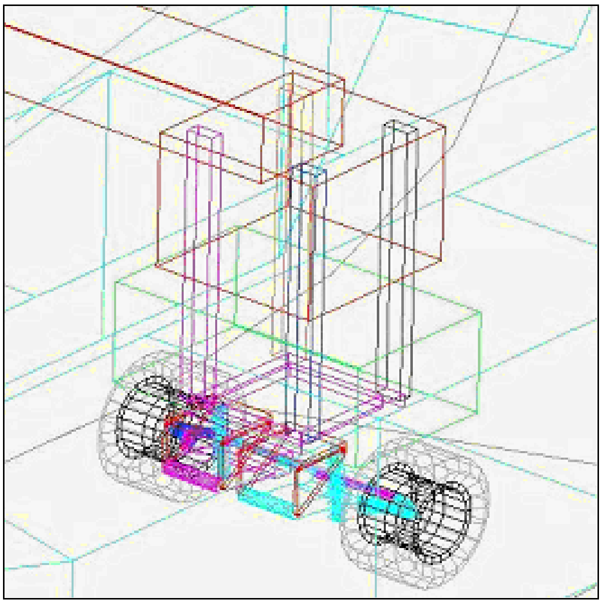

Figure 9 Multi-Body model of the loading trolley.

The MB models allows a wide set of data to be extracted from simulation runs, investigating the effects of critical factors on the performance of the APT facility and considering the relationships between relevant parameters. Examples of typical MB outputs are shown in the following paragraphs.
First of all, the dynamic forces applied to the pavement surface in standard stationary working conditions can be plotted for each wheel of the trolleys. This is shown in Figure 10, which refers to the condition of a perfectly flat pavement surface and a constant value of sideslip angle of 3°.
Secondly, the adopted model allows the evaluation of the forces exchanged between the elements of the trolley and the APT facility for each working condition of the system.

For example, Figure 11 gives the time history of the force acting along the axis of the tie rod for different values of tire sideslip angle. These values are fundamental for dimensioning the actuation system which is necessary to impose given values of the steering angle.

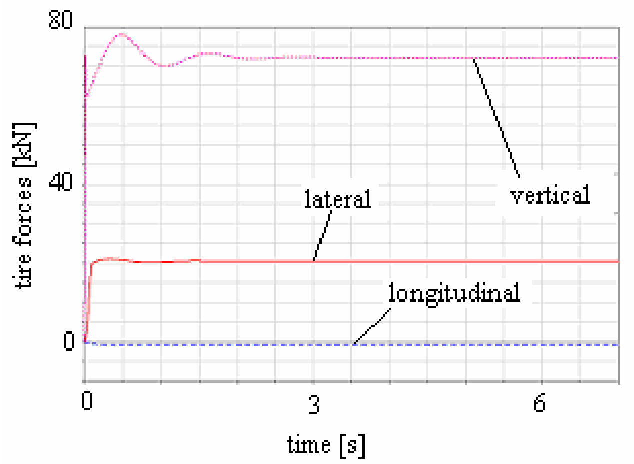

Figure 10 Forces acting on the pavement surface during APT testing.

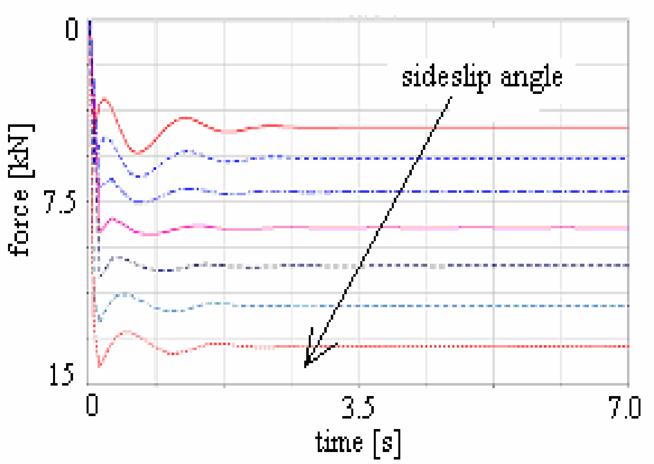

Figure 11 Forces acting along the axis of the tie rods during APT testing.

The MB model can also be used for the design of the ball bearings used to connect the trolleys to the horizontal arms of the APT device. In fact, the forces and the torques acting of each bearing can be calculated with a good level of approximation: this is shown in Figure 12, where the plotted data refers to simulations carried out by considering different values of the stiffness K of the ball bearings. Too stiff bearings can lead to a statically indeterminate structure, with abnormal values of torques or forces, due to the fact that the MB software does not consider the deformation of the rails or of the structure of the chassis.

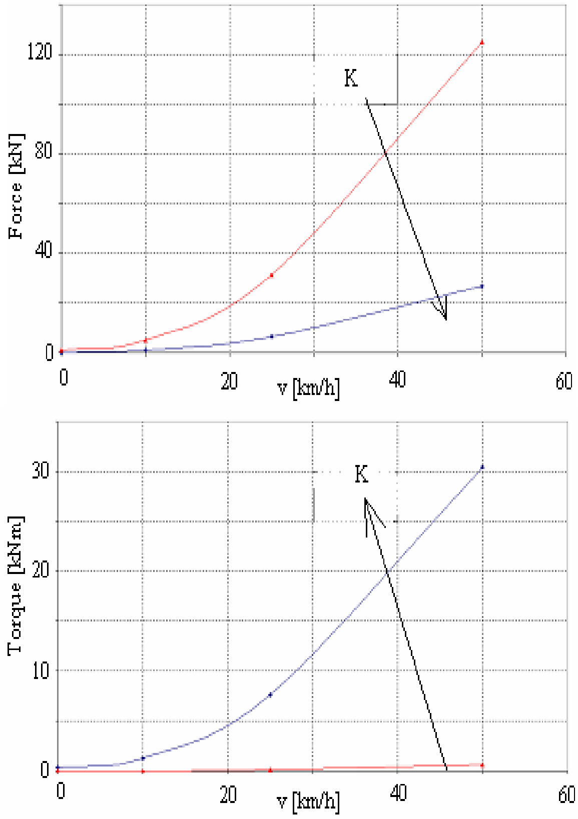

Figure 12 Forces (up) and torques (down) acting on the ball bearings.

Another interesting application of the MB model consists in its support to the optimization of the system of sensors with which the APT facility should be instrumented. For a system of the type considered in this study, the most expensive solution to measure the forces and torques acting on the wheels of each trolley consists in mounting a wheel hub equipped with sensors. However, this solution can be substituted by cheaper alternatives, which can be designed based upon the results of the MB model. For example, the estimation of tire sideslip angle can be performed on the basis of the measurement of tie rod displacement (the yaw rate motion and the sideslip motion of the trolley are limited by the arms of the APT facility). This is clearly shown in Figure 13, which highlights the existence of a precise correlation between the two dimensions estimated from MB simulations. Similarly, relationships can be obtained from MB simulations to link sideslip angle values to the side forces applied to the pavement surface. As a consequence, in a first approximation, side forces can be evaluated on the basis of tie rod position; in a second approximation (in any case cheaper than the solution of the sensors located directly in the wheel hub), side forces can be estimated as a function of the signals retrieved from force sensors located on the tie rods. Even in this case, by means of MB modelling, correlations between the forces at the tie rods and the side forces on the tires can be easily obtained.

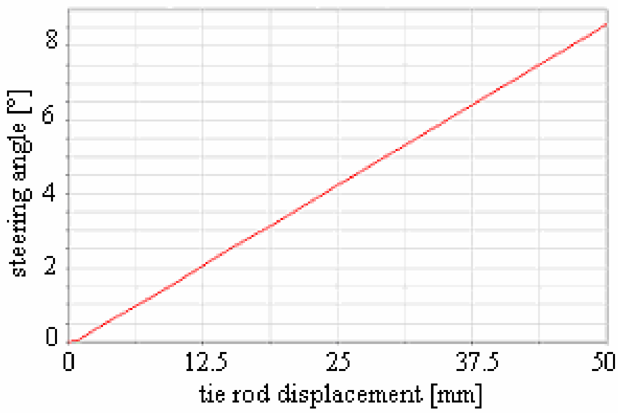

Figure 13 Tire steering angle as a function of tie rod displacement.

The last fundamental information which can be extracted from the MB model refers to the behaviour of the APT system in extreme dynamic conditions which may be encountered in the case of rough pavement profiles. This is shown in Figures 14 through 17, which refer to different MB simulations.

Figure 14 shows the oscillations of the torques which as a result of a sinusoidal pavement profile were calculated around the three axes of the motor shaft. These data are especially important for the design of the central shaft of the APT facility and for the selection of its bearing system. During prolonged testing, any damage to this core element of the facility should be prevented and therefore the use of refined modelling tools which support structural calculations is totally justified.

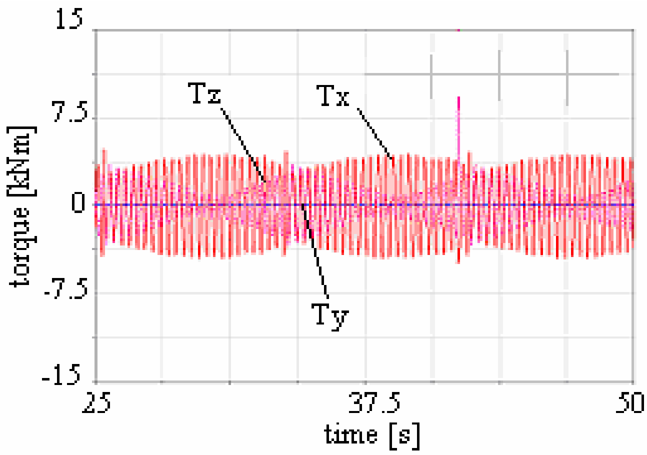

Figure 14 Torques on the bearings of the central shaft of the APT facility.

Figures 15 through 17 highlight the effects caused by rough profiles on the actual pavement loading history and prove the efficiency of the specific kind of suspension which was considered in the study. In all cases the trolleys of the APT

device encountered a flat surface in the right wheel track and a sinusoidal profile (2.5 m of wavelength, amplitude of 50 mm) in the left wheel track. Simulations were carried out at a speed of 10 km/h.
Figure 15 contains plots of the vertical force and displacement of the left wheel only: as expected, oscillations are non negligible and are certainly bound to affect pavement performance. The data plotted in Figure 16 refer to the same simulations: however, it should be noted that the time history of loading of the right wheel is not affected by the roughness of the left wheel track. This proves that the adopted trailing arms suspension system decouples the oscillations between the two sides of the trolley. If the suspension system is modified, with the introduction of a stiff bar connecting the two arms, totally different results are obtained: this is shown in Figure 17, where it can be observed that the loading histories of both wheels is characterized by a continuous oscillation. Since the left wheel provokes the motion of the right wheel, both tires are subjected to dynamic forces, which would be difficult to quantify by making use of simple models based on mass-spring-damper systems, like those indicated in literature [7].

CONCLUSIONS

The paper presents a procedure for the design of APT facilities based on the integrated use of static calculations and Multi-Body models. Such a methodology enables designers to optimize the configuration of the APT system with the possibility of taking into account the effects caused on pavements by tires side and longitudinal forces, in addition to those caused by vertical forces. Moreover, the procedure permits to compute the regulation diagrams of the system, fundamental to use its full potential for all working conditions.
Examples of the advantages associated to the use of the MB model are provided in the paper. These are certainly relevant in the context of the structural design of the various components of the test facility and can be especially useful to optimize the choice and positions of various force and displacement sensors. By running MB simulations it is also possible to appreciate the effects caused by different configurations of the suspensions of the trolleys.
The next step which will be performed within the research which is currently being develop by the Pavement Engineering and Vehicle Dynamics groups of the Politecnico di Torino will consist in the full implementation of a FEM model of the structure of the APT facility to be run in co-simulation with the MB model. Furthermore, results derived from MB and FE modelling will be used as input data for the evaluation of the stresses and strains induced in pavements by different loading systems.

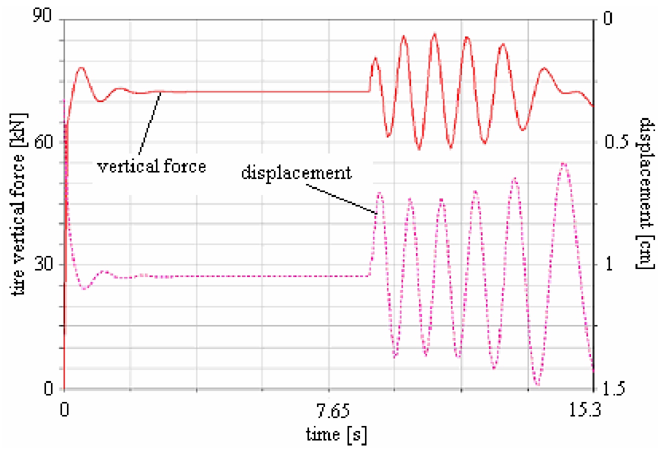

Figure 15 Wheel vertical force and displacement during a test on a sinusoidal pavement profile.

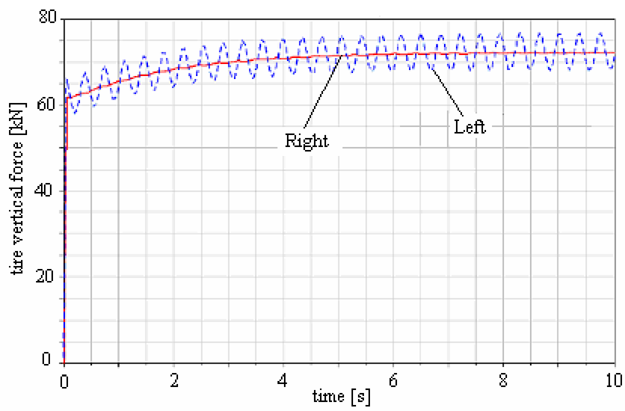

Figure 16 Tire vertical force in the case of trailing arm suspension and sinusoidal road profile for the left wheel.

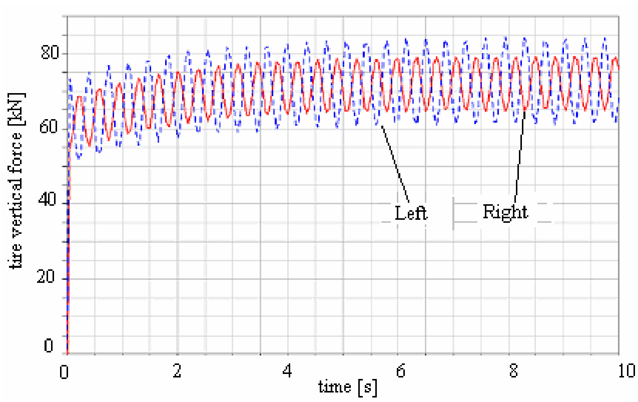

Figure 17 Tire vertical force in the case of modified suspension and sinusoidal road profile for the left wheel.

REFERENCES

[1] NCHRP Synthesis 325, Significant findings from Accelerated Pavement Testing. *Transportation Research Board 2004*, USA.

[2] NCHRP Synthesis 325, Application of Full-Scale Pavement Accelerated Testing. *Transportation Research Board 1996*, USA.

[3] Pacejka H.B., *Tire and Vehicle Dynamics*. SAE International, 2002.

[4] Cardano G., *Ars Magna*. Nurnberg, 1545.

[5] *ADAMS View® User's Manual*, MSC Software, 2001.

[6] Fiala E., *Seitenkrafte am rollenden Luftreifen*. VDI Zeitschrift, 1954.

[7] Steven B.D., De Pont J.J., Pidwerbeski B.D. and Arnold G., Accelerated Dynamic Loading of Flexible Pavements at CAPTIF. *1999 International Conference on Accelerated Pavement Testing*, 1999.

ISSN 1590-8844
International Journal of Mechanics and Control, Vol. 08, No. 02, 2007

A CHARACTERIZATION OF CAM TRANSMISSIONS THROUGH IDENTIFICATION OF LUMPED PARAMETERS

Giuseppe Carbone * Chiara Lanni * Giovanni Incerti ** Marco Ceccarelli *

* DiMSAT - University of Cassino, Italy
** University of Brescia - Italy

ABSTRACT

In this paper, a numerical-experimental procedure is proposed for an identification of parameters in cam transmissions. Models with lumped parameters are defined specifically for cam transmissions. Experimental tests are carried out on main components of a cam transmission in order to estimate the values of mass, damping and stiffness lumped parameters through a low-cost easy-operation procedure. Experimental tests are also carried out in order to characterize the dynamic behaviour of a whole cam transmission. A comparison of numerical and experimental results is used in order to calibrate the values of lumped parameters. Experimental tests have been carried out by means of suitable test-beds for cams that have been built specifically at University of Brescia and at LARM in Cassino as alternative testing solutions.

Keywords: Mechanical Transmission, Cams, Mechanism Analysis

1 INTRODUCTION

A cam is a mechanical element used for transmitting a desired motion to another mechanical element by direct point or line contact. Cam systems are generally composed by three basic parts: a cam, which is the driving member, a follower, and a fixed frame, [1]. The cam can rotate, translate, oscillate or even remain stationary. The follower can have a translating or oscillating motion. Due to the type of contact of the moving parts cam mechanisms form higher kinematic pairs, [2]. They are used for transmission of power or information, as pointed out in [3]. Cam systems are applied in a great variety of applications where simple and economic control systems are needed, [4]. They are frequently implemented in automatic and textile machinery, cutting and forming presses, engines, fast manufacturing, equipment.

Contact authors: Giuseppe Carbone[1], Giovanni Incerti[2]

[1] LARM: Lab. of Robotics and Mechatronics
DiMSAT – University of Cassino
Via Di Biasio 43 - 03043 Cassino (Fr), ITALY
E-mail: carbone@unicas.it

[2] Dept. of Mechanical Engineering
University of Brescia
Via Branze 38 - 25123 Brescia, ITALY
E-mail: giovanni.incerti@ing.unibs.it

The main design phase for a cam transmission consists in defining a suitable cam profile that can provide the prescribed displacement diagram of the follower, [1-3]. At LARM in Cassino a specific line of research has been devoted to design circular-arc cams with the aim to develop modern computer-oriented algorithms both for analysis and synthesis purposes. However, several dynamic aspects should be taken into account in the design process. Therefore, researches have proposed optimum design procedures to take into account both kinematic and dynamic aspects, [3, 5, 6]. But these optimum design procedures require the definition of a proper dynamic model.

Several researches have proposed dynamic models for cam transmissions, [6-18].

Methods for identification of damping parameters for a generic dynamic system are proposed for example in [19, 20]. An experimental procedure for an easy identification of the curvature of cam profiles is also proposed in [21, 22]. In this paper, the problem of identification of lumped parameters is addressed both from the theoretical and experimental point of view in a single procedure. A numerical-experimental procedure for parameter identification of lumped parameter models for cam transmission is discussed in order to be able to properly de scribe the dynamic behaviour of a real cam system. In addition, special attention has been addressed in defining proper models with lumped parameters.

In fact, models should take into account all the phenomena that characterize the real system but at the same time they should be as simple as possible. In fact, in a too complex model the solution of equations of motion can require high computational efforts and sometimes a feasible solution cannot be even found as pointed out, for example, in [23, 24].

2 CAM TRANSMISSIONS

Cam transmissions are characterized by the transmission capability due to the cam profile both in terms of kinematic and dynamic performances. Therefore, a suitable design of a cam transmission strongly depends on the cam profile and its characteristics for a theoretical synthesis and a practical application. Usually, a designer chooses a motion law for a definition of a cam profile and consequently all the other geometric and constructive parameters can be defined. However, only an experimental validation can guarantee that kinematic and dynamic behaviour of a built cam is acceptable for specific applications.
In addition, it is of fundamental importance to achieve an optimum kinematic design of a cam profile but it is important as well to determine the effects of design parameters and their errors on the operation performance in practical applications.
An experimental-numerical procedure for identification of lumped parameters can be useful for better characterizing the dynamical behaviour of a cam system.
The abovementioned procedure can be summarized in the following steps: 1) identification of design constraints and performance characteristics for a given application; 2) formulation of basic performances; 3) definition of N-dofs lumped parameter model; 4) identification of measurable numerical and/or experimental lumped parameters; 5) identification of non measurable lumped parameters; 6) fine tuning procedure of non measurable parameters by using an optimization technique; 7) validation of obtained lumped parameters; 8) experimentally validation of the obtained model in order to guarantee a predefined confidence error.
In this paper, a proper procedure defined by the abovementioned 8 steps is proposed in order to define suitable dynamic models of cam transmissions. This procedure is based on a combination of theoretical and experimental aspects in order to have suitable modelling of a real system behaviour. Thus, this model can be considered for design purposes without the need of using empirical safety coefficients.

3 MODELS WITH LUMPED PARAMETERS

A general model of multi-dof cam transmission can be defined by using lumped parameters as proposed in [2, 25]. In this type of models properties and behaviours of a real system are replaced by mass (or inertia), stiffness and damping elements that are concentrated in given points.
In general it is possible to assume that mass or inertia elements are rigid bodies with negligible damping. Usually these type of elements are lumped in their centre of mass. They can gain or loose kinetic energy only when the linear and/or angular velocity of the body changes and the forces and torques that it can apply are proportional to its mass and accelerations.
Stiffness elements are assumed to have negligible mass and damping. They are modelled as linear or torsional springs. They can store or loose potential energy and apply a force that is proportional to the deformation of the spring that is given as the displacement of one end of the spring with respect to the other one.
Damping elements are assumed to have negligible mass and stiffness. They are modelled as dampers. They describe the mechanism of gradual dissipation of vibrational energy of a system into heat and sound. A damping force is obtained only if there is a relative velocity between two ends of a damper.
Figure 1 shows a model with lumped parameters of a cam-follower. In this model, it has been assumed that: the cam operates at constant speed, regardless of forces acting on it; the reaction spring connected to the frame always prevents separation of the follower from the cam; the ground is assumed as rigid.
A two degrees of freedom model has been derived as shown in Fig.1. It is composed by one linear spring that represents the lumped stiffness parameters k_1 of the valve; one linear spring that represents the lumped stiffness parameters k_2 of the follower; one linear spring that represents the lumped stiffness parameters k_3 of the ground; one torsional spring that represents the lumped stiffness parameters k_T of the cam; three dampers that represent the lumped damping parameters c_1 of valve, c_2 of follower and c_3 of ground, respectively.
More complex models can be defined in order to take into account mass distributions, non constant input speed, reactions of the ground, effects of backlash and friction like for example the model with 5 degrees of freedom that is shown in Fig.2, [24].
The model of Fig.2 is based on the following assumptions: the displacements of the spring mass m_s, follower mass m_f,

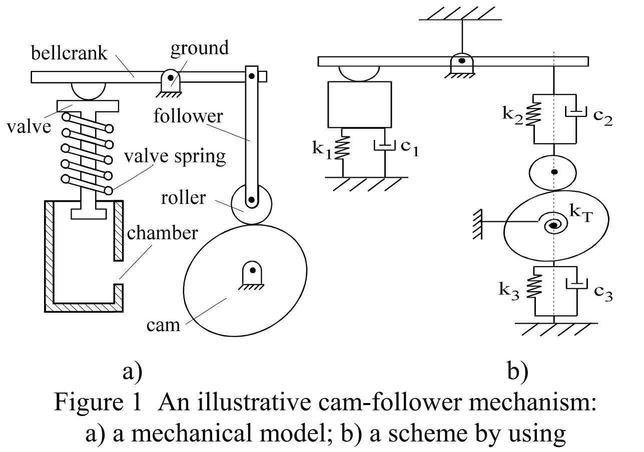

a) b)

Figure 1 An illustrative cam-follower mechanism: a) a mechanical model; b) a scheme by using lumped parameters.

roller mass m_r and cam mass m_c can be described with reference respect to the XY frame by means of the coordinates y_s, y_f, y_r, y_M and y_c, respectively. k_s and c_s are the structural stiffness and damping coefficients of the spring elements, respectively; k_f and c_f are the structural stiffness and damping coefficients of the follower; k_r is the structural stiffness coefficient for the roller; k_T is the structural torsional stiffness of the cam element; k_g and c_g are the structural stiffness and damping coefficients of the ground, respectively; g_f is a gap due to the clearance between the cam and follower; finally J_c is moment of inertia of the cam expressed with respect to its centre of rotation. Details are reported in [24].

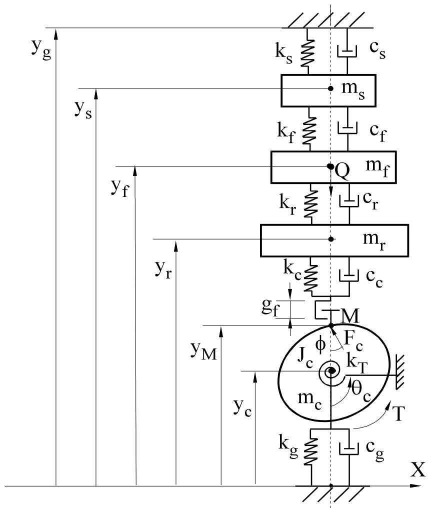

Figure 2 A lumped parameters model of a cam mechanism with 5 degrees of freedom, [24].

4 IDENTIFICATION OF CAM PARAMETERS

One of the main problems of using models with lumped parameters is the identification of numerical values for mass, stiffness and damping lumped parameters.
A lumped mass is used to collect all the mass properties of a mechanical component into a given point. The values of lumped mass parameters can be estimated by knowing the shape of the components and material densities. They can be also measured experimentally by means of a weight measurement.
A lumped stiffness is used to concentrate the rigidity properties of a mechanical component into a given point. The values of lumped stiffness parameters can be estimated by knowing the distribution of the applied forces, shape of the components, material density, Young's and shear modules. For example, the lumped stiffness parameter expressing the axial stiffness of a beam can be computed as

$$k=EA/L \tag{1}$$

where E is the Young's modulus of the material, A is the area of the cross section and L is the beam length. Other effects such as flexural and torsional stiffness can be similarly derived.
The mechanics of continuum theory can be also used for obtaining similar expressions as proposed, for example, by [25]. Alternatively, finite element methods can be used for objects of complex geometry. The stiffness properties can be also computed by measuring the linear and angular compliant displacements for unit forces and torques in static experiments.
A lumped damping parameter is used to concentrate the energy dissipation properties of a mechanical component into a given point. The values of lumped damping parameters depend on the processes that produce the energy dissipation. In particular, there are three main processes that contribute to the energy dissipation during vibratory processes: hysteresis, dry friction, and viscous friction.
In the case of viscous friction if one considers the squeeze-film of a lubricant between the surfaces of a disc cam and its roller follower when a constant viscosity of the lubricant and a constant pressure throughout the film thickness are assumed, the viscous damping c_v can be written as, [26],

$$c_v = 12\pi\eta b\left[\left(\frac{R_1R_2}{R_1+R_2}\right)\frac{1}{2t_f}\right]^{3/2} \tag{2}$$

where t_f is the film thickness; η is the viscosity of the fluid, b is the thickness of the cam or roller, R_1 is the roller radius and R_2 is the cam radius. A simplified empirical expression of the viscous damping c_v can be written for joints with narrow contact surfaces that are lubricated by a thin film of industrial mineral oil of average viscosity as, [27]

$$c_v = \frac{0.31}{\sqrt[3]{P_m}}\frac{m\omega_n}{\pi} \tag{3}$$

where P_m is the mean oil pressure on the contact surface expressed in MPa, m is the mass, $\omega_n = \sqrt{\frac{k}{m}}$ is the natural frequency with k being the lumped stiffness parameter of the same component. Similar empirical expressions for estimating the damping properties can be found in the literature also for different energy dissipation processes as reported for example in [26-28].
An experimental measure of damping parameters can be derived also by referring to modal theory. For example, for small values of damping one can write, [28],

$$\lambda \cong \frac{c\,\pi}{m\,\omega_n} = \ln\frac{A(t)}{A(t+\Delta t)} \tag{4}$$

where c is the damping parameter, λ is the logarithmic decrement, A(t) and A(t+Δt) are two consecutive amplitudes of the damped free vibration of a component. Thus, the experimental measure of two consecutive amplitudes can provide an approximate value of the damping parameter in one direction as, [28]

$$c \cong \frac{\lambda m \omega_n}{\pi} = \left(\ln \frac{A(t)}{A(t+\Delta t)} \right) \left(\frac{m \omega_n}{\pi} \right) \tag{5}$$

An alternative experimental method for measuring damping parameters consists in the identification of the so-called “half-power bandwidth”, [28], for a steady-state harmonic response. It can be used for small damping values and consists in applying a known harmonic external force $F(t)=F_0 \sin(\omega t)$ on the component and by studying the results in the frequency domain in terms of Bode diagrams, (Nashif et al. 1985). In these diagrams one can identify the so-called half-power points that correspond to the frequencies ω_1 and ω_2 of the external force in which the response amplitude is $1/\sqrt{2}$ times the maximum amplitude of deformation. It is worth noting that the relationship between ω_1 and ω_2 and damping parameter c depends on the processes that produce the damping effect. In hysteretic damping the energy loss per cycle is independent from the frequency of vibration and approximately proportional to the square of the amplitude. In this case, the hysteretic damping c_h can be estimated as, [28]

$$c_h = \frac{\omega_2 - \omega_1}{\omega_n} \tag{6}$$

In the case of viscous damping one can write

$$c_v = \sqrt{km}\,\frac{\omega_2 - \omega_1}{\omega_n} \tag{7}$$

The case of dry friction damping cannot be usually derived with the “half-power bandwidth” method since it can show high damping values and non-linearities, [28].

It is worth noting that even friction can affect significantly dynamical behaviour of a cam transmission. A dry friction or Coulomb friction model can be assumed when no lubrication is used between cam and follower contact surfaces.

For example in the case of dry contact the relationship on the viscous friction force F_d as a function of relative velocity can be expressed as proposed in [23] in the form

$$F_d = c_F \dot{y} \tag{8}$$

where c_F is the constant friction coefficient, $\dot{y}$ is the relative velocity between cam and follower. Handbooks such as [29-31], provide values or ranges of values for c_F as function of the materials that are in contact. However, speed, pressure, temperature, cleaning of surfaces can affect the value of c_F. Thus, experimental measures of c_F are often carried out. Nevertheless, the effect of friction can be considered negligible for low-speed cams when a roller with ball bearings and/or lubrication are used. Instead when a lubricant is used the coefficient c_F should be replaced by c_L. This coefficient can be experimentally measured or it can be experimentally estimated in standard conditions, for example, through the expression given by Ubbelhode, [29, 30, 32, 33], as

$$c_L = \rho \left(7.3\,E - \frac{6.3}{E} \right) 10^{-6} \tag{9}$$

where c_L is obtained [$m^2 s^{-1}$]; ρ is the lubricant density; E is a conventional measure of viscosity known as Engled degree, [29, 30, 32, 33], that can be given as

$$E = \frac{t_f}{t_w} \tag{10}$$

where t_f is the time of flow of 200 cubic centimetres of fluids and t_w is the time of flow of 200 cubic centimetres of water. Both t_f and t_w are measured at standard temperature that is usually equal to 20 °C. Nevertheless, the effect of friction can be negligible for low speed cams when a roller with ball bearings and/or lubrication are used. More details on other friction models in presence of lubrication can be found for example in [23].

It is worth noting that for some mechanical parts such as springs and joints, stiffness and damping properties are provided by manufacturers or an approximate value can be found in literature [27, 28]. Nevertheless, stiffness and damping are also affected by the environment conditions and by non-linear behaviours. Therefore, values that can be obtained by using the Eqs.(1) to (6) or by literature should be considered as approximate values or as valid under given conditions only. Starting from the abovementioned values a fine tuning of the stiffness and damping parameters could be carried out by using optimization procedures when experimental values are considered too. In fact, one can compare the numerical and experimental results by considering some lumped parameters as variables (within a given range of tolerance) and using as objective function a measure of difference between numerical and experimental data. An example of this approach is reported in [34, 35]. It is worth noting that the number of parameters that can be tuned with this procedure should be very limited. In fact, one can obtain similar values of the objective function with different non-coincident sets of lumped parameters, when their number is too high, as pointed out for example in [34].

5 A NUMERICAL-EXPERIMENTAL PROCEDURE

A theoretical and experimental procedure for identification of lumped parameters can be defined as proposed in the following. The aim of this procedure is to identify lumped parameters and validate them with proper experimental tests.

The step 1 of the proposed procedure consists in setting the values of ε, N, i, and j. In particular, ε is the maximum acceptable calibration error between the real behaviour of the cam transmission and results obtained though a model with lumped parameters. The value of ε should be chosen by considering the purpose of the model, whose lumped parameters are going to be defined. N is the number of degrees of freedom (dofs) that should be as low as possible. In particular, N has been set as equal to 1 because this is the lowest feasible value. The values for i and j are automatically set equal to 0 since i and j are just counters for the number of lumped parameters and number of measurable lumped parameter, respectively. After setting these values the procedure defines a model with lumped parameters having N dofs, and a maximum number of lumped parameters equal to I.
The next step 2 of the procedure consists in identifying the maximum number of lumped parameters J that can be experimentally measured. This step is achieved by means of a loop that starts with i equal to 0 and ends with i equal to I. At step 3 the J lumped parameters are experimentally measured by means of weight measurements for lumped masses, by measuring compliant displacements for unit forces in static experiments for the lumped stiffness parameters, by means of Eqs.(5) to (8) and harmonic response experiments for damping lumped parameters. At step 4 the (I-J) non experimentally measurable lumped parameters are numerically computed, for example by means of Eqs.(1) to (3).
Step 5 of the procedure consists in implementing a numerical simulation of the dynamic properties of the cam transmission as based on a mechanical model with N dofs and values of lumped parameters that have been obtained in previous steps. This numerical simulation provides as results linear and angular positions, velocities, accelerations, jerks, input and reaction forces and/or torques as functions of time. Then, the most significant simulation results are stored as a multi-array vector of numerical results $\mathbf{r_s}$.
In step 6 a proper test-bed for a real cam transmission is defined so that main dynamic properties of the system can be experimentally measured. The operation conditions are properly chosen so that they show significant results within the operating range of the system. They are also chosen so that experimental results are given at the same operation conditions of numerical simulations. Then, experimental results are stored in a multi array vector of experimental results $\mathbf{r_d}$.
At step 7 a calibration error Δ is computed as a function of comparison between numerical and experimental results. It is worth noting that there are several ways of computing the calibration error Δ. Among the many available techniques for data fitting, [36, 37]. The least-square method has been used since it is widely used in the literature and provides a single value for Δ. Thus, Δ can be formulated as a sum of the weighted square difference between the values of numerical computations and experimental results as

$$\Delta = \sum_i (r_{d_i} - r_{s_i})^2 w_i \qquad (11)$$

where r_{di} is a multi-array vector of numerical results ; r_{si} is a multi-array vector of experimental results; w_i is a weight factor.
This criterion used produces a minimum value which represents the best fit according to the least square criterion, as pointed out for example in [38]. In particular, this minimum values has been calculated by means of CONSTR code within the Matlab Optimization Toolbox.
The way of measuring the calibration error Δ is related with the type of results that are compared. Moreover, one should also consider the use of proper hardware and software filters in case of experimental results that have been obtained in presence of significant noise sources.
After that, the value of Δ has been properly computed, one can compare it with ε. If the calibration error Δ is higher than ε, the step 8 proceeds to a fine tuning of the J parameters that cannot be experimentally measured by means of a multicriteria optimization technique. In multicriteria optimization, one deals with a design variable vector **v**, which will satisfy all the constraints and makes the scalar performance index as small as possible. This index is calculated by taking into account each component of an objective function vector **F**(**v**). A possible approach to this problem is the so-called compromise programming as indicated for example in [36]. This approach does not provide unique solution to the problem but a set of solutions named as Pareto-optima set. The use of weighted objective functions is one of the most usual, alternative approaches for multi-objective optimization problems. It converts the multi-objective problem of minimizing the function vector **F**(**v**) into a scalar one by constructing a weighted sum of all the objectives.
A multicriteria optimization can be defined as

$$\mathbf{F(v)}=\min(\Delta) \qquad (12)$$

subjected to

$$\mathbf{G(v)}=0; \qquad \mathbf{H(v)}=0 \qquad (13)$$

where **v** is the vector of design variables; **F**(**v**) is the vector of objective functions that express the optimality criteria, **G**(**v**) is the vector of constraint functions that describe limiting conditions, and **H**(**v**) is the vector of constraint functions that describe the design prescriptions.
Optimality criteria for cam transmissions can be identified in terms of performance evaluations as for example:

- in a required rise law for the follower given in correspondence of a specific application;
- in a high force transmission ratio between cam and follower in order to guarantee a good mechanical efficiency;
- in a limited range of variation of the input torque in order to avoid the use of a big and/or small flywheel or

short working life for the input motor;
- in a dynamic behaviour of the follower in order to avoid vibratory phenomena.

The multi-objective function **F** can be formulated by using computer-oriented algorithms when its components are computed numerically through suitable analysis procedures. The constraint functions **G** and **H** can be formulated by using suitable evaluation of design and operation constraints
and also for additional constraints that are needed for computational issues. The problem for obtaining optimal results from multi-objective optimization problem can be subdivided in two basic parts such as:
- to choose a numerical solving technique;
- to formulate the optimality criteria with computational efficiency.

In particular, the solving technique can be selected as
- commercial software packages;
- non-linearity type;
- involved computations for the optimality criteria and constraints.

On the other hand, the formulation and computations for the optimality criteria and design constraints can be conceived and performed by looking also at the peculiarity of the numerical solving technique. Those two basic parts can be very helpful in order to obtain an optimal design procedure that can give solutions with no great computational efforts and with the possibility of engineering interpretation and guide.
It is worth to note that the formulated problem is intrinsically highly non-linear. Its solution will be obtained when the numerical evolution of the tentative solutions due to the iterative process converges to a solution that can be considered optimal within the explored range. But this solution can be considered only as a local optimum. This last remark makes clear once more the influence of suitable formulation with computational efficiency for the involved criteria and constraints in order to have a procedure, which is significant from engineering viewpoint and numerically efficient.
If the optimization technique does not provide feasible results or if the calibration error Δ is higher than ε, it means that a model with N dofs does not take into account all the main phenomena that characterize the real system. Therefore, the model with lumped parameters should be modified by considering more aspects and the procedure is iterated by going back to step 1. Otherwise, if the calibration error Δ is lower than ε, it means that a proper model of the real cam transmission has been identified. Thus, in the step 9 one can obtain as output the values of lumped parameters that have been identified and the validated mechanical model.
Main advantages of the proposed procedure are: definition of a model having the minimum set of lumped parameters; numerical and experimental identification of proper lumped parameters; experimental validation of both model and values of lumped parameters for a given calibration error.

6 TEST-BEDS AND RESULTS

Illustrative examples are reported as application of the proposed procedure for different systems in different institutions with different previous experiences.

6.1 EXPERIENCES IN BRESCIA

The indexing cam that is shown in Fig.3 has been studied at University of Brescia. This indexing cam is driven by an AC motor that is controlled by an inverter with an open loop control. This indexing cam is typically used in heavy-duty applications for producing cyclical movements of a moving platform. Models with lumped parameters have been developed for this indexing cam as shown in Fig.4.
Figure 4 shows a model for the indexing cam mechanism of Fig.3. The motor is described by its characteristic function $T_m = T_m(\dot{\gamma})$. The clearances of the gear speed reducer and the elasticity of the mechanical members are modelled by means of elastic elements, as reported in Fig.4. Backlash g_1 is due to the tolerances between the teeth of the speed reducer; its value is particularly important when the transmission ratio is high.
In this paper g_1 has been assumed equal to 0.8 deg. by considering results of experimental tests. The coupling between the table and the indexing mechanism output shaft mainly causes clearance g_2, which is generally very close to zero. Finally, the damping variables have been considered as scalar constant values, as well as all the moments of inertia.
The model with lumped parameters in Fig. 4 takes into

a)

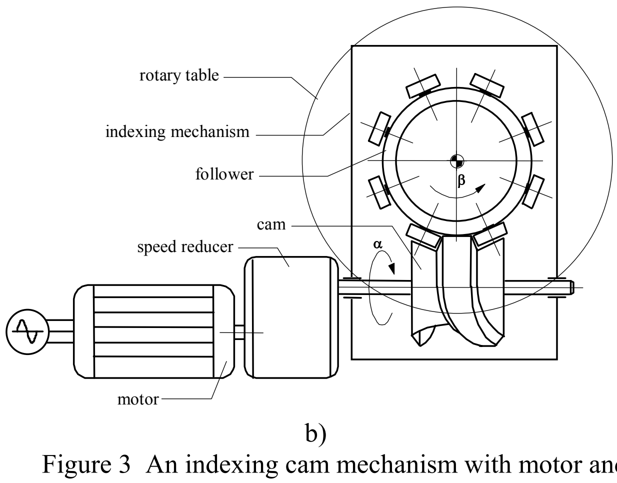

b)

Figure 3 An indexing cam mechanism with motor and speed reducer, [39]: a) a picture; b) a scheme.

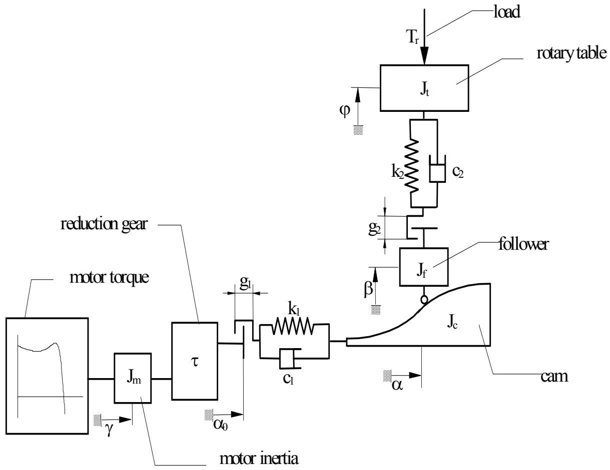

Figure 4 A lumped model for the indexing cam mechanism in Fig.3.

account the effects due to stiffness of the follower, damping of the follower, characteristics of the motor, presence of clearance in the gear speed reducer, elasticity and structural damping of the input shaft.

Further details on this model are reported in [34, 35]. The following equations have been derived for the model of Fig.4

$$\ddot{\alpha} = \frac{M_1 + \beta' M_2 - J_f \beta' \beta'' \dot{\alpha}^2}{J_c + J_f \beta'^2}$$
$$\ddot{\varphi} = -\frac{T_r + M_2}{J_t} \tag{14}$$
$$\ddot{\gamma} = \frac{T_m - \tau M_1}{J_m}$$

where dots indicate time derivatives, apices indicate derivatives calculated with respect to the angle α (rotation of the cam); of course, if the motor motion $\gamma(t)$ is known, it is sufficient to consider only the first two equations of the set in Eq.(12).

The symbols M_1 and M_2 represent the torques transmitted by the spring-damper elements; in presence of mechanical clearances, their analytical expressions are

$$M_1 = \begin{cases} 0 & \left|\alpha_0 - \alpha\right| \le \dfrac{g_1}{2} \\ k_1\left(\alpha_0 - \alpha - \dfrac{g_1}{2}\right) + c_1\left(\dot{\alpha}_0 - \dot{\alpha}\right) & \alpha_0 - \alpha > \dfrac{g_1}{2} \\ k_1\left(\alpha_0 - \alpha + \dfrac{g_1}{2}\right) + c_1\left(\dot{\alpha}_0 - \dot{\alpha}\right) & \alpha_0 - \alpha < -\dfrac{g_1}{2} \end{cases} \tag{15}$$

$$M_2 = \begin{cases} 0 & \left|\varphi - \beta\right| \le \dfrac{g_2}{2} \\ k_2\left(\varphi - \beta - \dfrac{g_2}{2}\right) + c_2\left(\dot{\varphi} - \dot{\beta}\right) & \varphi - \beta > \dfrac{g_2}{2} \\ k_2\left(\varphi - \beta + \dfrac{g_2}{2}\right) + c_2\left(\dot{\varphi} - \dot{\beta}\right) & \varphi - \beta > \dfrac{g_2}{2} \end{cases} \tag{16}$$

Numerical simulations have been carried out by using the model of Fig.4. In particular, the lumped parameters have reported in Table I.

In addition, experimental tests have been carried out on the indexing cam by using an incremental encoder Eltra L72 that is installed on the input shaft, an accelerometer Entran ECGSY-240D2-10 and an inertial load that are installed on the rotating platform. Experimental results have been obtained by using LabView software and a NI AT-MIO-16-H9 Acquisition Card. The abovementioned setup can measure the angular position of the input shaft and tangential acceleration of the rotating platform for different input angular velocities of the input shaft and for different inertial loads.

The plots in Fig.5 show numerical and experimental results for the indexing cam of Fig.3.

The comparison of results in Fig.5a) and b) shows a calibration error Δ=0.2 calculated by using Eq.(9). Thus, the model of Fig.5 and the values of lumped parameters in Table I have been validated for the indexing cam in Fig.3 when a maximum calibration error of 0.2 rad/s^2 is considered as acceptable. Therefore, the validated model can be considered as a useful tool for determining the effective performance of the indexing cam in Fig.3 but also for testing new design solutions and influence of the various design parameters.

Table I - Values of the lumped parameters for the model of Fig.4

k_1 (Nm/rad)	k_2 (Nm/rad)	C_1 (Nm/rad)	C_2 (Nms/rad)
$6.5 \cdot 10^5$	$3.5 \cdot 10^7$	2000	70000
τ	J_t (kg·m^2)	J_f (kg·m^2)	J_c (kg·m^2)
1/124	14500	92	7.6

6.2 EXPERIENCES AT LARM IN CASSINO

Another illustrative example has been carried out at LARM on a three circular-arc cam by means of the test-bed that is shown in Fig.6. Referring to Fig.6, one accelerometer S_1 has been installed on the follower.

The accelerometer gives the possibility to measure and monitor the acceleration and the motion of the follower. In addition, the dynamic performances can be experimentally evaluated by using a dynamic torsionmeter S_2, which has been installed on the motor shaft. Signal conditioner and amplifiers U_1 and U_2 have been used in order to provide the power supply to S_2, S_3, and S_4, respectively, and reduce the noise on the output of the sensors. One encoder S_3 and one tachometer S_4 have been installed on the camshaft In particular, the encoder gives the possibility to monitor the position of the camshaft, whereas the tachometer is used to monitor and measure the velocity of the camshaft. Three different power supply sources A_1, A_2 and A_3 have been used in order to provide different input voltage to the four sensors and motor. It has been used LabView software with

ISSN 1590-8844
International Journal of Mechanics and Control, Vol. 08, No. 02, 2007

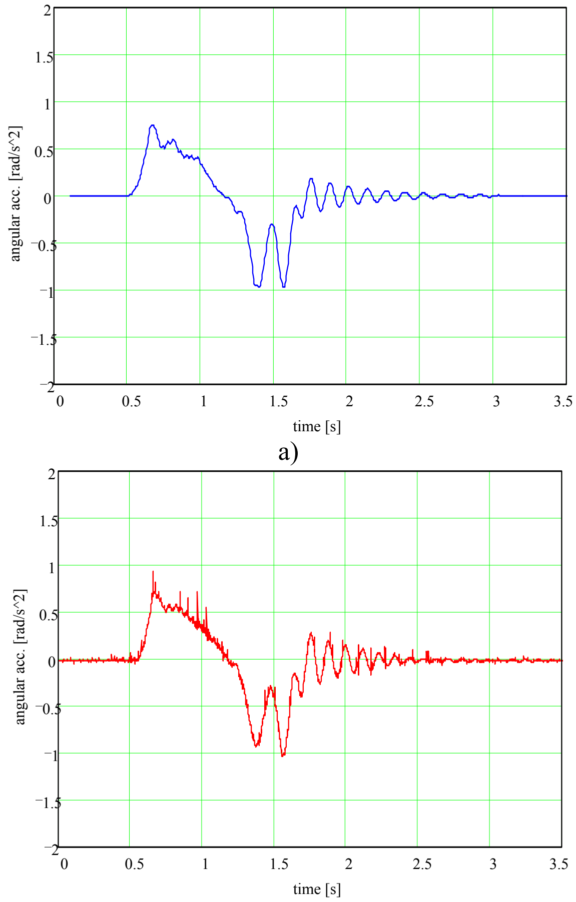

Figure 5 A comparison between numerical and experimental results for the indexing cam of fig.3: a) simulated acceleration; b) measured acceleration.

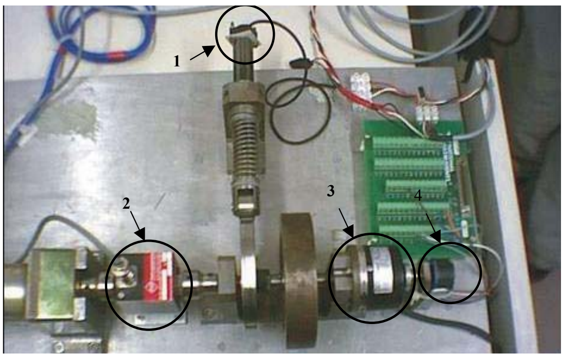

Figure 6 Test-bed for cam testing at LARM in Cassino: 1- accelerometer; 2- dynamic torsionmeter; 3- tachometer; 4- encoder.

NI 6024E Acquisition Card, to work with virtual instruments, which manage commercial sensors.
Figure 7 shows a simplified model of the cam system of Fig.6 under the condition of combined linear moving masses in which the equivalent mass m_s+m_f+m_r represents all the moving masses in the follower system.
The displacement of the total mass can be described with respect to the XY reference frame by means of the coordinate y_{rfs}. The internal damping c_{rfs} of the system element is represented by an equivalent viscous damping contribution of roller, follower, and spring.
The motivation of using this simplified model is based on the small size of the roller and spring with respect to the size of the follower. Thus, masses of roller and spring have been considered as negligible.
The dynamics of a cam system in Fig.7 can be expressed by the equations of motion in the following form

$$
\begin{aligned}
&(m_f + m_r + m_s)\ddot{y}_{rfs} = -k_s(y_{g0} - y_{rfs0}) + k_s(y_g - y_{rfs}) \\
&- c_{rfs}\,\dot{y}_{rfs} + k_c(y_{rfs0} - y_{M0}) - k_c(y_{rfs} - y_M) + \\
&- c_c(\dot{y}_{rfs} - \dot{y}_M) - Q
\end{aligned}
\tag{17}
$$

$$
\begin{aligned}
&Q\tan(\phi) = -k_c(y_{rf0} - y_{M0}) + k_c(y_{rf} - y_M) + \\
&+ c_c(\dot{y}_{rf} - \dot{y}_M)
\end{aligned}
\tag{18}
$$

The masses, stiffness and damping values have been assumed as reported in Table 2 by referring to a test-bed for cam systems that is available at LARM, Fig.6.
The plots of Fig.8a) show the result of the numerical simulation with the model in Fig.8 for an input shaft speed of 176 rpm. The plots of Fig.8b) show the experimental results for the same case. It is worth noting that in this case a complete rotation of the cam is obtained in 0.34 sec. The comparison of results in Fig.8a) and b) shows a calibration error Δ= 0.2 m/s^2 by using the expression in Eq.(9).
Thus, the model of Fig.7 and the values of lumped parameters in Table II have been validated for the cam system in Fig.6 when a maximum calibration error of 0.2 m/s^2 is considered as acceptable.
Therefore, the validated model can be considered as a useful tool for determining the effective performance of the cam system in Fig.6 but also for testing new design solutions and influence of the various design parameters.
The results of Fig.8 show a reasonable match between simulated values and measured acceleration values on the follower. It is worth noting that a satisfactory match has

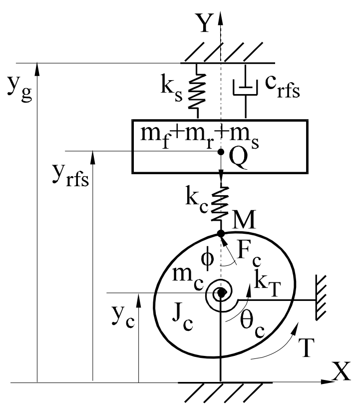

Figure 7 Simplified model of a cam system by using lumped parameters in the case of combined linear moving masses.

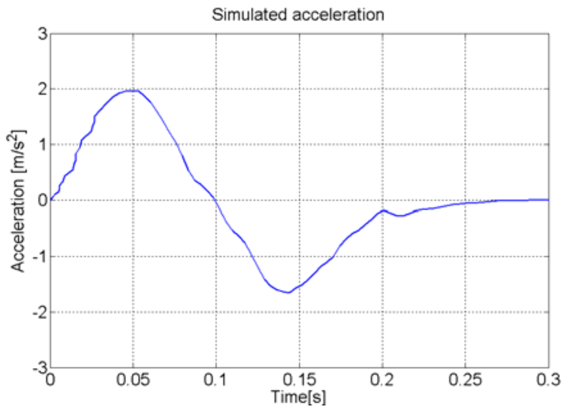

a)

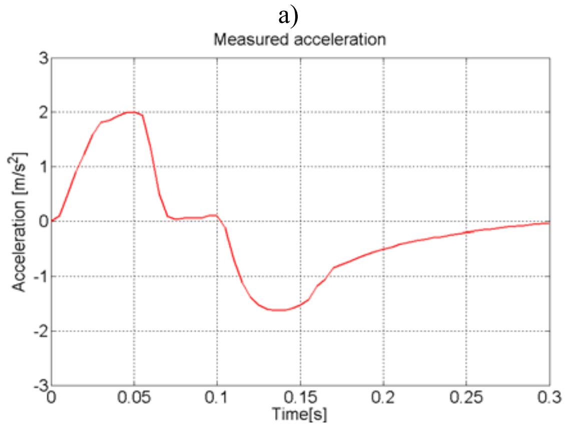

b)

Figure 8: A comparison between the numerical and experimental results for the circular-arc cam: a) simulated acceleration; b) measured acceleration.

Table II - Values of the lumped parameters for the model of Fig.7

m_c (kg)	m_s (kg)	m_r (kg)	m_f (kg)	c_{rfs} (Ns/m)
0.374	0.018	0.040	0.325	10
k_s (N/m)	k_T (Nm/rad)	k_c (N/m)	J_c (kg·m^2)	
235	5.00 10^4	10^7	3.76 10^{-3}	

been obtained for the case with a input speed of the camshaft equal to 176 rpm. Of course, the validation of the model of Fig.7 is suitable only for low speeds ranging from about 100 to 200 rpm. In fact, for the circular-arc cam that has been tested the actuator cannot guarantee the continuous motion of the cam system when the speed of the input shaft is less than about 100 rpm the inertial effects become dominants as pointed out [40]. When the speed of the input shaft is greater than about 200 rpm the dynamical effects become dominants and the spring cannot guarantee the continuous contact of follower with cam surface due to jump phenomena. The modeling of the abovementioned effects require models with higher number of dofs and more complex formulations, which are out of the scale of this paper.

CONCLUSIONS

This paper refers to the identification of proper dynamic models of cam transmissions for experimental identification of lumped parameters. In particular, a numerical-experimental procedure has been proposed for the identification and fine tuning of lumped stiffness and damping parameters specifically for cam transmissions. Experimental tests are carried out also to characterize the dynamic behaviour of cam transmissions as a whole. The experimental tests have been used in order to validate a dynamic model with lumped parameters. Then, a comparison of numerical and experimental results can be used in order to calibrate the values of lumped parameters by means of a suitable optimization algorithm that is proposed in the paper. The validated models can be considered as a useful tool for determining the effective performance of specific cam systems but also for testing new design solutions and the influence of the various parameters on the dynamics.

REFERENCES

[1] Rothbart H.A., *Cams design, dynamics and accuracy*. John Wiley & Sons, New York, 1956.

[2] Magnani P.L. and Ruggieri G., *Mechanisms for automatic machinery*. UTET, Torino, (Italian), 1986.

[3] Angeles J. and Lopez-Cajun C.S., *Optimization of cam mechanisms*. Kluwer Academic Publishers, Dordrecht, 1991.

[4] Uicker J.J.Jr., Pennock G.R. and Shigley J.E., *Theory of machines and mechanisms*. Oxford University Press, New York, 2003.

[5] Cardona A., Lens E. and Nigro N., Optimal design of cams. *Multibody System Dynamics*, Vol. 7, pp 285-305, 2002.

[6] Carbone G., Lanni C., López-Cajún C.S. and Ceccarelli M., Numerical and experimental simulation of dynamic operations of cams. *ECCOMAS Thematic Conference Multibody Dynamics 2005*, Madrid, CD Proceedings, paper n. MB02, 2005.

[7] Koster M.P., *Vibrations of cam mechanisms*. The Macmillan Press, London, 1974.

[8] Tesar D. and Matthew G.K., *The dynamic synthesis, analysis, and design of modelled cam systems*. D.C. Heath and Company, Lexington, Mass., 1976.

[9] Kim H.R. and Newcombe W.R., The effect of cam profile errors and system flexibility on cam mechanism output. *Mechanism and Machine Theory*, Vol.17, No.1, pp 57-72, 1982.

[10] Hanachi S. and Freudenstein F., The development of a predictive model for the optimisation of high-speed cam-follower systems with coulomb damping, internal friction and elastic and fluidic elements. *ASME Journal of Mechanisms, Transmission, and Automation in Design*, Vol. 108, pp 506-515, 1986.

[11] Dalpiaz G. and Rivola, A., A kineto-elastodynamic model of a mechanism for automatic machine. *IX. IFToMM Congress*, Milan, pp 327-3321995.

[12] Dresner T.L. and Barkan P., New methods for dynamic analysis of flexible single-input and multi-input cam-follower systems. *Transaction of ASME, Journal of Mechanical Design*, Vol.117, pp 150-155, 1995.

[13] Rao S.S., *Mechanical vibrations*. Addison-Wesley, Reading, 1995.

[14] Reeve J., *Cams for industry*. London, Paston Press Ltd, 1999.

[15] Carbone G., Lanni C., Ceccarelli M. and Lopez-Cajùn C., Dynamic effects of curvature change in the profile of two-circular-arc cams, *V Congresso Iberoamericano di Ingegneria Meccanica*, Merida, pp 1247-1252, 2001.

[16] Zongyu C., Ce Z., Yuhu Y. and Yuxin W., A study on dynamics of roller gear cam system considering clearances. *Mechanism and Machine Theory*, Vol.36, pp 143, 2001.

[17] Rivola A., Carlini A. and Dalpiaz G., Modelling the elastodynamic behaviour of a desmodromic valve train. *Proceedings of SMA2002 International Conference on Noise & Vibration Engineering*, Leuven, 2002.

[18] Carra S., Garziera R. and Pellegrini M., Synthesis of cam with negative radium follower and evaluation of pressure angle. *Mechanism and Machine Theory*, Vol.39, pp 1017-1032, 2004.

[19] Qaisi M.I., Non-linear normal modes of a lumped parameter system. *Journal of Sound and Vibration*, Vol. 205, No.2, pp 205-211, 1997.

[20] Lee J.-H. and Kim J., Identification of damping matrices from measured frequency response functions. *Journal of Sound and Vibration,* Vol. 240, No.3, pp 545-565, 2001.

[21] Ceccarelli M., Carbone G., Lanni C. and Ottaviano E., A fairly simple method to identify the curvature of a cam profile. *ASME International Design Engineering Technical Conferences IDETC'04*, Salt Lake City, paper n. DETC2004-57387, 2004.

[22] Ceccarelli M., Lanni C. and Carbone G., Numerical and experimental analysis of cam profiles with circular-arcs. *IX. International Conference on the Theory of Machines and Mechanisms*, Liberec, Keynote Lecture, pp 189-207, 2004.

[23] Norton R.L., *Cam Design and Manufacturing Handbook*. Industrial Press, Worcester Polytechnic, 2002.

[24] Lanni C., Carbone G., Ottaviano E. and Ceccarelli M., Modelling of cam transmissions. *Proceedings of First International Congress Design and Modelling of Mechanical Systems*, *CMSM'2005*, paper n. CMSM05LANNI, 2005.

[25] Pisano A.P. and Freudenstein F., An experimental and analytical investigation of the dynamic response of a high-speed cam-follower system. Part 2: A combined, lumped-distributed parameter dynamic model. *ASME Journal of Mechanisms, Transmission, and Automation in Design*, Vol. 105, pp 699-704, 1983.

[26] Chen F.Y, *Mechanics and design of cam mechanisms*. Pergamon Press, New York, 1982.

[27] Rivin E.I., *Stiffness and damping in mechanical design*, Marcel Dekker Inc., New York, 1999.

[28] Nashif A.D., Jones D.I.G. and Henderson J.P., *Vibration damping*. John Wiley & Sons, New York, 1985.

[29] Dinsdale A. and Moore, F., *Viscosity and its measuremen*t. Elsevier, Reinhold Publishing, New York, 1962.

[30] Schey J. A., *Tribology in metalworking: friction, lubrication and wear*. American Society For Metals, Metals Park, 1983.

[31] Ghigliazza R. and Galletti C.U., *Mechanics applied to machines*. UTET, Torino, 1986, (in Italian)

[32] Fuller D. O., *Theory and practice of lubrication for engineers*. John Wiley and Sons Inc., Second Edition, New York, 1984.

[33] Scotto Lavina, *Applications of mechanics applied to machinery*. Ed. Siderea, Roma, 1990, (in Italian).

[34] Bussola R., Faglia R., Incerti G., Magnani P.L. and Tiboni M., Indexing cam mechanisms: a complex mathemaical model for simulation. *Proceedings of the X IFToMM Congress*, Oulu, Vol.1, pp 246-251, 1999.

[35] Bussola R., Faglia R., Incerti G. and Tiboni M., Mechanisms for motion transformation driven by controlled actuators: an original approach for their dynamic optimization. *20th IASTED International Conference of Modelling, Identification and Control, MIC 2001*, Innsbruck, Vol.2, pp 617-622, 2001.

[36] Grace A., *Optmization toolbox for use with Matlab*. The MathWorks Inc., Natick, 1992.

[37] Arora J.S., *Introduction to Optimum Design*. McGraw-Hill Inc., Singapore, 1989.

[38] Press W. H., Teukolsky S.A., Vetterling W.T. and Flannery B.P., *Numerical recipes in c, The Art of scientific Computing*. Second Edition, Cambridge University Press, New York, 1992.

[39] Colombo Filippetti, webpage http://mycf.cofil.it/, 2006.

[40] Greco G., *Analysis and experiments of three circular-arc cams*, Master Thesis, LARM, University of Cassino, Cassino, 2002 (in Italian).

ACKNOWLEDGMENT

The authors wish to thank Dr. Hanfried Kerle of the Institute of Machine Tools and Production Technology at Technical University of Braunschweig (Germany) for the helpful comments and reviewing this paper.

ISSN 1590-8844
International Journal of Mechanics and Control, Vol. 08, No. 02, 2007

PSEUDO-DYNAMIC SIMULATION METHOD SOLVING HYDRAULIC STATIONARY PROBLEMS

Lorenzo Borello Matteo D. L. Dalla Vedova

Department of Aerospace Engineering, Politecnico di Torino
Corso Duca degli Abruzzi 24 – 10129 TORINO

ABSTRACT

The conception, layout and design of any dynamic system start from activities focused on the first-approach definition of the principal characteristics of the system itself, essentially from the point of view concerning the compliance of its performance with the customer requirements; such first-approach analysis, concerning the definition of the system steady state performance, is usually based on relatively simple physical-mathematical models able to match only the stationary phenomenons involved in their operation, neglecting the dynamic analysis. When such stationary models are mathematically represented by systems of non-linear algebraic equations of difficult or impossible solution in closed form, in order to solve the system itself, it is necessary to employ iterative methods specifically shaped on the definite problem and not necessary convergent; therefore, in order to overcome the aforesaid shortcomings, the authors tested the conception of an innovative mathematical method, inspired to the time simulation of proper dynamic behaviours having the considered stationary condition as a limit of a consequent asymptotic evolution to a constant input.

Keywords: non-linear equations system, new numerical method

1 INTRODUCTION

The conception, layout and design of any dynamic system start from activities focused on the first-approach definition of the principal characteristics of the system itself, essentially from the point of view concerning the compliance of its performance with the customer requirements; the definition of the system further characteristics (depending on its dynamic behaviour) is instead demanded to second-approach or first-refinement activities. The abovementioned first-approach analysis concerning the definition of the system steady state performance is usually based on relatively simple physical-mathematical models able to match only the stationary phenomenons involved in their operation, neglecting the dynamic analysis (typically used in the following design activities). For example, in order to obtain a first-approach model of a hydraulic, electric or pneumatic net work, defining the relative and absolute sizing of its components fitted to their specific duties or to solve several mechanical or structural problems, it is adequate (and sufficient) to define stationary models however characterised by all the non-linearities significant to the purpose. The stationary model may be mathematically represented by a system of non-linear algebraic equations of difficult or impossible solution in closed form; in this case, in order to solve the above-mentioned equations system, it is necessary to employ iterative (or recurring) methods specifically shaped on the specific problem and not necessarily convergent (therefore particularly undesirable to use). Therefore, in order to overcome the aforesaid shortcomings, the authors tested the conception of an innovative mathematical method (provisionally defined semi-dynamic or pseudo-dynamic mathematical method), conceived as a time simulation of proper dynamic behaviours having the considered stationary condition as a limit (for infinite time, at least conceptually) of a consequent asymptotic evolution to a constant input. Having told it, in the problem analysis, the advantage depending on the employment of simpler static models seams to fail; however it must be noted that, just by the introduction of some proper terms into their stationary equilibrium equations (provided with proper values

Contact author: Matteo D. L. Dalla Vedova

E-mail: matteo.dallavedova@polito.it

of their coefficients, selected with a view to optimize the performances of the algorithm), expressed in terms of first-order time derivatives of the unknown variables, it is possible, from the computational point of view, to solve one by one separately the different equations of the system. By means of the aforementioned mathematical method it is possible to turn, component by component, stationary dis-equilibriums into instantaneous pseudo-dynamic equilibriums, by which the convergence rate of the considered unknown variable (towards its stationary value) is definable and easily controllable through adequate numerical coefficients.
The proposed method cannot be strictly considered intrinsically convergent; however, the desired stationary condition, if characterised by a stable equilibrium, following proper selections of the values of the added terms coefficients, can be found by means of the time integration of the so obtained first-order equilibrium differential equations, that is by time integrating the first-order derivatives of the desired unknown quantities, till their stabilization (that is convergent to constant values of the desired quantities and null of their derivatives). If an unstable equilibrium conditions must be reached, the time back integration is adequate.

2 BASIC CONCEPTS CONCERNING THE PROPOSED METHOD

The proposed method consists of a new approach to the solution of any non-linear equations system both of algebraic and differential type: so, it is not a computational method specifically conceived to solve problems concerning structural, mechanical, hydraulic, pneumatic or electrical systems, but its validity is wider. In general, the solution of a non-linear equations system of any type needs numerical recurring or iterative methods; neither their convergence is always assured nor the rate of the eventual convergence is always controllable. The proposed method replaces the recurring computation by a sort of mathematical modelling and time simulation of a hypothetical, but possible, pseudo-dynamic phenomenon, able to spontaneously converge towards the desired stationary condition (initially unknown quantity and finally solution of the problem), under constant inputs and for theoretically infinite time.
All the transient dynamic conditions are solutions of the problem described by the hypothetical dynamic phenomenon; one of these only is stationary persistent and so it represents the solution of the primary problem.
The pseudo-dynamic phenomenon, which is mathematically modelled and time-simulated, is developed from the stationary one by a measure: it consists of assigning to each system equation the task concerning the computation of a specific unknown quantity of the problem (without necessarily making it explicit) by introducing an auxiliary further linear additive term, expressed in form of first order derivative of the unknown variable itself, multiplied by a proper coefficient.
The equation must be made explicit (it is always possible) in the further additive term in order compute, really, the first order derivative of the desired unknown quantity; the value of the "dynamic unknown variable" is thus defined, which, time-integrated, gives the value temporarily updated of the "stationary unknown variable".
By allowing the integration process going on for a sufficiently long time (permitting the transient of the pseudo-dynamic phenomenon to go out), the "stationary unknown variable" reaches a constant value: thus, the unknown quantity of the primary problem is defined; in fact, in this condition, the supplementary term of the equation becomes null, and the problem turns into the stationary one, primarily considered, having defined its solution.

3 MATHEMATICAL CONSIDERATIONS

Practically, for example, a physical problem, involving the resolution of a mathematical model consisting of a system of ***n*** algebraic non-linear equations containing ***n*** unknown quantities $\boldsymbol{x_i}$, as represented in (1), can be considered; the solution of the physical problem consists of the determination of the real roots of the equation system.

$$\begin{cases} f_1(x_1,\ldots x_i,\ldots x_n) = 0 \\ \ldots\ldots\ldots\ldots\ldots \\ f_i(x_1,\ldots x_i,\ldots x_n) = 0 \\ \ldots\ldots\ldots\ldots\ldots \\ f_n(x_1,\ldots x_i,\ldots x_n) = 0 \end{cases} \tag{1}$$

To this purpose, according to the proposed method, the system (1) must be modified in the set of independent non-linear equations (2) (no more an equation system), where the functions $\boldsymbol{f_i}$ are not assigned equal to zero, but equal to an auxiliary additive term in which $\boldsymbol{x'_i}$ are the time derivatives of each unknown variable.

$$\begin{aligned} & f_1(x_1,\ldots x_i,\ldots x_n) = c_1 \cdot \dot{x}_1 \\ & \ldots\ldots\ldots\ldots\ldots \\ & f_i(x_1,\ldots x_i,\ldots x_n) = c_i \cdot \dot{x}_i \\ & \ldots\ldots\ldots\ldots\ldots \\ & f_n(x_1,\ldots x_i,\ldots x_n) = c_n \cdot \dot{x}_n \end{aligned} \tag{2}$$

By introducing initial values of the unknown variables $\boldsymbol{x_i}$, the equations (2) can be independently solved to obtain the instantaneous values of the derivatives $\boldsymbol{x'_i}$ of the unknown variables $\boldsymbol{x_i}$ as in (3).

$$\begin{aligned} & \dot{x}_1 = f_1(x_1,\ldots x_i,\ldots x_n)/c_1 \\ & \ldots\ldots\ldots\ldots\ldots \\ & \dot{x}_i = f_i(x_1,\ldots x_i,\ldots x_n)/c_i \\ & \ldots\ldots\ldots\ldots\ldots \\ & \dot{x}_n = f_n(x_1,\ldots x_i,\ldots x_n)/c_n \end{aligned} \tag{3}$$

The derivatives x'_i, subsequently, can be time-integrated in order to compute the new values of the unknown variables x_i which can be reintroduced in the equations (2), to obtain the new values of the derivatives x'_i, and so on, as in a time-simulation of the behaviour of a dynamic system.

It must be noted that the method cannot be defined intrinsically convergent or not; the selection of the proper values of c_i, with respect to the integration time interval Δt, allows the control of the convergence and of its rate. When the values of the derivatives computed by the equations (2) are adequately small, the convergence is practically completed and the values assumed by the unknown variables x_i are stable between two successive integration steps.

In these conditions the equation set (2) is equivalent to the equation system (1), and the stabilized values of the unknown variables x_i represent the desired numerical solution of the system (1). If the system (1) has different solutions, the initial values assumed for the variables x_i act on what solution is found, as it is in the usual recurring or iterative computing methods. The proposed method can be applied to equation systems characterised by any type of algebraic functions f_i (non-linear, transcendental, exponential, etc…, provided that having no singularities within the field of values swept till the unknown variable), because, in the form of equations (2), they are solved in the terms containing the derivatives x'_i, which can be intrinsically represented in explicit form. In case of time-differential equations f_i, the method can be applied by some measure on the additional terms: this matter requests more careful studies. So it can be said in case of not-time- differential equations $f_i = 0$.

If a number k of unknown variables can be directly given in an explicit form within the same number k of system equations (one different variable in each equation), the introduction of the auxiliary terms, expressed in first order derivatives of the k unknown variables themselves, is unnecessary and inappropriate.

So, if the equations system (1) can be expressed as:

$$\begin{cases} f_{\Theta 1}(x_2,\dots x_i,\dots x_n) = x_1 \\ f_{\Theta 2}(x_2,\dots x_i,\dots x_n) = x_2 \\ \dots\dots\dots\dots\dots \\ f_i(x_1,\dots x_i,\dots x_n) = 0 \\ \dots\dots\dots\dots\dots \\ f_n(x_1,\dots x_i,\dots x_n) = 0 \end{cases} \tag{1bis}$$

the set of replacing equations to solve can be:

$$\begin{array}{l} f_{\Theta 1}(x_2,\dots x_i,\dots x_n) = x_1 \\ f_{\Theta 2}(x_2,\dots x_i,\dots x_n) = x_2 \\ \dots\dots\dots\dots\dots \\ f_i(x_1,\dots x_i,\dots x_n) = c_i \cdot \dot{x}_i \\ \dots\dots\dots\dots\dots \\ f_n(x_1,\dots x_i,\dots x_n) = c_n \cdot \dot{x}_n \end{array} \tag{2bis}$$

having the advantage of the reduction of the number of coefficients c_i to preset for the computing process, so simplifying it.

4 SIMPLIFIED HYDRAULIC APPLICATION

In order to explain the innovative mathematical method proposed by the authors, in the present paragraph the case of application of the aforesaid method to a simple hydraulic system is analysed. The examined hydraulic system, as shown in figure 1, is composed of a tank S having a higher capacity (able to assure, in operation, a constant value of the supply pressure p_S) connected, by means of a pipeline (ideally thought without fluid-dynamic losses), with a pressure relief valve VLP ad a hypothetic user U (able to absorb, or to supply upstream, an assigned flow Q_u). Downstream the tank S, a laminar-turbulent orifice St is placed.

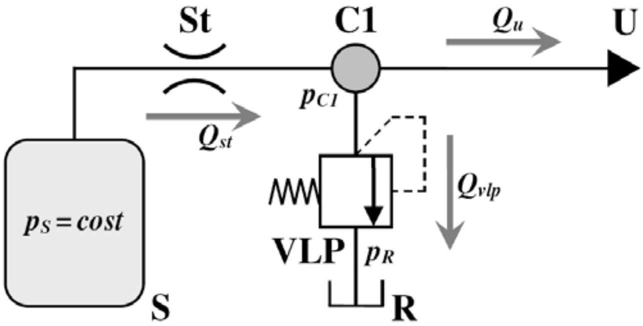

Figure 1 Schematic of simplified hydraulic system

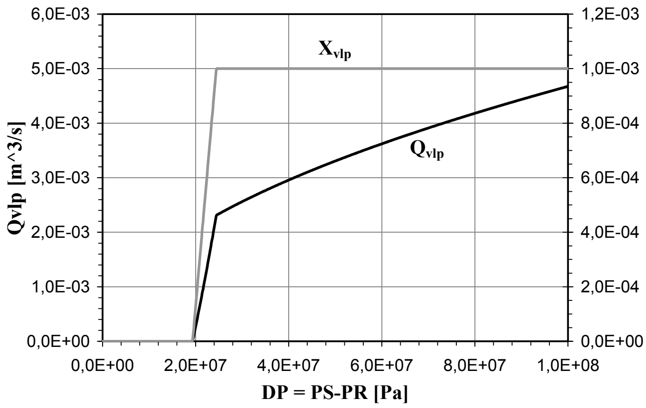

Figure 2 Hydraulic characteristic of the VLP valve

The pressure relief valve VLP, as shown in figure 2, acts by controlling the flow Q_{vlp}, drained to return R, for the purpose of limiting (to an assigned setting $FRV0$) the maximum value of the upstream pressure p_{C1}. If the upstream pressure p_{C1} overcomes the aforesaid calibration pressure p^* (in this case equal to 20 [MPa]), the VLP variable orifice modify its position (X_{vlp}), in order to drain the exceeding flow and maintain the upstream pressure close to its calibration value. The return pressure p_R and the tank supply pressure p_S are assigned and constant; also the fluid dynamics characteristics of laminar-turbulent orifice ***St*** and pressure relief valve ***VLP*** are known. Our goal is to compute, as a function of the volumetric flow $\boldsymbol{Q_u}$ required by the user ***U***, the values of the pressures (particularly the pressure $\boldsymbol{p_{C1}}$ downstream the orifice ***St*** in stationary conditions) and flows developed inside the hydraulic system. In order to approach in closed form the aforesaid problem, it is necessary to solve, contemporarily, all the equations representing the considered physical phenomenon; in this case, the equations describing the fluid dynamic behaviour of the examined system (shown in figure 1), are the following:

$$\begin{cases} Q_{st} = SIGN\left[\dfrac{\sqrt{RL_{st}^{\;2} - 4\cdot RQ_{st}\cdot(p_S - p_{C1})} - RL_{st}}{2\cdot RQ_{st}}, p_S - p_{C1}\right] \\ XRV = MIN\{MAX[0, (\mathrm{A_{vlp}}\cdot(p_{C1} - p_R) - FRV0)/\mathrm{KRV}], \mathrm{XRVM}\} \\ ARV = C_d\cdot\pi\cdot\Phi_{vlp}\cdot XRV \\ \mathrm{Q_{vlp}} = SIGN\left(ARV\cdot\sqrt{2\cdot|p_{C1} - p_R|/\rho}, p_{C1} - p_R\right) \\ \mathrm{Q_{st}} = \mathrm{Q_u} + \mathrm{Q_{vlp}} \end{cases} \tag{4}$$

where, the abovementioned coefficients, are the following:

$\boldsymbol{RL_{st}}$, $\boldsymbol{RQ_{st}}$	linear and quadratic resistance coefficients of the orifice ***St*** [kg/s/m^4] , [kg/m^7]
$\boldsymbol{A_{vlp}}$	effective area of the valve poppet on which the differential pressure is active [m^2]
FRV0	calibration preload of the pressure relief valve spring [N]
KRV	stiffness of the pressure relief valve spring [N/m]
XRVM	maximum value of the valve poppet travel [m]
ARV	value of the pressure relief valve turbulent orifice (it is proportional to the valve poppet position ***XRV***) [m^2]
$\boldsymbol{C_d}$	efflux coefficient of the pressure relief valve turbulent orifice [1]
$\boldsymbol{\Phi_{vlp}}$	diameter of the pressure relief valve turbulent orifice [1]

The equations shown in (4) are expressed by means of the Matlab (or FORTRAN) syntax, then the operators MIN(a,b), MAX(a,b) and SIGN(a,b) have to be intended in this way. The equations system (4) is composed by five different algebraic equations expressed as a function of three unknown variables (in this case the pressure $\boldsymbol{p_{C1}}$ and the flows $\boldsymbol{Q_{st}}$ and $\boldsymbol{Q_{vlp}}$). Since it is possible to merge (by means of simple mathematical operations) the second, third and forth equations in a single equation, the system (4) can be reduced to an equivalent system (5) composed by only three algebraic equations expressed as a function of the three aforesaid unknown variables.

$$\begin{cases} Q_{st} = SIGN\left[\dfrac{\sqrt{RL_{st}^{\;2} - 4\cdot RQ_{st}\cdot(p_S - p_{C1})} - RL_{st}}{2\cdot RQ_{st}}, p_S - p_{C1}\right] \\ \mathrm{Q_{vlp}} = SIGN\left(\Omega_{ARV}\cdot\sqrt{2\cdot|p_{C1} - p_R|/\rho}, p_{C1} - p_R\right) \\ \mathrm{Q_{st}} = \mathrm{Q_u} + \mathrm{Q_{vlp}} \end{cases} \tag{5}$$

where $\boldsymbol{\Omega_{ARV}}$ is equal to:

$$C_d\cdot\pi\cdot\Phi_{vlp}\cdot MIN\left\{MAX\left[0, \frac{A_{vlp}\cdot(p_{C1} - p_R) - FRV0}{KRV}\right], XRVM\right\}$$

The first and the second equations of the system (5) put in relation the flows $\boldsymbol{Q_{st}}$ and $\boldsymbol{Q_{vlp}}$ with the corresponding pressure drops (in other words the differential pressures $\boldsymbol{p_S - p_{C1}}$ and $\boldsymbol{p_{C1} - p_R}$), while the last one is the flow continuity equation; as the pressures $\boldsymbol{p_S}$ and $\boldsymbol{p_R}$ and the flow $\boldsymbol{Q_u}$ are given, all the three equations of the system (5) only are functions of the pressure $\boldsymbol{p_{C1}}$. In order to solve the equation system (5) in closed form, deducing the corresponding values of the unknown variables $\boldsymbol{p_{C1}}$, $\boldsymbol{Q_{st}}$ and $\boldsymbol{Q_{vlp}}$, it would be necessary to solve simultaneously all the three equations forming the aforementioned system; since the abovementioned procedure can result difficult to solve (particularly in case of non-linearities), this kind of problems is often approached by means of numerical approximate solving methods that, by a proper computing process (not always intrinsically convergent), give the approximate values of the desired unknown variables. Applying the proposed pseudo-dynamic method, it is possible to introduce into the third equation of (5) an opportune additive term (expressed as a function of the first order time derivative of the unknown variable $\boldsymbol{p_{C1}}$) and so modifying the system (5) obtaining the set of independent non-linear equations (6) (no more an equation system):

$$\begin{aligned} & Q_{st} = SIGN\left[\dfrac{\sqrt{RL_{st}^{\;2} - 4\cdot RQ_{st}\cdot(p_S - p_{C1})} - RL_{st}}{2\cdot RQ_{st}}, p_S - p_{C1}\right] \\ & \mathrm{Q_{vlp}} = SIGN\left(\Omega_{ARV}\cdot\sqrt{2\cdot|p_{C1} - p_R|/\rho}, p_{C1} - p_R\right) \\ & \mathrm{Q_{st}} - \mathrm{Q_u} - \mathrm{Q_{vlp}} = \mathrm{C}\cdot\frac{\mathrm{dp_{C1}}}{\mathrm{dt}} \end{aligned} \tag{6}$$

From a physical point of view, the adoption of the abovementioned additive term is equivalent to consider the presence of a hydraulic capacity, located downstream the orifice ***St***, in the physical model itself.

Computing the hydraulic flow compressibility through a fictitious coefficient (that is chosen appropriately in order to guarantee the calculation convergence), it is possible to express the temporal evolution of the pressure p_{C1} as a function of net flow that goes into the abovementioned capacity; in fact, the introduction of a hydraulic capacity allow to obtain a corrective term (in this case the first order derivative of p_{C1}) proportional to the flows imbalance. By that term, the flows unbalance influences the pressure value calculated in the following computation step producing its convergence towards equilibrium value that satisfies the flow continuity equation.

By introducing an initial value of the unknown variable p_{C1} (for example equal to the return pressure p_R), the equations (6) can be independently solved; the first and the second equations give directly the instantaneous value of the flows Q_{st} and Q_{vlp} and, by substitution, the third one gives the corresponding value of the derivative $p'_{C1} = d(p_{C1})/dt$.

The derivative p'_{C1}, subsequently, can be time-integrated in order to compute the new value of the unknown variable p_{C1} which can be reintroduced in the equations (6), to obtain the new values of the derivative p'_{C1} (besides the corresponding instantaneous value of the flows Q_{st} and Q_{vlp}), and so on, as in a time-simulation of the behaviour of a dynamic system. The equations (6) have been used to build a dedicated computer code in a general purpose language. Several simulation have been run (with different values of the flow Q_u) with the purpose to tests the effectiveness of the proposed pseudo-dynamic method.

The following figures explain the time history of the pressures and flows calculated during the numerical simulations; the transients, which are unnecessary in order to analyse the stationary performance of the examined system, are however reported in order to show the computation convergence towards the corresponding static values.

Basing the modelling of the system upon a first order mathematical model, their stationary conditions are equal to the asymptotic values of the corresponding variables (pressures and flows), calculated through the numerical simulations based upon the proposed method; obviously, the so obtained stationary values are also solutions of the equations system (4) or (5).

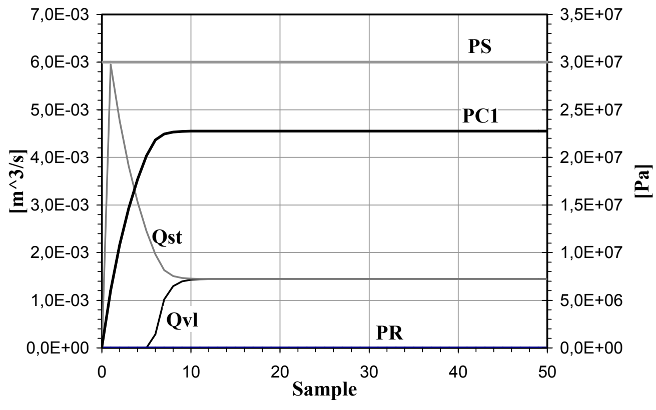

Figure 3

In figure 3 the case of null flow Q_u is considered; the whole flow Q_{st}, which flows across the laminar-turbulent orifice St, is drained towards return R through the pressure relief valve VLP (in fact, their simulated values are asymptotically equal). The stationary value of the pressure p_{C1} (about 23 [MPa]) is correctly lower than the supply pressure p_S (in fact, flowing across the nozzle, the hydraulic fluid produces indeed a pressure drop).

Using the first equation of (6), it is also possible to verify the correct relationship between the calculated flow Q_{st} (about 1,4 [l/s]) and the pressure drop p_S - p_{C1}.

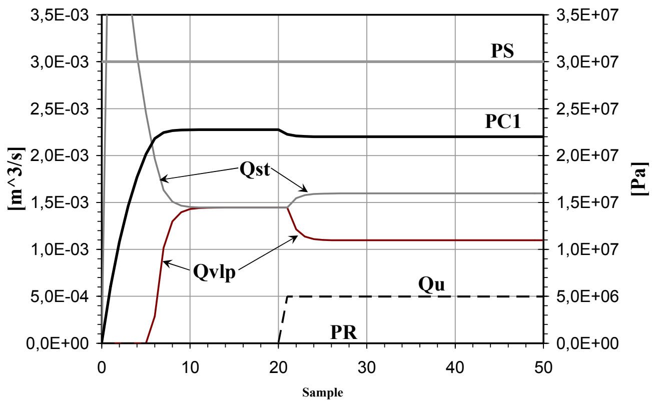

Figure 4

In figure 4 it is possible to state as, introducing a drained flow Q_u greater than zero (this means that the user is absorbing the abovementioned flow), the stationary values of p_{C1}, Q_{st} and Q_{vlp} result modified (as regards the previous case). As regards the previous case, the absorbed flow Q_u (in this case equal to 0,5 [l/s]) produces an increase of the overall value of flow Q_{st} that flows across the laminar-turbulent orifice St; such flow increase performs a greater pressure drop p_S - p_{C1} and, therefore, reduces the pressure value p_{C1} downstream the aforesaid orifice. This pressure decrease modifies the equilibrium of translation of the forces acting on the VLP poppet and so reduces the orifice stroke XRV (and consequently reduces also the poppet control area). The contemporaneous drop of p_{C1} and XRV gives rise to a corresponding reduction of the flow Q_{vlp} drained across the pressure relief valve VLP. The aforesaid flow absorption (Q_u) produces a transient that, however, converges asymptotically towards the new stationary conditions shown in figure 4.

In figure 5 it is possible to state as, increasing further the drained flow Q_u (in this case equal to 2,5 [l/s]), the stationary values of p_{C1}, Q_{st} and Q_{vlp} result noticeably modified; the greater flow absorbed by the user, reduces the pressure value p_{C1} under the calibration pressure p^* of the VLP and, consequently, sets at zero the value of the flow Q_{vlp} (in fact, if the upstream pressure p_{C1} is smaller than the corresponding setting value p^*, the pressure relief valve doesn't absorb any flow). In this case, since the pressure relief valve doesn't work, the flow Q_u (absorbed by the user) is exactly equal to what goes through the orifice St.

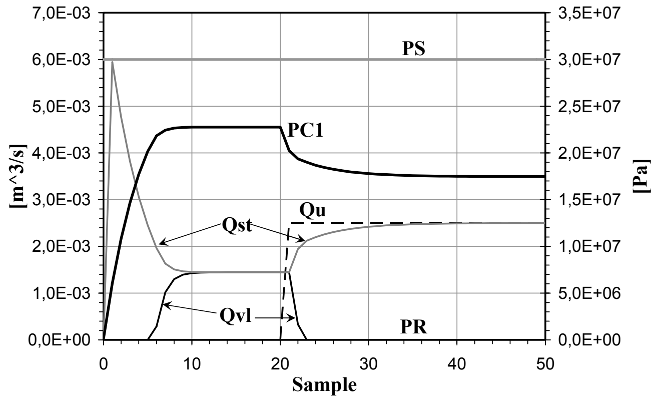

Figure 5

Figure 6 shows the evolution of the calculated variables of the system (towards the corresponding stationary values) in case of $\boldsymbol{Q_u}$ = 5,95 [l/s]; this case represents a limit condition of the examined system, in fact, more elevated values of the flow $\boldsymbol{Q_u}$ would produce cavitations phenomenons (reducing $\boldsymbol{p_{C1}}$ under the corresponding vapour pressure value).

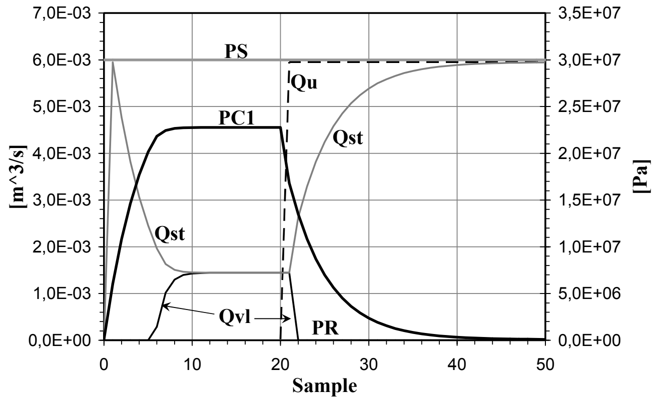

Figure 6

Figure 7 shows the case of absorbed flow $\boldsymbol{Q_u}$ = 7 [l/s]; since such flow is greater than the limit condition value (shown in the previous case), cavitations phenomenons are produced downstream the orifice ***St*** (and the pressure $\boldsymbol{p_{C1}}$ decreases up to reach the vapour pressure value).

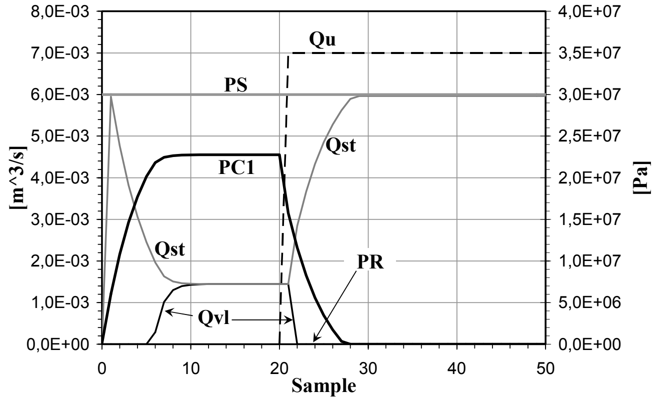

Figure 7

Figures 8, 9 and 10 show the simulation performed for the case of hydraulic system subjected to a backflow $\boldsymbol{Q_u}$ ($\boldsymbol{Q_u}$ smaller than zero, that is the user forces the flow back through the pipeline). In these cases, increasing the value of the backflow $\boldsymbol{Q_u}$, both the pressure $\boldsymbol{p_{C1}}$ and the flow $\boldsymbol{Q_{vlp}}$ are consequently increased.

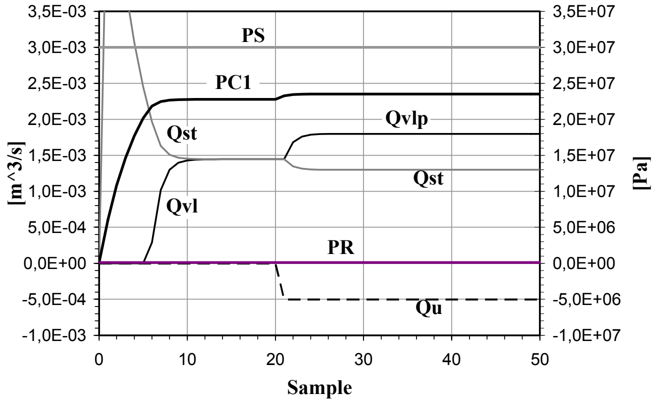

Figure 8

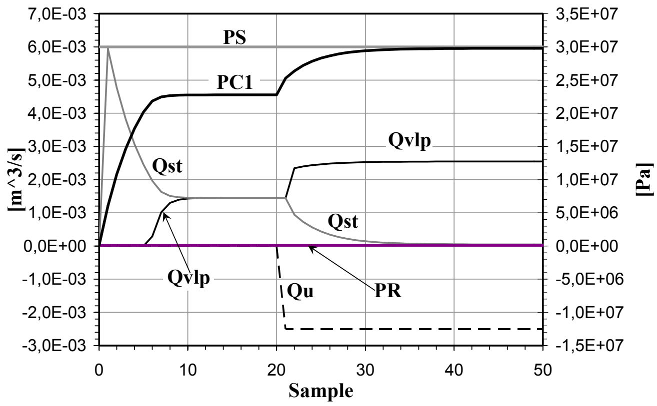

Figure 9

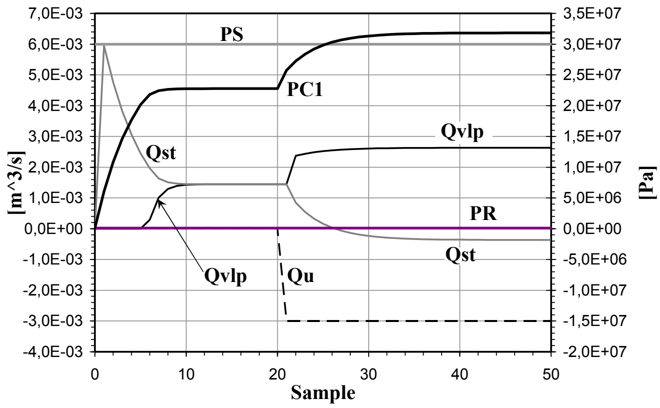

Figure 10

In figures 8 it is also possible to state as, adopting a backflow $\boldsymbol{Q_u}$ equal to -0,5 [l/s], the stationary value of the flow $\boldsymbol{Q_{st}}$ results smaller than the corresponding value calculated in case of $\boldsymbol{Q_u}$ = 0; in fact, the abovementioned growth of the pressure p_{C1} modifies the equilibrium condition (of the hydraulic fluid through the orifice) reducing the corresponding value of Q_{st}.

The comparison between the results reported in figures 9 and 10 allows to state how, increasing the backflow Q_u, the pressure p_{C1} can be greater than the corresponding supply pressure p_S (which is assumed constant and equal to 30 [MPa]) and it is therefore possible to reduce at zero the flow Q_u or even to obtain a backflow through the orifice ***St***.

5 HYDRAULIC SYSTEM APPLICATION

In order to explain the new mathematical method proposed by the authors, in the present paragraph a further case of application of the aforesaid method is considered.

The examined hydraulic system, as shown in figure 11, is composed of:

- a fixed-displacement volumetric pump ***GAQF*** that supplies a constant flow Q_{n1},
- a connection pipeline (ideally thought without fluid dynamic losses),
- a pressure relief valve ***VLP*** (already shown in the previous paragraph),
- a 4-way continuous positioning control valve ***SV***,
- a 2-way proportional flow control valve ***RQ2*** (in which, in order to assure a load-compensation of the drained flow, the pressure compensator (***SVP***) keeps the differential pressure across the metering orifice (***SM***) always at a constant value),
- an adjustable laminar-turbulent orifice ***St***.

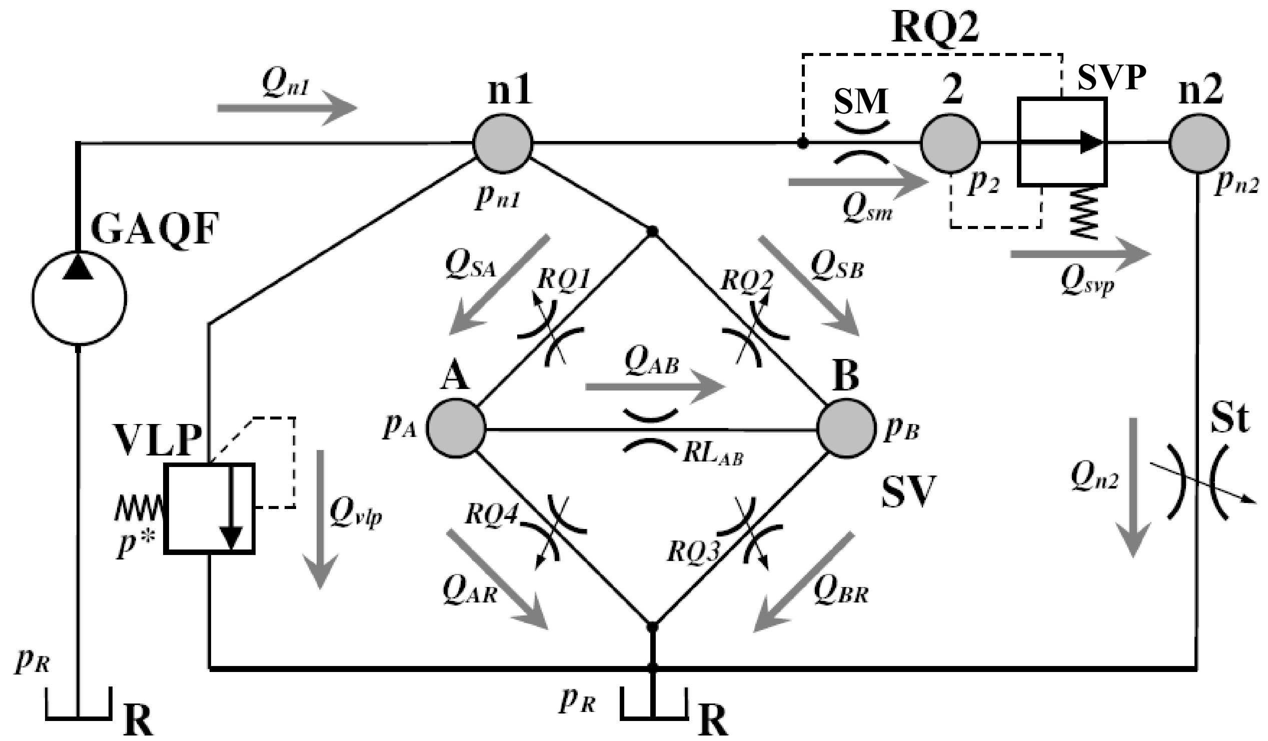

Figure 11

As shown in figure 12, the abovementioned control valve ***SV*** consists of a control spool regulating the passing flow modifying its position (***XSV***); in fact, the connection of the pressure supply port (***S***) to an actuator port and, at the same time, the connection of the other actuator port to the return flow port (***R***) are performed by means of four adjustable turbulent orifice, having variable areas depending on the spool position. The actuation ports ***1*** and ***2*** are connected each other through a pipeline producing a flow proportional pressure drop and so represented by a laminar orifice.

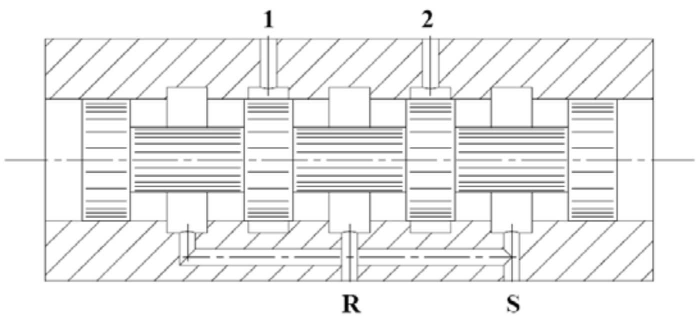

Figure 12 Schematic of control valve spool

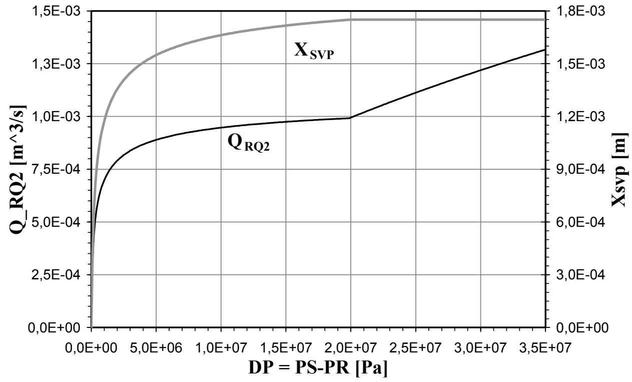

Figure 13

The 2-way proportional flow control valve ***RQ2***, as shown in figure 13, operates in order to assure a load compensation of the passing flow; in fact, when the valve is within its control field, the pressure compensator (***SVP***), properly modifying its port area, keeps always the differential pressure across the metering orifice (***SM***) at a constant value. The equations that describe the fluid dynamic behaviour of the aforementioned ***RQ2*** valve are the following:

$$\begin{cases} Q_{sm} = SIGN\left[\dfrac{\sqrt{RL_{sm}{}^{2} - 4\cdot RQ_{sm}\cdot\left(p_{n1}-p_2\right)} - RL_{sm}}{2\cdot RQ_{sm}}, p_{n1}-p_2\right] \\ Xsvp = MIN\left\{MAX\left[0\,,\mathrm{AR_{svp}}\cdot\left(p_{n1}-p_2-p^*\right)/\mathrm{Ksvp}\right],\mathrm{Xsvpm}\right\} \\ Asvp = \left(Xsvp0 - Xsvp\right)\cdot Wsvp \\ RQ_{svp} = \rho/\left(2\cdot Cd^2\cdot Asvp^2\right) \\ Q_{svp} = SIGN\left[\dfrac{\sqrt{RL_{svp}{}^{2} - 4\cdot RQ_{svp}\cdot\left(p_2-p_{n2}\right)} - RL_{svp}}{2\cdot RQ_{svp}}, p_2-p_{n2}\right] \end{cases} \qquad (7)$$

where, the abovementioned coefficients, are the following:

RL_{st} ; RQ_{st}	linear , quadratic resistance coefficients of the metering orifice ***SM*** [kg/s/m^4];[kg/m^7]
AR_{svp}	effective area of the ***SVP*** valve poppet [m^2]
P*	calibration preload of the ***SVP*** valve spring [N]
Ksvp	stiffness of the ***SVP*** valve spring [N/m]
Xsvpm	maximum value of the valve poppet's travel [m]
Wsvp	circumferential width of the ***SVP*** valve orifice [m]
Asvp	value of the ***SVP*** valve orifice (it's proportional to the poppet position ***Xsvp***) [m^2]
C_d	efflux coefficient of the pressure relief valve's turbulent orifice [1]
ρ	hydraulic fluid density [kg/m^3]
RL_{svp} ; RQ_{svp}	linear, quadratic resistance coefficients of the metering orifice ***SVP*** [kg/s/m^4];[kg/m^7]

In order to compute in closed form the stationary system behaviour, it is necessary to solve, contemporarily, all the equations that describe the examined physical phenomenon. Also in this case the problem can be approached by means of the proposed pseudo-dynamic method; in fact, applying the procedures shown in the previous paragraph, it is possible to introduce, into the system equations composing the mathematical model of the considered hydraulic system, five proper additive terms (expressed as a function of the first order time derivative of the five unknown variables) and so modifying the corresponding equations system, obtaining a set of independent non-linear equations. From a physical point of view, the introduction of the abovementioned additive terms is equivalent to introduce five hydraulic capacities (called as ***n1***, ***2***, ***n2***, ***A*** and ***B***), properly located inside the physical model itself (in figure 11, they are represented by five grey dots); in this case the five unknown quantities are the pressure values characterising the aforesaid hydraulic capacities (that is the pressures p_{n1}, p_2, p_{n2}, p_A and p_B shown in figure 11). Computing the fluid compressibility through fictitious coefficients (that are properly selected in order to assure the computing process convergence), it is possible to express the time history of the unknown variables as a function of the net flows entering the abovementioned capacities; in fact, the introduction of hydraulic capacities furnishes the corrective terms (in this case the pressure first order derivatives) proportional to the corresponding flows unbalances. By introducing an initial value of the unknown variables (in this case equal to the return pressure p_R), the equations can be independently solved (obtaining the stationary values of the pressure and the corresponding flows). As it was already shown in the previous paragraph, the so obtained equations have been used to build a dedicated computer code. Several simulations have been run for the purpose of testing the effectiveness of the proposed pseudo-dynamic method. The following figures show the time history of the pressures and flows calculated during the numerical simulations; the transients, which are unnecessary in order to analyse the stationary performance of the examined system, are however reported for the purpose of showing the computation convergence towards the corresponding static values. The above mentioned computer code allows to modify many operational parameters of the considered hydraulic system (in order to analyze the behaviour of the proposed pseudo-dynamic method in case of non-linear mathematical models and, particularly, to test its computing stability and convergence rate under mutual interaction between the different unknown variables acting on the phenomenon). Such parameters are:

- the supply flow Q_{n1} generated by pump,
- the control port area of the adjustable orifice ***St*** (through an opportune numerical coefficient α_{St} variable between 0 and 1; condition of closed orifice are simulated assuming $\alpha_{St} = 0$, whereas conditions of fully open orifice are simulated with $\alpha_{St} = 1$),
- the position of the control valve spool ***XSV*** (variable between the corresponding values of valve end of travel ± ***XSVM***; as shows in figure 13, the closed valve condi-

tion, in which all the valve passageways are closed, is corresponding to the centred spool position).

In figure 14 and 15 it is possible to state as, in case of both control valve ***SV*** and adjustable orifice ***St*** closed (that is ***XSV*** and α_{St} null), in stationary conditions the supply flow Q_{n1} (equal to 1 [l/s]) is fully drained towards return ***R*** by means of the pressure relief valve ***VLP***. In fact, since the abovementioned valves are closed, the whole supply flow increases the pressure of the hydraulic capacities ***n1***, ***2*** and ***n2*** as long as the ***VLP*** is below its working field and, only when the pressure p_{n1} at last overcomes the ***VLP*** calibration value p^* (in this case equal to 20 [MPa]), such flow is drained through the pressure relief valve. The stationary values of the pressures p_{n1}, p_2, p_{n2} are the same (see figure 14) and correspond with the ***VLP*** pressure drop that verifies the equality $Q_{n1} = Q_{vlp}$ between supplied and drained flows (see figure 15).

Figures 16 and 17 show the system behaviour in case of supply flow Q_{n1} = 1 [l/s], control valve ***SV*** fully open (in which the spool position ***XSV*** corresponds to its positive end of travel ***XSVM***) and adjustable orifice ***St*** closed (α_{St} = 0); since the control valve is able to request a limited flow, also in this case a portion of the supply flow Q_{n1} is drained to return through the pressure relief valve ***VLP***.

In figure 17 it is possible to state how, at the end of the transient (when the system pressures are stabilized), the values of the flows through the control valve are the same ($Q_{sa} = Q_{ab} = Q_{br}$) and the continuity equation is satisfied ($Q_{n1} = Q_{ab} + Q_{vlp}$).

In figures 18 and 19 the system behaviour in case of supply flow Q_{n1} = 1 [l/s], control valve ***SV*** closed (null spool position ***XSV***) and adjustable orifice ***St*** fully open (α_{St} = 1) are shown; in this case the stationary value of the supply pressure p_{n1} (developed downstream the pump ***GAQF***) is lower than the ***VLP*** calibration value p^*, so that the pressure relief valve doesn't work and the whole flow is drained to return ***R*** through the abovementioned adjustable orifice ***St***. As the supply flow is lower than the corresponding flow control valve ***RQ2*** calibration value, in this case this component doesn't work.

Figures 20 and 21 show the system behaviour in case of control valve ***SV*** and adjustable orifice ***St*** fully open (having the spool position ***XSV*** corresponding to its positive end of travel ***XSVM*** and α_{St} = 1); also in such operational condition (such as in the previous ones), the supply flow Q_{n1} (equal to 1 [l/s]) passes through ***SV*** and ***St*** (requiring no ***VLP*** action).

In figures 22 and 23 it is possible to state as, increasing the supply flow Q_{n1} to 2 [l/s], even if all the other parameters are unchanged, the stationary values of the calculated pressure and flows are modified. The augmented supply flow, that should cross the system branches towards ***R***, increasing the pressure p_{n1}, causes the ***VLP*** working; in fact, in this case, the pressure relief valve ***VLP***, in order to control the abovementioned pressure p_{n1}, develops a drained flow Q_{vlp} reducing the net flows across the ***SV*** and ***RQ2*** – ***St*** valves.

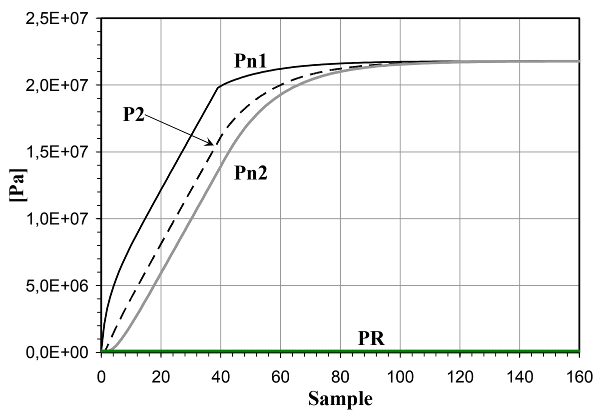

Figure 14

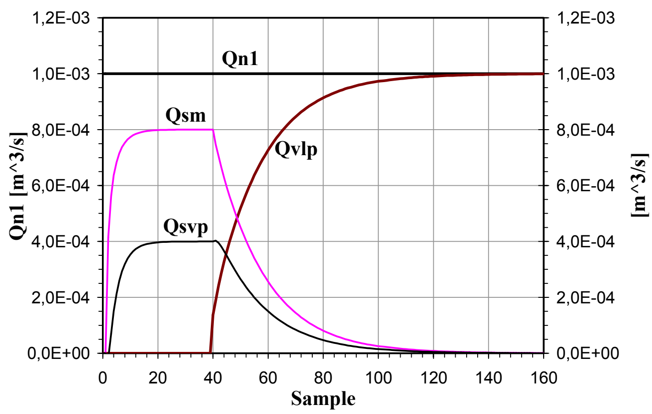

Figure 15

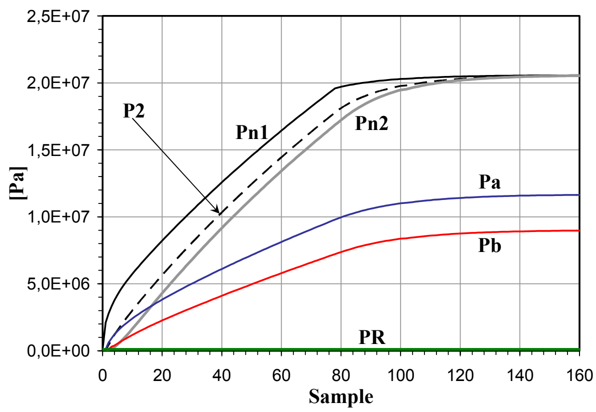

Figure 16

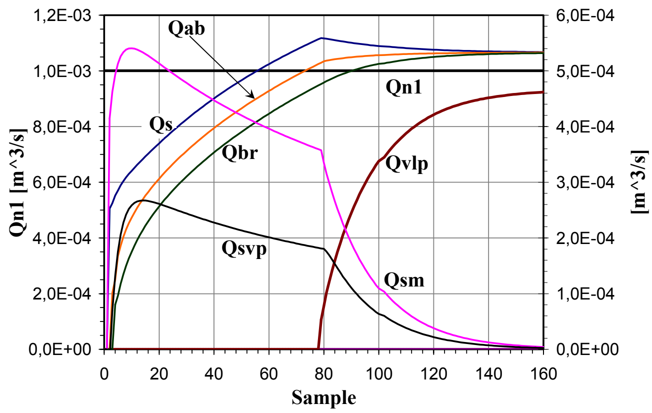

Figure 17

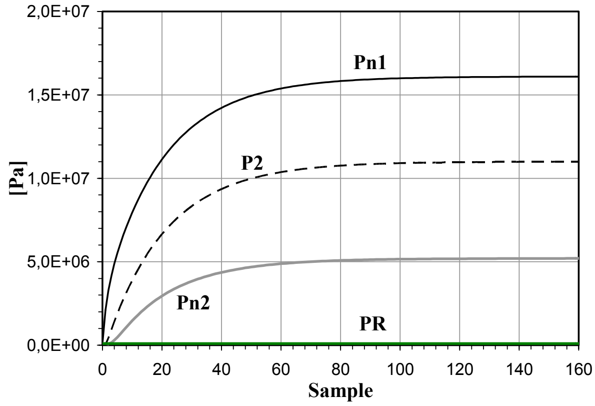

Figure 18

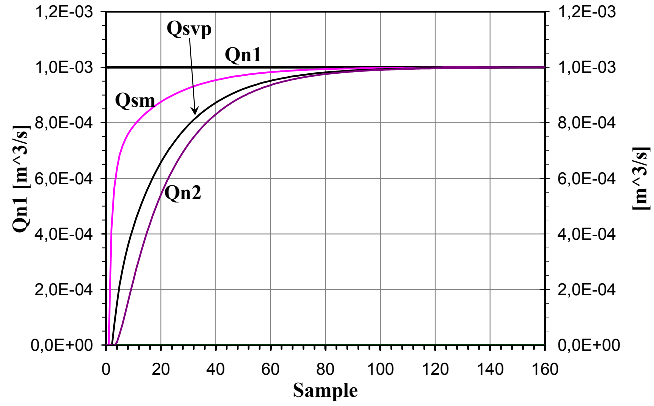

Figure 19

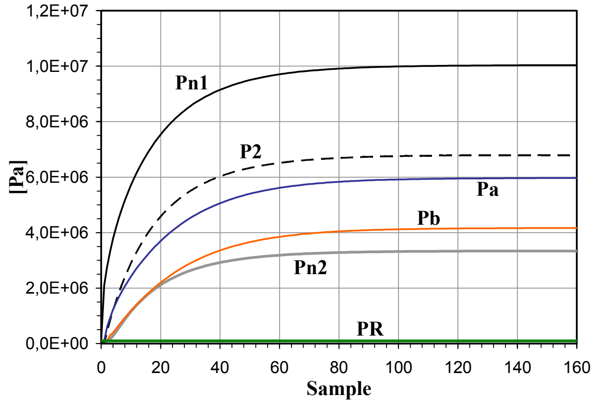

Figure 20

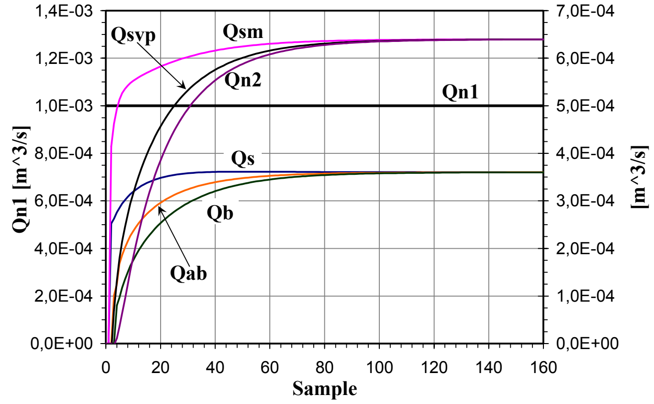

Figure 21

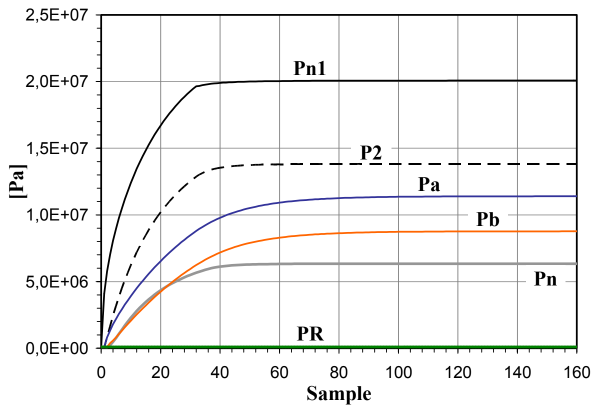

Figure 22

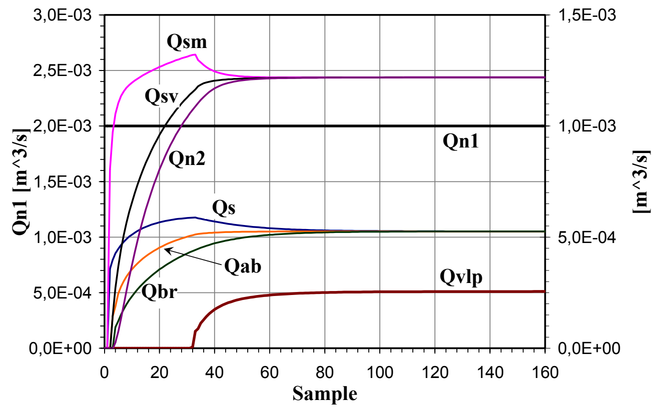

Figure 23

CONCLUSIONS

In conclusion the new method is based upon the computing, step by step, of the value representing the unbalance of each equation; by means of a proper coefficient, the unbalance term is used to compute the new value to assign to each variable to the next step. By the abovementioned new value, a new unbalance term can be computed and so a new value to assign to each variable and so on, till the convergence is reached. The proposed method is able to solve any type of functions forming the equation system, thus being widely of general purpose type. In the present work the proposed method is validated by applying it on typical hydraulic problems. Further works will prove the effectiveness of the method in other fields: mechanical, electrical and structural.

REFERENCES

[1] Viersma T.J., *Analysis Synthesis and Design of Hydraulic Servo-systems and Pipelines*, Elsevier, Delft, 1980.

[2] Dransfield P., *Hydraulic Control Systems. Design and Analysis of their Dynamics*, Springer Verlag, Berlin, 1981.

[3] Keller G. R., *Hydraulic system analysis*, Penton IPC, Cleveland, 1969.

[4] Akers A., Gassman M., Smith R., *Hydraulic power system analysis*, Boca Raton, 2006.

ISSN 1590-8844
International Journal of Mechanics and Control, Vol. 08, No. 02, 2007

TEMPLATE FOR PREPARING PAPERS FOR PUBLISHING IN INTERNATIONAL JOURNAL OF MECHANICS AND CONTROL

Author1*   Author2**

*   affiliation Author1

**   affiliation Author2

ABSTRACT

This is a brief guide to prepare papers in a better style for publishing in International Journal of Mechanics and Control (JoMaC). It gives details of the preferred style in a template format to ease paper presentation. The abstract must be able to indicate the principal authors' contribution to the argument containing the chosen method and the obtained results. (max 200 words)

Keywords: keywords list (max 5 words)

1 TITLE OF SECTION (E.G. INTRODUCTION)

This sample article is to show you how to prepare papers in a standard style for publishing in International Journal of Mechanics and Control.
It offers you a template for paper layout, and describes points you should notice before you submit your papers.

2 PREPARATION OF PAPERS

2.1 SUBMISSION OF PAPERS

The papers should be submitted in the form of an electronic document, either in Microsoft Word format (Word'97 version or earlier).
In addition to the electronic version a hardcopy of the complete paper including diagrams with annotations must be supplied. The final format of the papers will be A4 page size with a two column layout. The text will be Times New Roman font size 10.

Contact author: author1[1], author2[2]

[1]Address of author1.

[2]Address of author2 if different from author1's address.

2.2 DETAILS OF PAPER LAYOUT

2.2.1 Style of Writing

The language is English and with UK/European spelling. The papers should be written in the third person. Related work conducted elsewhere may be criticised but not the individuals conducting the work. The paper should be comprehensible both to specialists in the appropriate field and to those with a general understanding of the subject.
Company names or advertising, direct or indirect, is not permitted and product names will only be included at the discretion of the editor. Abbreviations should be spelt out in full the first time they appear and their abbreviated form included in brackets immediately after. Words used in a special context should appear in inverted single quotation mark the first time they appear. Papers are accepted also on the basis that they may be edited for style and language.

2.2.2 Paper length

Paper length is free, but should normally not exceed 10000 words and twenty illustrations.

2.2.3 Diagrams and figures

Figures and Tables will either be entered in one column or two columns and should be 80 mm or 160 mm wide respectively. A minimum line width of 1 point is required at actual size. Captions and annotations should be in 10 point with the first letter only capitalised *at actual size* (see Figure 1 and Table VII).

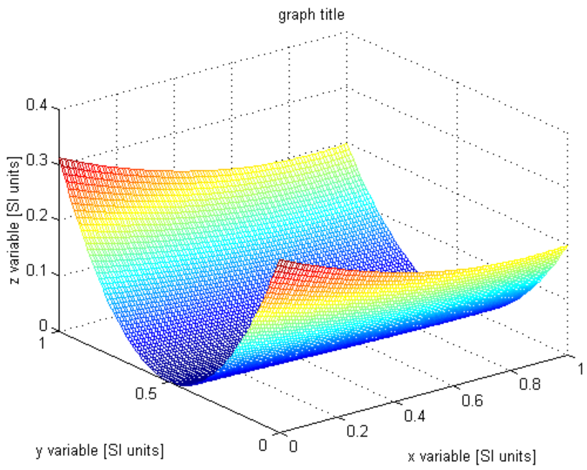

Figure 1 Simple chart.

Table VII - Experimental values

Robot Arm Velocity (rad/s)	Motor Torque (Nm)
0.123	10.123
1.456	20.234
2.789	30.345
3.012	40.456

2.2.4 Photographs and illustrations
Authors could wish to publish in full colour photographs and illustrations. Photographs and illustrations should be included in the electronic document and a copy of their original sent. Illustrations in full colour …

2.2.5 Equations
Each equation should occur on a new line with uniform spacing from adjacent text as indicated in this template. The equations, where they are referred to in the text, should be numbered sequentially and their identifier enclosed in parenthesis, right justified. The symbols, where referred to in the text, should be italicised.

- point 1
  - point 2
    - point 3

1. numbered point 1
   2. numbered point 2
      3. numbered point 3

$$W(d) = G(A_0, \sigma, d) = \frac{1}{T}\int_0^{+\infty} A_0 \cdot e^{-\frac{d^2}{2\sigma^2}} dt \qquad (1)$$

3 COPYRIGHT

Authors will be asked to sign a copyright transfer form prior to JoMaC publishing of their paper. Reproduction of any part of the publication is not allowed elsewhere without permission from JoMaC whose prior publication must be cited. The understanding is that they have been neither previously published nor submitted concurrently to any other publisher.

4 PEER REVIEW

Papers for publication in JoMaC will first undergo review by anonymous, impartial specialists in the appropriate field. Based on the comments of the referees the Editor will decide on acceptance, revision or rejection. The authors will be provided with copies of the reviewers' remarks to aid in revision and improvement where appropriate.

5 REFERENCES (DESCRIPTION)

The papers in the reference list must be cited in the text. In the text the citation should appear in square brackets [ ], as in, for example, "the red fox has been shown to jump the black cat [3] but not when...". In the Reference list the font should be Times New Roman with 10 point size. Author's first names should be terminated by a 'full stop'. The reference number should be enclosed in brackets.
The book titles should be in *italics*, followed by a 'full stop'. Proceedings or journal titles should be in *italics.* For instance:

REFERENCES (EXAMPLE)

[1] Smith J., Jones A.B. and Brown J., *The title of the book*. 1st edition, Publisher, 2001.

[2] Smith J., Jones A.B. and Brown J., The title of the paper. *Proc. of Conference Name*, where it took place, Vol. 1, paper number, pp. 1-11, 2001.

[3] Smith J., Jones A.B. and Brown J., The title of the paper. *Journal Name*, Vol. 1, No. 1, pp. 1-11, 2001.

[4] Smith J., Jones A.B. and Brown J., *Patent title*, U.S. Patent number, 2001.

International Journal of Mechanics and Control – JoMaC
Published by Levrotto&Bella
TRANSFER OF COPYRIGHT AGREEMENT

NOTE: Authors/copyright holders are asked to complete this form signing section A, B or C and mail it to the editor office with the manuscript or as soon afterwards as possible.	*Editor's office address:* Andrea Manuello Bertetto Elvio Bonisoli *Dept. of Mechanics* *Technical University – Politecnico di Torino* *C.so Duca degli Abruzzi, 24 – 10129 Torino – Italy* *e_mail: jomac@polito.it* *fax n.: +39.011.564.6999*

The article title:

By:____

To be Published in ***International Journal of Mechanics and Control JoMaC***
Official legal Turin court registration Number 5320 (5 May 2000) - reg. Tribunale di Torino N. 5390 del 5 maggio 2000

A Copyright to the above article is hereby transferred to the JoMaC, effective upon acceptance for publication. However the following rights are reserved by the author(s)/copyright holder(s):
1. All proprietary rights other than copyright, such as patent rights;
2. The right to use, free or charge, all or part of this article in future works of their own, such as books and lectures;
3. The right to reproduce the article for their own purposes provided the copies are not offered for sale.
To be signed below by all authors or, if signed by only one author on behalf of all co-authors, the statement A2 below must be signed.

A1. All authors:

SIGNATURE____________________________DATE__________ SIGNATURE____________________________DATE__________

PRINTED NAME__________________________________ PRINTED NAME__________________________________

SIGNATURE____________________________DATE__________ SIGNATURE____________________________DATE__________

PRINTED NAME__________________________________ PRINTED NAME__________________________________

A2. One author on behalf of all co-authors:
"I represent and warrant that I am authorised to execute this transfer of copyright on behalf of all the authors of the article referred to above"

PRINTED NAME__________________________________

SIGNATURE____________________________ TITLE____________________________ DATE______________

B. The above article was written as part of duties as an employee or otherwise as a work made for hire. As an authorised representative of the employer or other proprietor. I hereby transfer copyright to the above article to Editel-Pozzo Gros Monti effective upon publication. However, the following rights are reserved:
1. All proprietary rights other than copyright, such as patent rights;
2. The right to use, free or charge, all or part of this article in future works of their own, such as books and lectures;
3. The right to reproduce the article for their own purposes provided the copies are not offered for sale.

PRINTED NAME__________________________________

SIGNATURE____________________________ TITLE____________________________ DATE______________

C. I certify that the above article has been written in the course of employment by the United States Government so that no copyright exists, or by the United Kingdom Government (Crown Copyright), thus there is no transfer of copyright.

PRINTED NAME__________________________________

SIGNATURE____________________________ TITLE____________________________ DATE______________

CONTENTS

next number scheduled titles:

Performance Estimation of Cam Transmissions through Identification of Lumped Parameters
G. Carbone, C. Lanni, G. Incerti, M. Ceccarelli

Nonlinear Elastic Characteristic of Magnetic Suspensions through Hilbert Transform
E. Bonisoli

Proposal of Innovative Fluid Dynamic Nonlinear Servovalve Models
L. Borello, M. D. L. Dalla Vedova

A Stress Evaluation Strategy for Designing Squat Structures
C. Rosso

Dynamic Root Stress Analysis in a Spur Gear under Impact Moving Load
T. Jingwei, X. Buqing, W. Shibin, B. Picasso